



Australian Government
Department of Defence
Defence Science and
Technology Organisation

A Review and Assessment of Current Airframe Lifting Methodologies and Tools in Air Vehicles Division

W. Hu, Y.C. Tong, K.F. Walker, D. Mongru, R. Amaratunga and P. Jackson

Air Vehicles Division
Defence Science and Technology Organisation

DSTO-RR-0321

ABSTRACT

The Air Vehicles Division of Defence Science and Technology Organisation (DSTO) owns and/or uses a large number of software tools for crack-initiation and crack-growth analyses of aircraft structures. These tools represent a substantial body of knowledge of fatigue and fracture of engineering materials and structures that has been created and accumulated over the years. This report presents a review and assessment of the methods underpinning the more commonly-used software tools and approaches in Air Vehicles Division. The key points of the principle of each method are discussed, and different implementation considerations are highlighted, to demonstrate the similarity and difference between the models. A start is made on the compilation of a compendium of benchmark problems and challenging problems in order to assist the evaluation and consistent validation of existing and newly-developed tools. The objectives of the review are to help to increase the responsiveness and robustness of the advice DSTO provides to its clients by identifying the strengths and limitations of the commonly-used methods and tools; identifying and recommending software platforms for future improvement, and horizon-scanning the field of fatigue and fracture for new and emerging methodologies for aircraft structural life prediction. It is expected that the recommendations presented in this review will be addressed in follow-on work.

RELEASE LIMITATION

Approved for public release

Published by

*DSTO Defence Science and Technology Organisation
506 Lorimer St
Fishermans Bend, Victoria, 3207 Australia*

*Telephone: (03) 9626 7000
Fax: (03) 9626 7999*

*© Commonwealth of Australia 2006
AR-013-826
December 2006*

APPROVED FOR PUBLIC RELEASE

A Review and Assessment of Current Airframe Lifting Methodologies and Tools in Air Vehicles Division

Executive Summary

One of the science and technology areas of the Defence Science and Technology Organisation (DSTO) is to provide high quality advice to the Royal Australian Air Force (RAAF) on the management of structural integrity of aircraft over a range of fleets, to reduce the cost of ownership and to increase the readiness of the RAAF fleet. Currently, the structural integrity of Australian Defence Force aircraft is managed in part according to the design philosophies of the original equipment manufacturers (OEMs), which invariably involve both fatigue life and crack-growth-based analyses and supporting tests. DSTO's fatigue lifting analyses and crack-growth-based Durability and Damage Tolerance Analyses (DADTAs) are often performed using the software tools provided by the OEMs. In some cases, generic codes sourced commercially or as freeware/shareware, or locally-developed codes and methodologies are also used. Consequently, DSTO uses, owns and maintains a number of platform-specific software tools based on a number of different methodologies and philosophies. The difference between each set of tools could be substantial or minor, but the use and maintenance of a series of tools with similar capabilities not only increases the cost in skill retention and transfer, but also requires the maintenance of consistent but different material databases for the same material. It is, therefore, highly desirable to review and assess the software tools used in DSTO. The objective of this report, the first from the newly formed "Methods Group" within Structures Branch of Air Vehicles Division, is to identify the advantages, disadvantages and limitations of each software tool in order to fully understand and utilise its strengths whilst compensating for any limitations, to identify and recommend software platforms for future incremental improvement, and to horizon-scan the field for new and emerging methodologies for aircraft structural life prediction. The report will also allow both customers and DSTO researchers to discuss and plan follow-on review and development activities on the basis of a consistent and firm understanding of the underlying theories of fatigue and the attributes of the existing DSTO software tools. The report also commences the task of compiling a list of benchmark problems that are currently successfully modelled by a specific tool, as well as challenging problems that cannot be reasonably modelled, with the aim of providing a database for the verification and validation of future development of lifting tools. The work presented in this report will enable DSTO to continue to provide responsive advice to its clients on aircraft structural integrity with the most accurate methods and tools available, whilst improving the efficiency of its data management and analysis processes.

Authors

W. Hu

Air Vehicles Division

Weiping Hu joined DSTO in 1998 as a research scientist. He is currently a senior research scientist leading the development of modelling capabilities for the analysis of structural integrity of aircraft structures.

After obtaining his PhD degree in 1993 at Dublin City University, Ireland, he held various academic positions at Dublin City University, Monash University and Deakin University. His current research interests include fatigue and fracture of engineering materials and structures, fatigue crack growth in aircraft structures, constitutive models and plasticity, and numerical methods in engineering.

Y.C. Tong

Air Vehicles Division

Mr Chee Tong is a research engineer in the Air Vehicles Division of DSTO. He joined AVD-DSTO in 1999 after graduating from the Royal Melbourne Institute of Technology with a Bachelor Degree in Aerospace Engineering with honours. He is currently undertaking his Ph.D. study with the University of Sydney and support from AVD-DSTO focusing in the area of statistical and probabilistic fracture mechanics and fatigue life assessment. Since joining DSTO in 1999, Mr Tong has worked in the fields of structural risk and reliability, propulsion systems life management, and fatigue crack growth modelling and fracture research.

K.F. Walker

Air Vehicles Division

Mr Walker graduated in 1983 with a Bachelor of Aeronautical Engineering (with distinction) from RMIT. He then served for eight years with the RAAF, including a posting to the USA where he gained a Masters of Science in Aeronautics and Astronautics from Purdue University. He then worked for three years in private industry before joining DSTO AVD in early 1994. His work at DSTO has included fatigue crack growth and damage tolerance analysis studies (mainly related to the F-111 aircraft), fatigue monitoring systems, development, design, validation and substantiation of bonded composite repairs, and development of improved fatigue crack growth analysis software. He is currently the lead structures engineer for surveillance aircraft including the P3 Maritime Patrol and the Boeing 737 based AEW&C aircraft.

D. Mongru

Air Vehicles Division

Mr Mongru graduated from RMIT in 1990 with a Bachelor of Aerospace Engineering (Honours). He commenced work at DSTO in 1994 working on loads development and fatigue interpretation for the PC9 fatigue test. He joined IFOSTP in 1996 performing fatigue analysis of critical components on the aft fuselage of the F/A-18. In 2001 he commenced work on the P-3 SLAP. His primary functions included fatigue test interpretation and provision of technical support to the P-3 empennage test. He is currently working on the standards and lifing methodologies task.

R. Amaratunga

Air Vehicles Division

Mr Amaratunga graduated in 1997 with a Bachelor of Engineering (Aeronautical) from the University of Sydney. Since commencing employment at the then Aeronautical and Maritime Research Laboratory in 1998, Mr Amaratunga has worked in the fields of aircraft structural integrity, risk and reliability assessment of fixed wing aircraft, and Air6000 cost and capability. Mr Amaratunga's experience ranges from repair design, probabilistic assessment of aircraft, to configuration comparison between high performance fighter aircraft. Mr Amaratunga is currently working in the Structural Life Assessment task.

P. Jackson

Air Vehicles Division

Philip Jackson graduated from the Royal Melbourne Institute of Technology in 1981 with a Bachelor of Aeronautical Engineering (with Distinction). He spent the next 15 years as an engineering officer with the Royal Australian Air Force in both squadron and staff engineering posts specialising in aircraft structural integrity and fatigue management. In 1988 he completed a Masters of Science in Aerospace Vehicle Design at Cranfield Institute of Technology, UK and from 1991-94 was attached to the Canadian National Research Council, Ottawa, Canada as part of the F/A-18 International Follow-on Structural Test Project. He joined DSTO in 1997 and has been the technical and program lead for the DSTO contributions to the international P-3 Service Life Assessment Program (SLAP). He is currently Head, Helicopter and Transport Aircraft Structural Integrity in the Aircraft Structures Branch of Air Vehicles Division as well as leading a divisional research effort on airworthiness and aircraft design standards.

Contents

1. OVERVIEW	1
1.1 Purpose and Objectives	1
1.2 The Scope of the Report.....	2
1.3 An Overview of the Development of Numerical Tools and Some Fundamentals	3
1.3.1 Fatigue Loading.....	3
1.3.2 Fatigue.....	5
1.3.3 Fatigue Life Programs at DSTO.....	6
1.3.4 Crack Growth.....	6
1.3.4.1 Pre ‘Paris’	7
1.3.4.2 Paris, Gomez and Anderson	7
1.3.5 Cycle Counting	11
1.4 Outline of the Report	12
2. APPROACHES FOR MODELLING FATIGUE LIFE	13
2.1 Stress-Based Approach	13
2.1.1 Effect of Mean Stress	14
2.1.2 Issue of the Fatigue Limit	15
2.1.3 Cycle History and Linear Damage Summation	16
2.1.4 Developing and Using ‘Working’ $S - N$ Curves.....	17
2.2 Strain-Based Approach	18
2.2.1 Cyclic Stress-Strain Behaviour at Notch Root	18
2.2.2 Strain-Life Curves.....	20
2.2.3 Equivalent Strain Equations.....	21
2.2.4 Notch Root Stress and Strain Response.....	22
2.2.5 A Generic Flowchart for Crack Initiation Life Prediction.....	24
3. SOFTWARE TOOLS FOR FATIGUE LIFE PREDICTION	26
3.1 CI89	26
3.2 FAMS.....	27
3.3 Comparison of FAMS and CI89	29
4. MODELLING OF FATIGUE CRACK GROWTH.....	30
4.1 The Fundamental Principle for Crack Growth Analysis-LEFM	30
4.2 Similitude Principle	33
4.3 Crack Growth Rate Curve and the Factors that Influence Crack Growth ...	33
4.3.1 Region I: Threshold Growth	35
4.3.2 Region II: Stable Growth	35
4.3.3 Region III Growth: Fast Fracture.....	35
4.3.4 Stress Ratio Effect	36
4.3.5 Sequence Effect, Crack Growth Acceleration and Retardation	36
4.4 Short Cracks	37
4.4.1 Experimental Evidence	37
4.4.2 Modelling Technique	38

4.5	Crack Closure Concept	39
4.5.1	Crack Opening Stress under Constant Amplitude Loading	40
4.5.2	Crack Opening Stress under Spectrum Loading	40
4.6	Constraint or Thickness Effects	40
4.6.1	Fracture Toughness	40
4.6.2	Crack Growth.....	40
5.	SOFTWARE TOOLS FOR FATIGUE CRACK GROWTH ANALYSIS	42
5.1	AFGROW	42
5.2	Broek	42
5.3	ADAMSys	42
5.4	METLIFE	43
5.5	CG90	45
5.6	FASTRAN	46
5.6.1	Crack Opening Stress under Constant Amplitude Load	49
5.6.2	Crack Opening Stress under Variable Amplitude Load	51
5.6.3	Crack Growth Rate Equation	53
5.6.4	Crack-Tip Plastic Zone	54
5.6.5	Constraint Factor α for Three-Dimensional Effect	54
5.6.6	Short Crack Model.....	54
5.7	CGAP	55
5.7.1	Cyclic Plasticity Model	56
5.7.2	Stress Distribution Ahead of a Notch Root.....	58
5.7.3	Weight Function/Green's Function Approach	60
5.8	Other Developments in Fatigue Crack Growth Modelling	63
5.8.1	Modelling Crack Growth under Spectrum Loading	63
5.8.1.1	Modelling Crack Growth by an Exponential Function	63
5.8.2	Effective Block Approach	66
5.8.3	Discussion.....	68
6.	PROBABILISTIC APPROACH	70
6.1	Statistical approach	71
6.1.1	Failure-Time Data Analysis	71
6.1.2	Failure-Time with Censored Data Analysis.....	74
6.1.3	Zero Failure Data (Weibayes) Analysis	76
6.2	Statistical Analysis Software Tools	78
6.3	Probabilistic Approach	78
6.4	Probabilistic Fatigue Life Assessment Software Tools	79
6.4.1	PROF	80
6.4.2	CGAP	81
6.5	Probabilistic Certification Requirement	82
7.	DISCUSSIONS AND COMPENDIUM OF PROBLEMS	84
7.1	Comparison of Fatigue Life Approaches	84
7.2	Challenging Issues in Modelling Fatigue Crack Growth	84
7.2.1	Short Crack Behaviour	84

7.2.2	Threshold Growth	85
7.2.3	Sequence Effect	87
7.2.4	Tensile Growth and Shear Growth	87
7.3	Limitations and Caveats for FASTRAN and CGAP.....	88
7.3.1	Negative Stress Ratio	88
7.3.2	The Geometry Factor β	88
7.3.3	The Shifting of Crack Growth Curves	89
7.4	Compendium of Problems	90
8.	RECOMMENDATIONS AND CONCLUDING REMARKS	91
8.1	Concluding Remarks.....	91
8.1.1	Fatigue Life Approaches and Tools	91
8.1.2	Crack Growth Approaches and Tools	91
8.1.3	Probabilistic Approaches.....	93
8.2	Recommendations	93
APPENDIX A	VARIOUS IMPLEMENTATIONS OF THE STRESS-LIFE METHOD AT DSTO.....	99
A.1.	ESDU S-N Algorithm	99
A.2.	PC-9 Minsum Algorithm.....	100
A.3.	P-3 SLMP Algorithm.....	100
A.4.	Modified Goodman Algorithm	101
A.5.	Case Study	102
APPENDIX B	BENCHMARK PROBLEMS FOR FATIGUE LIFE ANALYSIS	105
B.1.	Benchmark Problems for Constant Amplitude Loading.....	105
B.2.	Benchmark Problems for Spectra Loading	107
APPENDIX C	CHALLENGING PROBLEMS FOR FATIGUE LIFE ANALYSIS.	111
C.1.	Challenging Problems for Constant Amplitude Loading.....	111
C.2.	Challenging Problems for Spectra Loading	113
APPENDIX D	BENCHMARK PROBLEMS FOR FATIGUE CRACK GROWTH ANALYSIS	121
D.1.	Mirage Spectrum Loading Example	121
D.2.	F-111 Wing Pivot Fitting Lower Plate Cracking Example.....	126
D.3.	F-111 Horizontal Tail Pivot Shaft Example	131
D.4.	F-111 Wing Pivot Fitting Upper Plate Fuel Flow Vent Hole Example	133

List of Abbreviations

ADF	Australian Defence Force
APOL	Australian post-LEX (spectrum)
ASTM	The American Society for Testing and Materials
AVD	Air Vehicles Division
CCT	Central-crack tensile
cdf	Cumulative distribution function
CF	Canadian Forces
DADTA	Durability and damage tolerance analysis
CPLT	Cold proof load test
DBI/SST	Database Interface / Spectra Sequencing Tool
DSTO	Defence Science and Technology Organisation
EBA	Effective block approach; or effective block approach
EDM	Electrical discharge machining
EIFS	Equivalent initial flaw sizes
ERFS	Equivalent repair flaw sizes
FCA	Fatigue critical area
FFVH	Fuel flow vent hole
FSFT	Full-scale fatigue test
hf	Hazard function
HCF	High cycle fatigue
IFOSTP	International Follow-On Structural Test Project
LCF	Low cycle fatigue
LEFM	Linear elastic fracture mechanics
MCS	Monte Carlo simulation
MIPS	Millions of inch pounds
NAWC	Naval Air Warfare Centre (US)
NLR	National Aerospace Laboratory (the Netherlands)
OEM	Original equipment manufacturer
pdf	Probability density function
RAAF	Royal Australian Air Force
SBI	Safety by inspection
sf	Survival function
SIF	Stress intensity factor
SLAP	Service Life Assessment Program
SLMP	Service Life Monitoring Program
SLEP	Service Life Evaluation Program
USN	United States Navy
WPBM	Wing pivot bending moment
WPF	Wing pivot fitting

Nomenclature

a	Crack depth, or half depth for a symmetric crack.
a_i	Initial crack depth or half depth for a symmetric crack.
b'	Fatigue strength exponent.
c	Crack length, or half length for a symmetric crack.
c'	Fatigue ductility exponent.
c_0	A material constant which represents a small crack size: $c_0 \approx \frac{1}{\pi} \left(\frac{\Delta K_0}{\Delta \sigma_e} \right)^2$.
c_i	Initial crack length, or half length for a symmetric crack.
c_f	Final crack length, or half length for a symmetric crack.
C	Crack growth rate coefficient in Paris law.
C_5	Cyclic fracture toughness.
e	Remote strain.
E	Modulus of elasticity.
$f(x_i)$	Influence function, representing the displacement caused at point i by a unit external stress.
f_p	Probabilistic density function.
F	Cumulative distribution function of probability.
$g(x_i, x_j)$	Influence function, representing the displacement caused at point i by a unit internal stress acting at point j .
G	Threshold function, $G = 1 - (\Delta K_0 / \Delta K_{\text{eff}})^p$.
h	Hazard function.
H	Fracture function, $H = 1 - (K_{\text{max}} / C_5)^q$.
L_i	The length of element i .
m	Crack growth rate exponent in Paris law.
n'	Material constant in Romberg-Osgood equation.
N	Number of cycles.
N_e	Number of strip elements in FASTRAN or CGAP.
N_f	Fatigue life; the number of cycles to fatigue failure.
K	Stress intensity factor.
K'	Material constant in Romberg-Osgood equation.
K_C	Fracture toughness.
K_{IC}	Plane strain fracture toughness.
K_{max}	Maximum stress intensity factor.
K_{open}	crack opening stress intensity factor
K_t	Theoretical stress concentration factor.
K_ε	Actual strain concentration factor, $K_\varepsilon = \varepsilon / e$.
K_σ	Actual stress concentration factor, $K_\sigma = \sigma / S$.
ΔK	Stress intensity factor range.
ΔK_0	Long crack threshold. It is considered to be a material constant, and in particular, independent of crack length.

ΔK_{eff}	Effective stress intensity range.
ΔK_{th}	Threshold stress intensity factor range below which there is no crack growth. For long cracks, $\Delta K_{\text{th}} = \Delta K_0$ and for short cracks, ΔK_{th} decreases with decreasing crack length.
R	Stress ratio of a load cycle, $R_s = S_{\min} / S_{\max}$.
S	Applied remote stress.
S_a	Amplitude or alternating stress of a load cycle.
ΔS_{eff}	Effective stress range, $\Delta S_{\text{eff}} = S_{\max} - S_{\text{open}}$
S_{\max}	The maximum stress in a load cycle.
S_{mean}	The mean stress of a load cycle.
S_{\min}	The minimum stress in a load cycle.
S_N	(Hypothetical) notch elastic stress.
S_o	Crack opening stress.
S_p	Survival function.
S_{peak}	The maximum stress in a load spectrum.
ΔS	Applied stress range. $\Delta S = S_{\max} - S_{\min}$.
V_i	The current crack surface displacement at element i .
w	Specimen width or half width for symmetric crack.
$W(x)$	Green's function or weight function for stress intensity factor calculation.
β	Geometry correction factor, which is a function of crack size and component geometry.
β_L	A constant in the log-linear approach.
ε	Local strain.
$\Delta \varepsilon$	Local total strain range.
ε_a	Local strain amplitude.
$\varepsilon_e, \varepsilon_p$	Local elastic and plastic strain, respectively.
$\Delta \varepsilon_e, \Delta \varepsilon_p$	Local elastic and plastic strain range, respectively.
ε_f'	Fatigue ductility coefficient.
ε_{\max}	Local maximum strain.
$\varepsilon_{\text{mean}}$	Local mean strain.
ε_{\min}	Local minimum strain.
ρ	Plastic zone size.
σ	Local stress.
σ_0	Averaged flow stress, $\sigma_0 = (\sigma_y + \sigma_u) / 2$.
$\Delta \sigma_e$	Endurance limit.
σ_{cy}	Cyclic yield stress of material.
σ_f'	Fatigue strength coefficient.
σ_i	Stress in element i .
σ_{\max}	Local maximum stress.

σ_{mean}	Local mean stress.
σ_{min}	Local minimum stress.
σ_u	Ultimate stress of material.
σ_y	Uniaxial yield stress of material.
$\sigma_{yy}(x)$	Distributed stress, perpendicular to the crack plane, at point x .
ω	Dugdale cyclic plastic zone size.

List of Tables

<i>Table 1 Examples of equivalent strain equations implemented in CI89 and FAMS (Shah 2004).....</i>	<i>22</i>
<i>Table 2 Comparison of FAMS and CI89.....</i>	<i>29</i>
<i>Table 3 Examples of some typical probabilistic requirements assigned for certification of aerospace structures and components</i>	<i>82</i>
<i>Table 4 Summary of tools for fatigue life analysis: input, output and capabilities.....</i>	<i>95</i>
<i>Table 5 Summary of tools for crack growth analysis: input, output and capabilities.....</i>	<i>96</i>
<i>Table 6 Analysis Results from Algorithm Comparison Case Study for FCA301</i>	<i>103</i>
<i>Table 7 Test Matrix for the Spectrum Analysis Coupons</i>	<i>109</i>
<i>Table 8 Coupon Test Program.....</i>	<i>113</i>
<i>Table 9 F-111 Sequences used for Coupon Test</i>	<i>114</i>
<i>Table 10 Experimental and numerical total fatigue lives for the coupon with a gross stress concentration factor of $K_t = 3.24$ subjected to constant amplitude loading.....</i>	<i>116</i>
<i>Table 11 Experimental and numerical total fatigue lives for the coupon with a gross stress concentration factor of $K_t = 5.00$ subjected to constant amplitude loading.....</i>	<i>116</i>
<i>Table 12 Experimental and numerical total fatigue lives for the coupon with a gross stress concentration factor of $K_t = 1.00$ subjected to constant amplitude loading</i>	<i>117</i>
<i>Table 13 Coupon Test Results for F/A-18 APOL Spectrum</i>	<i>117</i>
<i>Table 14 Spectrum Analysis results for FCA301</i>	<i>117</i>
<i>Table 15 Spectrum Analysis results for FCA361</i>	<i>118</i>
<i>Table 16 Low Load Transfer Coupon Test results.....</i>	<i>118</i>
<i>Table 17 Total Life recorded for the FASS 226 Fatigue Life Coupons.....</i>	<i>118</i>
<i>Table 18 Coupon Test Results for F/A-18 FT55 Spectrum. Stress Level: 57.5 ksi</i>	<i>119</i>
<i>Table 19 Flight segment spectra</i>	<i>124</i>
<i>Table 20 Sequence of flight segments in a block representing 100 flights, 66.6 hours (1989 cycles)</i>	<i>124</i>
<i>Table 21 A-4 Right Hand Wing Fatigue Test Blocked Spectrum</i>	<i>128</i>

List of Figures

Figure 1 Constant amplitude cyclic loading	4
Figure 2 Fracture process zone, plastic zone and K-dominated zone	9
Figure 3 A schematic of a stress-life ($S - N$) curves and the effect of mean stress on fatigue life. S_a is the alternating stress, and N_f is the number of cycles to failure.....	14
Figure 4 Low cycle and high cycle fatigue.....	15
Figure 5 Transient and stead-state cyclic elastic-plastic stress-strain response at a notch root	19
Figure 6 Cyclic stress-strain response of aluminium 7050 under strain-controlled test, demonstrating the gradual relaxation of mean stress (Hu and Wang 2000)	20
Figure 7 Schematic of strain-life curve.....	21
Figure 8 A graphical illustration of Neuber's rule and the equivalent strain energy method	24
Figure 9 A generic flow chart for strain-based fatigue life analysis program.....	25
Figure 10 Schematic illustration of da/dN versus ΔK curve. The crack growth may be divided into three regions; the threshold region, the stable growth region and fast fracture region. The growth rates in these regions are influenced, to different extent, by the microstructure, mean stress, thickness and environment. Adapted from (Ritchie 1979).....	32
Figure 11 Crack growth curves predicted using Paris law, illustrating the effect of different parameters on crack growth.....	34
Figure 12 Fatigue crack growth rate for 7050-T7451 aluminium alloy tested at a variety of R ratio values correlated on ΔK (compiled from (Sharp, Byrnes and Clark 1998))	37
Figure 13 Illustration of typical long and short crack growth rates as a function of stress intensity factor range, under constant amplitude loading. Short cracks grow at ΔK below the threshold value. They may either develop into long cracks or arrest. Short cracks emanating from notches usually develop into long cracks (adapted from (Suresh and Ritchie 1984)).	39
Figure 14 A flow chart for fatigue crack growth analysis using the plasticity-induced crack closure model.....	48
Figure 15 Normalised crack opening stress under constant amplitude loading and simulated plane stress condition.($\alpha = 1$).....	50
Figure 16 Normalised crack opening stress under constant amplitude loading and simulated plane strain condition.($\alpha = 3$).....	50
Figure 17 The influence of constraint factor on crack-opening stress. $S_{\max} / \sigma_0 = 0.4$	51
Figure 18 Schematic of loading and coordinate system for the analytical plasticity-induced crack closure model (after Newman 1981a)	53
Figure 19 The determination of material constants for the cyclic plasticity model. A single back stress is only suitable for modelling a small strain range.....	58
Figure 20 A plate component containing a generic notch subjected to remote tensile loading	59
Figure 21 The cold proof load sequence applied to Damage Item 36 (DI36) coupon.....	59
Figure 22 Cyclic stress-strain response under CPLT sequence shown in Figure 21	60

Figure 23 Crack growth curves for a single through-thickness crack emanating from the edge of a central hole in a plate subjected to constant amplitude loading	62
Figure 24 Crack growth curves for a single through-thickness crack emanating from the edge of a central hole in a plate subjected to CPLT sequence and four blocks of service spectrum, each block representing 500 flight hours	63
Figure 25 Experimental fatigue crack growth curves for 7050-T7451 aluminium alloy specimens subjected to IARPO3a + marker load spectrum, crack depth a versus blocks of spectrum loading	64
Figure 26 The dependence of β_L on the peak stress of the spectrum, according to Equation (36). $A_L = 10^{-8.404}$, $q_L = 3.028$	65
Figure 27 Fatigue test data for various peak stress factors correlated using Equation (3)	66
Figure 28 Crack growth rate curves for 7050-T7451 aluminium alloy specimens subjected to IARPO3a + marker load spectrum.....	67
Figure 29 The collapse of the crack growth rate curves on to a single curve using Equation (39) for 7050-T7451 aluminium alloy specimens subjected to IARPO3a + marker load spectrum..	68
Figure 30 The relationship between the equivalent initial crack size and the stress level of a spectrum	69
Figure 31 Variation in fatigue life data for aluminium 7050 alloy specimens tested under a normalised fighter aircraft spectrum with various peak stress levels, life versus blocks of spectrum loading	72
Figure 32 Statistical analysis of the variation in fatigue life data shown in Figure 31 using the constant standard deviation (σ) method.....	73
Figure 33 Statistical analysis of the variation in fatigue life data shown in Figure 31 using the constant coefficient of variation (COV) method.....	74
Figure 34 Example demonstrating maximum likelihood estimate of the distributions with and without right censored data for fatigue life data shown in Figure 31 using the constant standard deviation (σ) method.....	76
Figure 35 Zero failure reliability or the Weibayes analysis example	77
Figure 36 Probability of failure is the hyper volume under the joint pdf bounded by $Y(X) \leq y$	79
Figure 37 Kitagawa diagram and the threshold stress prediction by El Haddad model. ΔK_{th} is the long crack threshold stress intensity factor range, $\Delta \sigma_e$ is the endurance limit, and F is the geometry factor.....	86
Figure 38 Normalised threshold stress intensity factor range for short cracks. ΔK_0 is the long crack threshold and is considered to be a constant (Suresh and Ritchie 1984; McClung and Feiger not dated).....	87
Figure 39 Beta factors defined against different crack measurements	89
Figure 40 Effect of shifting crack growth curves. The red, dashed line represents the crack growth curve obtained using a smaller initial crack size, and it was shifted leftward to align up with the black solid line, which was obtained using a larger initial crack size	90
Figure 41 Stress-life data for 7075-T6 (Schwarmann 1988), with cubic curve-fitting	102

<i>Figure 42 S-N algorithms & FAMS normalised fatigue lives for FCA301</i>	103
<i>Figure 43 Geometry for coupons with $K_t = 3.24$</i>	106
<i>Figure 44 Geometry for coupons with $K_t = 5.00$</i>	106
<i>Figure 45 Geometry for coupons with $K_t = 1.00$</i>	107
<i>Figure 46 Geometry for FS488 Flange Fillet Coupons</i>	108
<i>Figure 47 Geometry for Low Load Transfer Coupons</i>	112
<i>Figure 48 Fixed End Centre Crack 7075-T651 Specimen</i>	122
<i>Figure 49 Representative segments from the Unmodified and 6.5 g limit spectra</i>	123
<i>Figure 50 Representative segments from the 5 g limit and 8.5 g peak spectra</i>	123
<i>Figure 51 Experimental crack growth results for four Mirage spectra variations</i>	125
<i>Figure 52 DADTA Item 86</i>	127
<i>Figure 53 Comparison of Observed Crack Growth with Analysis</i>	129
<i>Figure 54 A-4 Right Hand Wing Fatigue Test Observed Crack Growth Compared with Analyses</i>	130
<i>Figure 55 DADTA Item 36</i>	131
<i>Figure 56 Typical Coupon Dimensions</i>	132
<i>Figure 57 DI 36 coupon crack growth test and analysis results</i>	133
<i>Figure 58 DI 92b</i>	134
<i>Figure 59 DI 92b coupon</i>	135
<i>Figure 60 DI92b coupon crack growth and analysis data</i>	136

1. Overview

1.1 Purpose and Objectives

The Defence Science and Technology Organisation's (DSTO) mission is to apply "science and technology to protect and defend Australia and its national interests" (DSTO mission statement). One of DSTO's science and technology areas is to provide high quality advice to the Australian Defence Force (ADF) on the management of the structural integrity of airframe structures in order to preserve airworthiness, reduce the cost of ownership and increase the operational effectiveness and readiness. Currently, the structural integrity of ADF aircraft is managed, in part, according to the design philosophies adopted by the original equipment manufacturers (OEMs), which invariably involve both fatigue life and crack-growth-based analyses. DSTO's lifing analyses and crack-growth-based Durability and Damage Tolerance Analyses (DADTAs) are often performed using the software tools provided by the OEMs. In some cases, generic codes sourced commercially or as freeware/shareware, or locally developed methodologies/codes are also used. Consequently, DSTO uses, owns and/or maintains a variety of platform-specific software tools based on different methodologies or design philosophies. For example, the fatigue life of F/A-18 airframe structures were analysed using CI89 (McDonnell Douglas 1991b), an OEM computer program, while similar predictions of P3-C structures are analysed using FAMS (Naval Air Warfare Center 1995). Both CI89 and FAMS are based on the strain-life approach and require essentially the same or equivalent input data, and have very similar capability in predicting fatigue lives. Similarly, quite a number of software tools are used for fatigue crack growth analyses on different platforms, such as FASTRAN (Newman 1992b) for P3-C. Sometimes several crack growth tools have been used on the same platform, e.g., AFGROW (Harter 2004), ADAMSys (Lockheed Martin not-dated), METLIFE, FASTRAN (Newman 1992a) and CGAP (Hu and Walker 2006a) for the F-111. The difference between each set of tools could be substantial. For instance, FASTRAN and CGAP are based on a plasticity-induced crack closure model, which is substantially different from the crack-growth models implemented in METLIFE. Alternatively the difference may also be minor, such as that between CI89 and FAMS which are both based on the same methodology and require essentially the same input data. The use and maintenance of many tools not only increases the cost in retaining skill sets to carry out competent analyses, but also requires the maintenance of different material databases for the same material.

In "A Strategic Plan for Fracture Research" (Rose and Preston 1999), notch-root stress-strain response and short crack growth were identified as two technical issues for improving the predictive capabilities in fatigue life and crack growth. Progress has been made on both issues within the Air Vehicles Division (AVD), with the development and implementation of an advanced notch plasticity model (Wang, Hu and Sawyer 2000), the development of an in-house software tool, CGAP (Hu and Walker 2006a), to explicitly model crack growth in the notch zone, and the development of methods for modelling short crack growth (Jones, Molent and Pitt 2006). On the other hand, due to changes in external environment, the Defence Procurement Review, DSTO Renewal and DSTO Culture change, DSTO is not only compelled to continue to provide *responsive* advice to its clients based on the best knowledge available,

but also to raise the level of rigour applied to its data management and analysis processes. In other words, DSTO not only needs to create knowledge, but also needs to manage and use knowledge effectively, in order to operate successfully in an increasingly competitive environment.

It is, therefore, highly desirable to comprehensively review and assess the methodologies and implementations of software tools used in DSTO to identify their advantages, disadvantages and limitations, in order to:

1. understand and utilise the strengths of each tool;
2. delineate between mature algorithms and capabilities under development and evaluation;
3. identify and recommend software platforms for future incremental improvement;
4. horizon-scan the field for new and emerging methodologies for aircraft structural life prediction.

This report, the first from the newly formed “Methods Group” within the Structures branch of AVD, commences this process by firstly describing some of the fundamental theories behind the current models and then reviewing the fatigue life and crack growth models in use within the Structures Branch of AVD. The report identifies where a more thorough or critical review of a specific model or methodology is still required or where additional work is needed to either improve existing tools or develop new approaches. The report also commences the process of compiling a list of benchmark problems that can be successfully modelled and some challenging problems that cannot be reasonably modelled by the current tools, in order to provide a (hopefully constantly expanding) database for the verification and validation of any future development in lifing tools.

1.2 The Scope of the Report

This report focuses on fatigue tools currently used and maintained in Structures Branch of AVD in DSTO for the prediction and assessment of fatigue life (either time to crack initiation or total life) and fatigue crack growth of aircraft structures subjected to mechanical loading. As a result, the fatigue cracks considered are all mode I cracks, as is the general case for airframes. The effect of environment on crack growth is not considered beyond its influence on the crack growth rate. Only limited mention is made of the structural fatigue testing programs carried out in DSTO, which are detailed in a recent report by Molent (2005), nor the significant work in fractography as exemplified in (Goldsmith and Clark 1990). Experimental work is only discussed in the context of model verification and validation.

As the emphasis of the report is on the methodologies rather than the operation of the software tools, no systematic comparison was made on the methods of running the software tools. For the use of the software tools covered here, the reader should refer to the corresponding user manuals for which references are provided.

Another important aspect of structural integrity, stable tearing, in which cracks could extend by millimetres under the action of a single high load, has been observed in a number of aircraft materials. Although the problem was identified as an aspect of crack modelling (Rose and Preston 1999) and some work has been carried out in AVD, the outcome is yet to be

implemented in a software tool for structural assessment. No attempt was made here to cover that topic, but the interested reader should refer to the report by Liu and Hamel et al (2005).

1.3 An Overview of the Development of Numerical Tools and Some Fundamentals

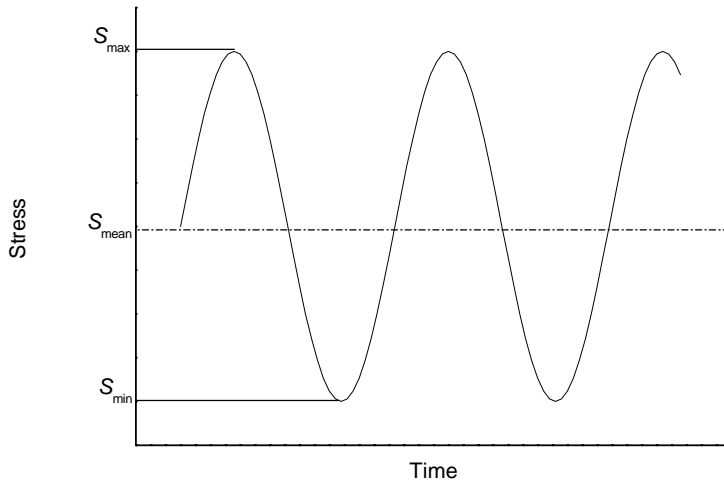
This section presents a brief review of the historical development of the methodologies to be assessed in this report and defines some of the common terms used in later sections. This is neither a comprehensive review of the physics of fatigue and fracture nor an in-depth review of the mathematical modelling of fatigue and fracture. Rather, it serves to set the context of the assessment of different approaches and tools presented in later sections. A brief but comprehensive review of the development of fatigue as an engineering discipline was given in Stephens and Fatemi et al (2001) and Schijve (2003).

1.3.1 Fatigue Loading

The loading that causes fatigue damage to engineering structures may vary in magnitude and direction, and for aircraft the variation is often random (for example gust events) or semi-random (such as flight manoeuvres). According to the variation in magnitude and direction, there can be two types of fatigue loading, constant amplitude and variable amplitude loading, described as follows:

A constant amplitude loading is uniquely specified by the maximum S_{\max} and minimum stress S_{\min} as shown in:

- (1) Figure 1. Alternatively, it may be defined by the amplitude $S_a = (S_{\max} - S_{\min})/2$ and the mean stress $S_{\text{mean}} = (S_{\max} + S_{\min})/2$; or the maximum stress S_{\max} and the stress ratio $R = S_{\min}/S_{\max}$, or a combination of any two of S_{\max} , S_{\min} , S_a , S_{mean} and R . The loading conditions experienced by rotating machinery such as turbomachinery, propellers and helicopter blades may be approximated as constant amplitude loading, but it is mainly used in laboratory tests to determine the so called stress-life ($S - N$) curves or strain-life ($\varepsilon - N$) curves or the crack growth rate curves;



Basic definitions:

$$\Delta S = S_{\max} - S_{\min}$$

$$S_a = \frac{S_{\max} - S_{\min}}{2} = \frac{\Delta S}{2}$$

$$R = \frac{S_{\min}}{S_{\max}}$$

$$S_{\text{mean}} = \frac{S_{\max} + S_{\min}}{2}$$

Figure 1 Constant amplitude cyclic loading

- (2) A variable amplitude load spectrum is defined by a series of peak-valley stress (or load) points. It can also be characterised by a spectrum-wide peak stress S_{peak} and a normalised spectrum. This can be either a repetition of blocks of constant amplitude loading with different amplitudes and mean stress, or a limited number of cycles of varying amplitudes and mean stresses, or semi- or completely random stress sequences. The latter cases are usually known as spectrum loading. Block loading is principally designed to study the effect of loading sequence on fatigue damage of material, such as the damage accumulation law, crack growth retardation and acceleration, while the load sequences encountered in airframes are semi-random. Complicating this definition, however, is that a sequence of load points, whether random or semi-random, destined to be applied repeatedly to a fatigue test specimen is often referred to as a 'block' of loading.

Spectrum loading is by far a more realistic representation of the actual loading condition on machinery in general and on aircraft structures in particular. In the analysis of fatigue lives of airframes, spectrum loading sequences may be obtained from the recordings of the strain gauges attached to aircraft structures, or based on recorded parametric data. The load sequence at a particular selected critical location is then obtained by applying appropriate conversion factors, and they represent the loading conditions experienced by the aircraft structure during taxiing, take-off, manoeuvring, landing, etc. A load spectrum is essentially defined by a sequence of stress points of peak-valley or valley-peak pairs, and may be characterised by the maximum spectrum stress S_{peak} and a sequence normalised by S_{peak} , when $S_{\text{peak}} > 0$.

For constant amplitude loading, a cycle is clearly defined by the sequence $S_{\max} - S_{\min} - S_{\max}$, or $S_{\min} - S_{\max} - S_{\min}$, when the ending stress coincides with starting stress. For variable amplitude loading, the concept of cycle is not that clear. Consequently, a number of cycle

counting methods were devised to identify complete cycles and half cycles based the concept of hysteresis loops, such as the widely used rain flow counting and range pair counting.

1.3.2 Fatigue

Earlier studies on fatigue aimed at avoiding failure altogether. It was noted that under fully reversed cyclic loading the number of cycles that could be endured by a bar under periodic bending depends more on the range of the bending stress than the maximum stress. By varying the amplitude of the fully-reversed cyclic loading, a curve of stress amplitude versus the number of cycles to failure could be plotted. This is commonly known as the *S – N curve*, which is normally represented in a linear axis for stress amplitude and a logarithmic axis for the number of cycles. The highest stress range that does not cause fatigue failure, hence giving an infinite fatigue life, is known as the *fatigue limit*, but for practical reasons, “does not cause fatigue failure” is normally interpreted as enduring a large number of cycles such as one million or ten million, i.e., 10^6 or 10^7 cycles. The fatigue limit thus defined is often referred to as the *endurance limit*. It should be noted that the life includes crack nucleation, growth and final fracture, and the curve is based on median lives or fifty percent survival, according to ASTM standard (ASTM 2000).

For a component or specimen of a given material subjected to a specified loading spectrum, the fatigue life is estimated by first forming cycles from the loading spectrum. The *S – N curve* is then used as a look-up table to determine the amount of damage caused by each specific cycle. Finally, the damage incurred by each cycle is summed up according to a predetermined rule to assess whether the component has failed. This method is known as the stress-life approach. The most commonly used damage accumulation law is the so called Miner’s rule (Miner 1945), which treats the damage from each cycle independently, i.e.

$$D = \sum \frac{n_i}{N_i}$$

where n_i is the number of repeated cycles for the current stress level, and N_i is the number of cycles to failure at the same stress level. $D = 1$ indicates failure. Miner’s rule was originated in 1923 (Palmgren 1923), and is still the most widely used damage accumulation law in spite of its deficiencies discussed below.

From the early days it was realised that in many cases failures occurred when the accumulated damage according to Miner’s rule was either less than or greater than one. Reasons for this include the effects of material surface condition, inaccuracies in the estimation of local stresses or the existence of contributing mechanisms such as fretting. Once these are dealt with, however, the basic technical issues involved in the modelling of fatigue life include accounting for the *mean stress effect*, *notch effect* and *sequence effect*. Whilst the principal driving force for fatigue damage is the amplitude of the alternating stress, the mean stress also has a significant effect. As illustrated in Figure 3, a tensile mean stress tends to shorten the fatigue life and a compressive mean stress tends to lengthen the fatigue life. Sufficient experimental data have been generated to show this effect and in analyses the mean stress effect is normally accounted for using models such as the Goodman equation (for more details see Section 2.1). The effect of a notch on the fatigue life of a component is non-linear with the stress concentration factor K_t , and in the stress-life approach the effect is generally covered by the

generation and use of $S - N$ curves for a variety of notch configurations. Significant amounts of data have been developed and published world-wide for combinations of material and notch types, including joints and fastener systems.

For notched components, local plasticity may occur under service load, particularly for fighter type aircraft where structural stresses are high and design service lives are short. In this case, it has often been found that the predictions based on a *strain-life* ($\epsilon - N$) approach gives a better correlation to experimental data than the stress-life approach. The strain life approach uses notch or 'local' strain derived from the remote stresses and the notch geometry, together with relationships such as Neuber's rule (Neuber 1961). In this way the cyclic history of local strain, related intuitively to the amount of irreversible work done to the material, is the key driver. The fatigue life of a notched part is related to the life of a small smooth specimen that is cycled to the same strains as the material at the notch root. Once again Miner's rule is the most widely used damage accumulation law.

The strain-life approach is superior to the stress-life approach when there is notch plasticity and it is in principle identical to the stress-life approach when there is no notch plasticity. Another advantage of the strain life approach is that coupon test data at different notch configurations is not needed. A Neuber notch concentration factor, K_n , is instead calculated for each application. Coupon data are most often recorded for failure of the specimen but sometimes the time or cycles to crack 'initiation' data are collected as well.

1.3.3 Fatigue Life Programs at DSTO

Fatigue life tools used by DSTO up to the mid-1980s were invariably based on the stress-life approach. These computer programs were based on the early hand-calculations and tables, and included cycle counting routines. Several of these are still available and are briefly discussed in Section 2. With the introduction of the F/A-18 came the strain-life method and tools in use at the time by McDonnell Douglas, St Louis and Northrop. These tools generally (but not always) use coupon data of life to 'crack initiation', where crack initiation was defined as the time to develop a small crack, say 0.010 inches or a fraction of the notch radius, ρ . This is different to the usual definition of fatigue life which implies the combination of both a crack initiation and a crack growth component. Currently, the two commonly used strain-based programs at DSTO are CI89 by McDonnell Douglas (McDonnell Douglas 1991b) used on F/A-18 work and FAMS by the US Naval Air Warfare Centre (NAWC) used on the P-3 Service Life Assessment Program (SLAP).

1.3.4 Crack Growth

According to the structural integrity management philosophy of damage tolerance, flaws are assumed to exist in structures on day one in service. These flaws could be caused by the manufacturing process, or the handling process. The objective of crack growth modelling is, then, to predict how these flaws behave under the applied cyclic load and the service environment. Depending on the level of load and the geometry of the structure, some flaws may remain dormant during the whole service life; others may develop into micro-cracks. Some of the micro-cracks may cease to propagate after in initial growth phase, while others may continue to grow slowly to develop into macro cracks. When the macro-cracks reach a certain critical size, catastrophic fracture follows. The purpose of a crack growth analysis is

then to predict the growth behaviour of the fastest growing crack so that an inspection interval or life can be established to avoid the crack reaching the critical size unchecked.

1.3.4.1 *Pre 'Paris'*

In 1957 Frost and Dugdale (1958) measured cracks growing from a small (typically 0.15 in) central slit in thin (typically 0.080 in) sheets of mild steel, aluminium and copper, subjected to various constant amplitude loading with $R > 0$. The work by Irwin (1957) on the analysis of a stress field around the tip of a crack was not known to Frost and Dugdale, although they did know from earlier work by Weibull and from Timoshenko and Goodier that there was an effect on the stresses at a central crack from the finite width of a sheet (effects included in the geometry correction factor β for the later stress intensity based models). As any theory to account for this was not yet satisfactory, they avoided the problem by only studying cracks up to one eighth of the width of the plate (at this point $\beta = 1.06$). They postulated that, if the material was homogeneous and through thickness stresses were not significant, i.e., crack length $l \gg t$ (they used the net crack length l instead of an operational crack length a), then geometric similitude suggested that the stresses around a crack (and thus also the mechanism driving crack growth) are only related to the length of the crack. From this reasoning, the crack growth rate is given by

$$dl / dN = C_l l \quad (1)$$

where N is the number of cycles, C_l is a material constant. Liu derived the same relationship through logical deduction and dimensional analysis, but noted more stringent conditions, e.g., plane strain (Liu 1991). The integration of the above rate equation yields

$$l = l_0 \exp(C_l N)$$

or

$$\log l = \log l_0 + C_l N$$

which gives a log-linear relationship between the net crack length and the number of cycles. For the crack lengths studied, this is indeed what Frost and Dugdale found earlier (Frost and Dugdale 1958).

It is worth noting that the Frost and Dugdale original hypothesis and their results were limited to a special condition where β is constant and the through thickness crack length is much greater than the thickness. Their hypothesis and results were not related at all to small cracks ($l \ll t$) where the through thickness stress variations are present and β varies with crack length.

1.3.4.2 *Paris, Gomez and Anderson*

The stress field around the tip of a crack of arbitrary size and subjected to arbitrary mode I tension, bending or both, may be analysed using the theory of elasticity, e.g., Broek (1986). Near the crack tip and along the crack plane the stress normal to the crack path is given by

$$\sigma_{yy} = \frac{K}{\sqrt{2\pi x}}, \quad (2)$$

where x is the distance measured from the crack tip along the crack plane, and K is the mode I stress intensity factor. As the stress at the crack tip should be proportional to the applied

stress S , from Equation (2) we have $K \propto S$. Similarly, for a through crack of length $2a$ in an infinite plate, the stress intensity factor should be proportional to the only length parameter, a . Detailed analysis (e.g., Anderson 1995, p. 111) gives

$$K = S\sqrt{\pi a}$$

for this particular problem. It is customary to express the stress intensity factor for other crack problems in the following format

$$K = S\beta\sqrt{\pi a},$$

where β is a factor to account for the effect of finite geometry and the crack length.

For fatigue crack growth, Liu recognised that the factor $\Delta S\sqrt{a}$ determines the crack growth rate (Liu 1963; Liu 1991). Paris and Erdogan proposed the now well-known Paris law which relates the fatigue crack growth rate to stress intensity range (Paris and Erdogan 1963)

$$\frac{da}{dN} = C\Delta K^m.$$

This relation was developed based on the experimental evidence obtained under long crack, constant amplitude tests and it only applies in region II or 'Paris region'. More discussion about region I, II and III growth will be presented in Section 4.3 on p. 33.

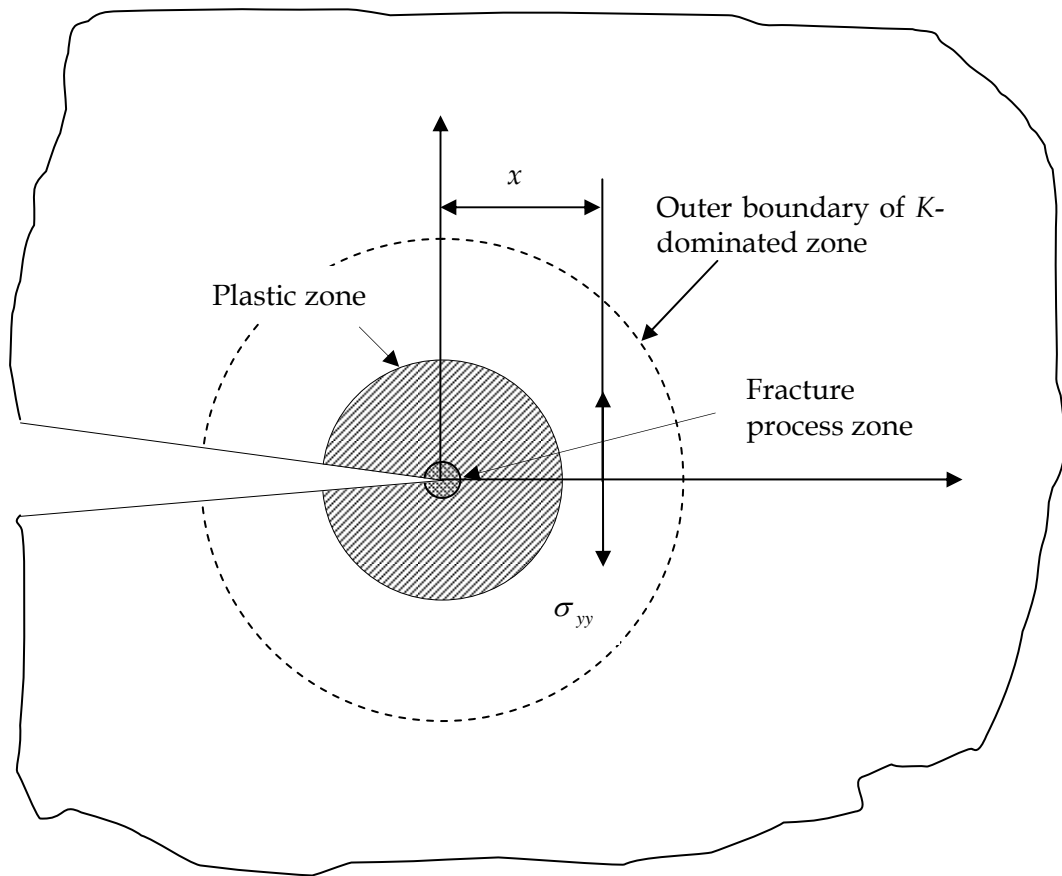


Figure 2 Fracture process zone, plastic zone and K -dominated zone

It should be noted that the equation for stress σ_{yy} is only applicable to a small region in the vicinity of the crack tip, in an area often referred to as the K -dominated zone as shown in Figure 2. The plastic zone at the crack tip resides inside the K -dominated zone and is much smaller than it. This condition is known as small scale yielding. K (and ΔK) is thus an averaged global description of the intensity of the activities occurring near the crack tip, and it is not a mechanistic variable. As a result, the use of ΔK to characterise the crack growth rate does lead to complications when we try to plot practical experimental data of da/dN versus ΔK . Examples are:

- Thickness effect. The thickness of the part in which the crack is growing affects the stress state in the material (plane stress for thin material through to plane strain for thick material) and thus affects the size of the plastic zone at the crack tip. If the size of the plastic zone is somehow related to the crack growth then different rates will be measured for different thicknesses. This is indeed what is observed.
- Short crack effect. The stress state for short cracks (typically non-through the thickness cracks such as corner flaws or semi circular flaws) is more likely to be closer to plane strain than plane stress. Geometry factors may be difficult to determine and/or may not be unique for each flaw shape. In addition, for very small cracks, the underlying

assumptions for continuum mechanics is no longer valid, and the concept of stress intensity factor does not capture the influence of the microstructure features such as grain size and boundaries on the fracture process.

- c. The environmental effect. The effect of adverse environments on crack growth is well known and extensive data exists. It is also known that crack growth rates in a vacuum (taken either from tests in a vacuum or from cracks internal to a specimen) are lower than growth rates in normal air, implying that a chemical interaction process is taking place at the tip of the crack.

As well as the above complications, the same basic technical issues that affect fatigue life calculations also affect crack growth calculations; namely the mean stress effect, the notch effect and the sequence effect. These complications are discussed further in Section 3.

The modelling methodologies for fatigue crack growth discussed in this report are all empirical in the sense that the crack growth rates are obtained by performing fatigue crack growth tests rather than derived from first principles or relating to fundamental material properties. Linear elastic fracture mechanics (LEFM) is the basis of all the existing classical crack growth software tools used in AVD. It is implicitly accepted in these codes that two cracks of different lengths subjected to the same stress intensity factor (SIF) range, ΔK (or ΔK_{eff} when crack closure is modelled), will grow at the same rate, hence SIF range is considered a unique parameter for correlating crack growth rate. This principle, known as *the principle of similitude*, applies in the slow, stable growth stage, and it is known to break down in the short crack regime (Suresh and Ritchie 1984) where the crack length is either comparable to the size of the micro structures, or it is comparable to the crack tip plastic zone size.

The DADTA of the F111 initially used METLIFE, a fatigue crack growth program developed by Ball from Lockheed Martin (Ball 2005a), for certain locations. It uses variations of the Paris law (Paris and Erdogan 1963) to describe the crack growth rate. The effect of stress ratio was taken into consideration by using the Walker or Forman equations, or a tabular look-up procedure. The sequence effect, the effect of overload and underload were taken into consideration by adopting models based on crack tip residual plastic zone size, such as Wheeler's (1970) and Willenborg models (Willenborg, Engle and Wood 1971). One of the advantages of METLIFE is that it provides a set of Green's function solution for a variety of crack configurations. A special feature of METLIFE is that it attempted to model crack growth in a notch plastic zone. The local stress-strain response was determined using Neuber's rule and a kinematic hardening constitutive equation of Ziegler-type (Ball 1990), and the stress intensity factor was obtained using the Green's function approach. Unfortunately, a numerical error in the implementation, as documented in Swanton (2005), has hindered the timely assessment of this feature.

FASTRAN, a crack growth program based on Elber's plasticity-induced crack closure model (Elber 1971) and developed by Newman at NASA (1992a), has been used at DSTO on different platforms. The crack opening stress was used as a means to account for the observed stress ratio effect, and the load sequence effect such as retardation and acceleration following an overload or underload. FASTRAN version 3.8 was subsequently selected by US Navy as the

tool for fatigue crack growth life estimation for P3-C, and at DSTO it has been made available under the graphical user interface of CGAP (Hu and Walker 2006a).

To overcome the numerical difficulties encountered in METLIFE (Swanton 2005), to make use of a more advanced cyclic plasticity model (Hu, Wang and Barter 1999) and to exploit the plasticity-induced crack closure model as implemented in FASTRAN (Newman 1992a), a Windows-based crack growth analysis program, CGAP, was developed at DSTO (Hu and Walker 2004; Hu and Walker 2006b).

In addition, AVD also uses other crack growth programs such as AFGROW, ADAMSys and CG90.

1.3.5 Cycle Counting

Although it is not explicitly stated, the concept of using crack growth data from constant amplitude testing to predict a spectrum loading case relies on the assumption that the crack growth accumulates in a manner similar to the concepts of linear cumulative damage advanced by Palmgren (1923) and Miner (1945). The crack growth calculation can be performed numerically on a cycle by cycle basis, and with modern computing equipment this is generally a feasible approach. For each cycle of loading, the increment of crack extension is readily computed and the growth of the crack is tracked in a cumulative fashion. The essential elements are:

- a. defining the “cycle”, i.e., matching a maximum and minimum load to form a pair;
- b. knowing the stress intensity range relating to the current cycle; and
- c. relating the stress intensity range to the crack growth rate.

One important difference for the crack growth modelling case compared to the fatigue life estimation case as per Palmgren/Miner is that the process is not linear. With Palmgren/Miner’s linear cumulative damage approach a cycle of given minimum and maximum (or mean and amplitude) is assumed to impart the same damage regardless of when/where it occurs. In the case of crack growth modelling, the amount of crack growth is dependent on the stress intensity range which, for a given applied load/stress range, increases with crack length. It is therefore a non-linear process. The rate is also influenced by other interaction (retardation/acceleration), constraint, and short crack effects (these are discussed elsewhere in this report).

The issue of cycle counting in the crack growth analyses context requires some discussion here. Analysis of fatigue life using the Palmgren-Miner linear cumulative damage approach has been shown to produce a more accurate result when the sequence is range pair or rain flow counted (Miner 1945). This has been explained by reference to hysteresis loop tracking, or by arguing that in fatigue, intermediate fluctuations are less important than the overall difference between high and low loads. However, when performing a crack growth analysis using a cycle by cycle approach, there seems to be little or no justification for cycle counting the spectrum using a scheme such as range pair or rain flow counting. It is sometimes done, however. In the case of the F-111 aircraft, normal practice for the manufacturer, Lockheed Martin, is to range pair count the spectrum before performing an LEFM based crack growth

analysis (Ball 1997b). The rationale is that the analysis using the range pair counted spectrum produces a more accurate result compared to the non-range pair counted spectrum. In the case of no range pair counting, cycles are still formed by simply assuming that each peak/valley is matched with the subsequent valley/peak. There does not seem to be any physical basis for the range pair counting in this case, and if the results are different, this is at odds with experimental evidence such as (Finney 1986) where very little difference was found in either total life or crack propagation life for specimens tested under range pair counted, flight by flight and randomised versions of the same spectrum. The references used by Lockheed (Ball 1997b) to justify this decision are all based around fatigue life analysis rather than crack growth analysis.

1.4 Outline of the Report

Following the introduction of this section, Section 2, "Approaches for Modelling Fatigue Life", outlines the methods for fatigue life analysis, including both the stress-life and strain-life (crack initiation) approaches. Section 3, "Software Tools for Fatigue Life Prediction", then presents a review and comparison of the software tools currently in Structures Branch for fatigue life modelling. Different methodologies and approaches for the modelling of fatigue crack growth are reviewed in Section 4, "Modelling of Fatigue Crack Growth", with detailed discussions about the issues such as short crack effects, load sequence effects, and crack closure concepts. Section 5, "Software Tools for Fatigue Crack Growth Analysis", discusses each of the software tools used within Structures Branch for crack growth analysis, with emphasis on FASTRAN (Newman 1992b) and CGAP (Hu and Walker 2006a). This section also includes an initial review of the recent developments in the modelling of crack growth under spectrum loading by Molent and Jones et al (Molent, Jones, Barter and Pitt 2006). Section 6, "Probabilistic Approach", is devoted to the review and assessment of probabilistic fatigue crack growth approaches. Appendix B through Appendix D present a list of benchmark problems and challenging problems for crack initiation and crack growth analyses, respectively. Finally, discussions of some of the difficulties in fatigue crack growth modelling are given in Section 7 "Discussions and Compendium of Problems", followed by recommendations and conclusions in Section 8.

2. Approaches for Modelling Fatigue Life

As briefly mentioned in Section 1.3.2 on p. 5, there are essentially two damage accumulation approaches to the modelling of fatigue life, the *stress-life approach* and the *strain-life approach*. The stress-life method is based on experimentally developed $S - N$ curves using constant amplitude loading on specimens with different K_t features, and is most suitable for structures subjected to moderate loading, without causing plasticity at the location of interest. The technical issues in modelling include accounting for the effects of non-zero mean stress, the effect of stress concentration and the load sequence effect, and the research efforts over the years have lead to the development of different mean stress equations and damage accumulation rules. These will be discussed in more detail in the subsequent sections. As the classical stress-life models do not account for the effect on fatigue life of notch plasticity, this effect is taken into account by selecting underlying $S - N$ data from a specimen that matches the feature being analysed. Furthermore, many material based factors may affect the characteristics of the baseline $S - N$ curve, such as the microstructure, surface finish and size of the specimen, however these are beyond the scope of the current report. More information on this topic may be found in (Stephens, Fatemi, Stephens and Fuchs 2001), for example.

The strain-life method is also based on experimentally developed $\varepsilon - N$ curves. This method was developed to deal with the observed elastic-plastic deformation at the notch root and is most appropriate for moderately notched features. The baseline $\varepsilon - N$ curves are typically generated by conducting a series of strain-controlled experiments on smooth specimens subjected to fully reversed constant amplitude loading, although notched specimens are sometimes also used. In addition to the issues encountered in the stress-life approach, the models based on the strain-life approach need to deal with the determination of the stress and strain at the notch root, from given applied load. This is usually done by using either Neuber rule or Glinka's method, together with the material stress-strain relationship; however the advantage of the strain-life approach is that, with notch plasticity being modelled, the expense of producing coupon data for different K_t features is not required.

2.1 Stress-Based Approach

The pioneering work on metal fatigue by the German engineer Wöhler established that the stress range, ΔS , rather than the maximum stress, S_{\max} , is the key factor for fatigue failure. When plotted on a log-log coordinate system, the alternating stress (also known as the stress amplitude) the fatigue life N_f has an approximate linear relationship, as illustrated in Figure 3. The baseline stress-life data, represented by the solid black line in the figure, is obtained under fully-reversed constant amplitude loading from small specimens subjected to either bending or axial loading. As the stress amplitude decreases, the fatigue life increases. Below a certain amplitude S_f the fatigue life becomes infinity ($\geq 10^6$ or 10^7 cycles in practice) and that stress amplitude is referred to as the fatigue limit of the material. Physically, the fatigue limit represents a stress range at or below which the microscopic flaws in the material does not develop into micro cracks, or, in the case of high K_t features, micro-cracks may initiate but fail to progress into the bulk of the material beyond the high K_t region.

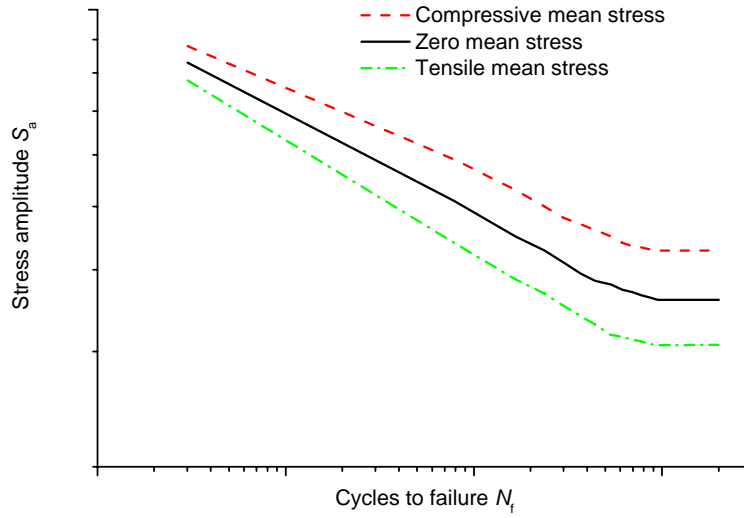


Figure 3 A schematic of a stress-life ($S - N$) curves and the effect of mean stress on fatigue life. S_a is the alternating stress, and N_f is the number of cycles to failure

2.1.1 Effect of Mean Stress

The (red) dashed line and (green) dash-dotted line in Figure 3 illustrate the effect of mean stress on fatigue life. The rule of thumb is that a tensile mean stress will reduce fatigue life and a compressive mean stress will increase fatigue life. In numerical approaches, the effect of mean stress is considered by using the modified Goodman line, the Gerber parabola, or the Morrow line (Stephens, Fatemi, Stephens and Fuchs 2001 p. 77).

ESDU data sheet 89046 provides a process for determining and applying the modified Goodman adjustment. The equation used in the approach is

$$S_{eq} = \frac{S_a}{1 - S_m / \sigma_u},$$

where S_{eq} is the equivalent amplitude at zero mean stress ($R = -1$) that is expected to generate the same damage as the non-zero mean stress cycle S_a with mean stress S_{mean} . σ_u is the ultimate tensile strength of the material.

Another approach that is claimed to produce better results (Dowling 2005) is the method of Smith, Watson and Topper (SWT),

$$S_{eq} = \sqrt{S_{max} S_a} \text{ or } S_{eq} = S_{max} \sqrt{\frac{1 - R}{2}}.$$

Alternatively, where data have been generated for a number of R ratios, the Walker equation can be used to fit the data using a parameter γ ,

$$S_{eq} = \gamma S_{\max} \sqrt{\frac{1-R}{2}}.$$

Obviously if the data at different R ratios does not condense onto one line using the Walker approach then the equation is not a valid one to use. Another typical error is to use either of the above equations for R values outside the range for which they have been either verified or originally derived. It is noteworthy that both the SWT and the Walker equations have a related form in the strain-life approach.

2.1.2 Issue of the Fatigue Limit

The earliest interests in fatigue were with the prevention of failures in machinery and so the issue of a fatigue limit was important at that time. The fatigue limit issue is also important for the rotating components in helicopters which are subject to cyclic frequencies of the order of 5 Hz. In practice, because of the time taken to conduct testing, the fatigue limit is generally defined as the alternate stress that gives a fatigue life in the range of 10^6 to 10^7 cycles. Helicopter designers (and engine designers) generally talk about low cycle fatigue (LCF) and high cycle fatigue (HCF), as illustrated in Figure 4.

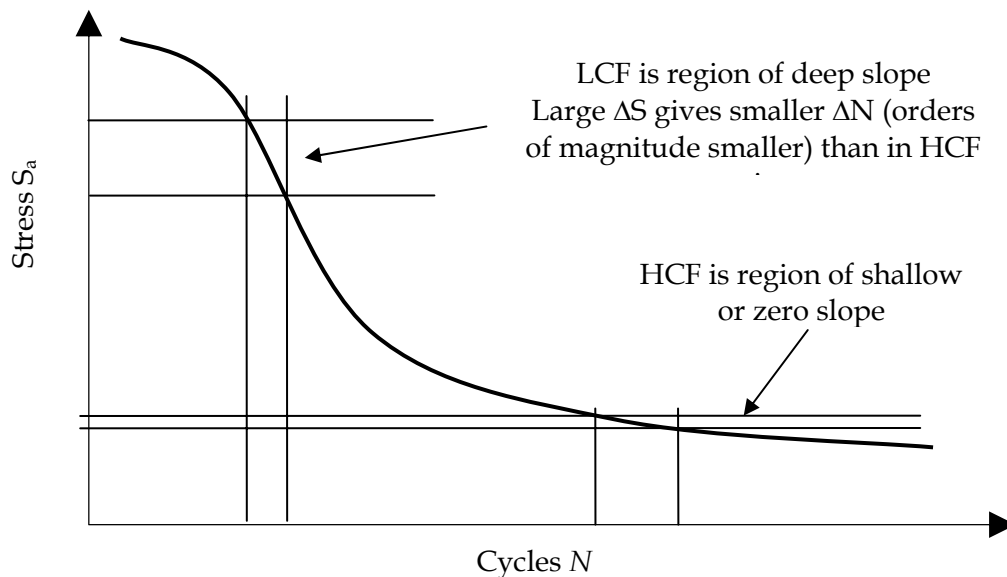


Figure 4 Low cycle and high cycle fatigue

In Figure 4, the alternating stress is plotted against the number of cycles to failure on a linear scale in Figure 4 to highlight the distinction between HCF and LCF. As shown in the figure, a small change in stress in the HCF region can lead to a large change in fatigue life. A rule-of-thumb that might be applied at the steep end of the $S - N$ curve is that for every 10% increase in stress amplitude, the fatigue life could be reduced by less than a factor of two, while at the flat end a 10% change in stress amplitude may affect the life by orders of magnitude. Thus, an approach based on determining and factoring the fatigue life using stress information may become meaningless for HCF. Uncertainties in the magnitude of the applied stress or location of the $S - N$ curve on the stress scale are thus taken into account during design by placing an adjustment on the stress level defining the fatigue limit.

A further complication arises under variable amplitude spectra. Cracks nucleated under a load that is above the fatigue limit may continue to develop during the subsequent application of cyclic load below the fatigue limit that would otherwise have not contributed to the damage had they been applied as the only loading. For this type of problem one solution has been to abandon the fatigue limit and continue the slope of the $S - N$ curve. There has been more than one suggestion about whether the slope should continue with the same value or whether another slope should be used. Either way, the approach is an empirical adjustment to get around the problem of predicting lives under variable amplitude spectra from data collected under constant amplitude tests.

2.1.3 Cycle History and Linear Damage Summation

The traditional stress-life approach is based on the linear damage summation concept and thus neglects any influence of loading history. This is both its strength and its weakness. The lack of any reliance on load history means that cycle counting methods can be simple. Indeed simple cycle counting methods were all that were possible in the time before personal computers were widely available, either because the loading data was not collected against a time base (g counters for example) or because of the limitation of hand calculations. Within a block of variable amplitude loading, the sequential pairing of the largest peaks and valleys, sometimes called the modified H1 method, is regarded as the most consistent for life prediction. With the advent of computers, the rainflow counting (or range-pair counting) method became practicable and this method is generally regarded as the one that most effectively captures the content of the damage incurred by the load sequence. This is not that surprising as the method closely replicates the hysteresis loops that are the foundation of local strain models.

By the 1960s, however, there was evidence that the order of load application affects the experimental outcome. Blocks of variable amplitude loading could be applied with an internal ordering of load amplitude from highest to lowest (Hi-Low), lowest to highest (Low-Hi), symmetrically (Low-Hi-Low) or semi randomly. Whereas the Miner's summation would produce the same numerical value for damage accumulation under these loading, coupon tests often showed different fatigue lives. Lives under Hi-Low sequences were generally the shortest, but the effect depended on the stress levels, the stress concentrator under test, the length of the variable amplitude test block and the number of times it was repeated during the test. Consequently, the non-linear effect of local yielding at a notch was considered an influence. For this reason the engineering practice for full scale fatigue tests moved from the application of loads via block loading (e.g., C130 early 1960's) to flight-by-flight replication of the load sequence (e.g., P-3A also early 1960's). Nevertheless, with the effect of load sequence implicitly included in the outcomes of properly ordered tests, a simple exceedance pairing method can still be expected to be a suitable approach for examining small changes in spectrum content within an overall usage that retains the major 'order of load' characteristics of the tested load sequence.

The inability to adequately model the retarding effect of high loads demands that caution be exercised when designing test sequences using elevated loads, in order to accelerate the testing process. Peak loads in the scaled-up sequence need to be kept below a certain level to

prevent unwanted yield at local stress concentrators, or they should be clipped at the same peak stress levels in the original load sequence.

2.1.4 Developing and Using 'Working' $S - N$ Curves

$S - N$ curves are invariably generated from the mean of the coupon data that has been collected for the purpose. However, the obvious scatter inherent in the results needs to be addressed in the pursuit of a durable and safe structure. Companies engaged in design may have processes to take into account the scatter in results by applying factors to the mean curve to make it more conservative, i.e., move the curves shown in Figure 3 to the left and/or downwards. These curves are then called 'working' curves. In the helicopter industry where the fatigue limit is of particular importance for the design of components subject to large numbers of alternating stresses, a factor on stress at the fatigue limit is also applied. Factors on life at the high end of curve can typically be 3, but they can even be as large as 10. Factors on stress may be up to 1.5. Typically, companies also have proprietary processes that enable their designers to adjust the usually limited $S - N$ data for such effects as product forms, surface effects and life enhancement processes such as interference fit fastener systems.

For the analysis of the fatigue life of aircraft components or structures that have already been designed, the usual process is to use a relevant mean $S - N$ curve and then apply factors on life to the final numerical result (called safety factors or scatter factors) to arrive at the equivalent fatigue life for a desired probability of failure. However, once again an $S - N$ curve generated from small specimens, with their generally consistent surface preparation and machining, is not likely to produce the same life as a full scale aircraft with its likely larger variation in built quality and surface preparation. This problem, as well as the effects of errors in stress estimation and the influence of non-primary stress components, are dealt with by a process of *pegging* to the full scale test result. After an $S - N$ curve is selected with a shape that reflects the stress concentrator of the feature being analysed the curve is then expanded or contracted on the vertical scale so that when the test spectrum is applied the resulting damage sum $\sum n/N$ equals one at the life achieved or demonstrated by the full scale test. It should be noted that on occasions, a $\sum n/N$ value of greater or smaller than one may be chosen to account for known or expected inaccuracies in the linear damage summation rule. In practice, the input spectrum is multiplied by a factor on stress or load. The most important step in this process is to select a curve with an appropriate shape, as the shape of the $S - N$ curves will change with the stress concentration of the feature being studied. Once the $S - N$ curve has been so pegged to the full scale test result, analysis can proceed for different spectra or for moderate changes in both stress concentration factor or working stresses. If the features under assessment are subject to local plasticity, the linear damage summation rule should be used with caution, and the departure from the conditions under which the life was pegged should be limited, as the linear summation rule cannot account for the resulting 'retardation' effect.

Def STAN 00-970 (UK Ministry of Defence 1999) advocates and defines a specific process for generating a working curve for the use in test interpretation. Called the *Safe $S - N$ method*, it defines life factors for the steep part of the $S - N$ curve and stress factors for the high cycle end, both based on the number of components in the aircraft and the desired probability of

failure, with a description on how to blend the two parts of the curve together. The result is a curve that obviates the need for the application of a fixed scatter factor at the end of the life determination process, and in fact results in a variable scatter factor vis-à-vis the life resulting from the use of the mean curve depending on the severity of the applied spectrum. The *Safe S – N* approach has been used for the latest versions of the F/A-18 test interpretation, see (Moews 2003).

Appendix A on p. 99 details four implementations of stress-life approach that have been used in the P-3 structural integrity management program and then compares the result to an equivalent strain-life analysis. Interested readers may refer to (Stephens, Fatemi, Stephens and Fuchs 2001 pp. 67-89), for further examples.

2.2 Strain-Based Approach

For notched specimens, local plasticity may occur under service loads. When this happens it is more appropriate to use the strain-life approach based on $\epsilon - N$ curves rather than the stress-life approach, as the material under consideration may undergo elastic-plastic deformation, and when this happens, local strain becomes a more sensitive parameter for fatigue damage.

2.2.1 Cyclic Stress-Strain Behaviour at Notch Root

Fatigue failures in engineering structures often occur at locations where there is a sudden change of geometry, such as notches and holes. At these locations, the local stress may exceed the yield stress due to stress concentration, even when the nominal remote stress is well below the yield stress. Under the cyclic remote load, the material at the notch root may undergo cyclic plastic deformation, and the local stress-strain response may be complex, as schematically illustrated in Figure 5. Figure 5a shows the experimental observation that the yield stress in compression will be reduced by the yielding in tension, the well-known Bauschinger effect. The Masing's rule postulates that the hysteresis loops are self-similar, i.e., if they are shifted to coincide at one turning point, the curves will also coincide, as illustrated in Figure 5b. This postulation allows the hysteresis loops to be constructed from the points on the cyclic stress-strain curve, which itself is formed by connecting the tips of the stabilised hysteresis loops under fully-reversed constant amplitude loading. However, as sketched in Figure 5e and f, this may not be the case for transient responses. Figure 6 presents the experimental data and model predictions for aluminium 7050 specimens subjected to strain-controlled loading (Hu and Wang 2000), where the numerical results were obtained using a non-linear kinematic hardening model (Chaboche 1986; Hu, Wang and Barter 1999). The non-closing hysteresis loops obviously violates Masing's postulate, but for critical locations under severe loading, it is important to model the local transient stress-strain response accurately. Figure 5c and d show the phenomena of cyclic softening and hardening, in which the cyclic stress becomes smaller and greater than the uniaxial yield stress, respectively. As a general rule, hardened material tends to soften cyclically while annealed material tends to harden cyclically.

The current methods for crack initiation life modelling ignore most of the above characteristics of cyclic plasticity. The general approach is to adopt Masing's rule and use the Ramberg-Osgood equation to represent the cyclic stress-strain curve and the hysteresis loops. This omission of the transient behaviour may affect the capability in capturing the load sequence

effect on fatigue damage. More detailed discussion is given in Section 2.2.4 “Notch Root Stress and Strain Response.”

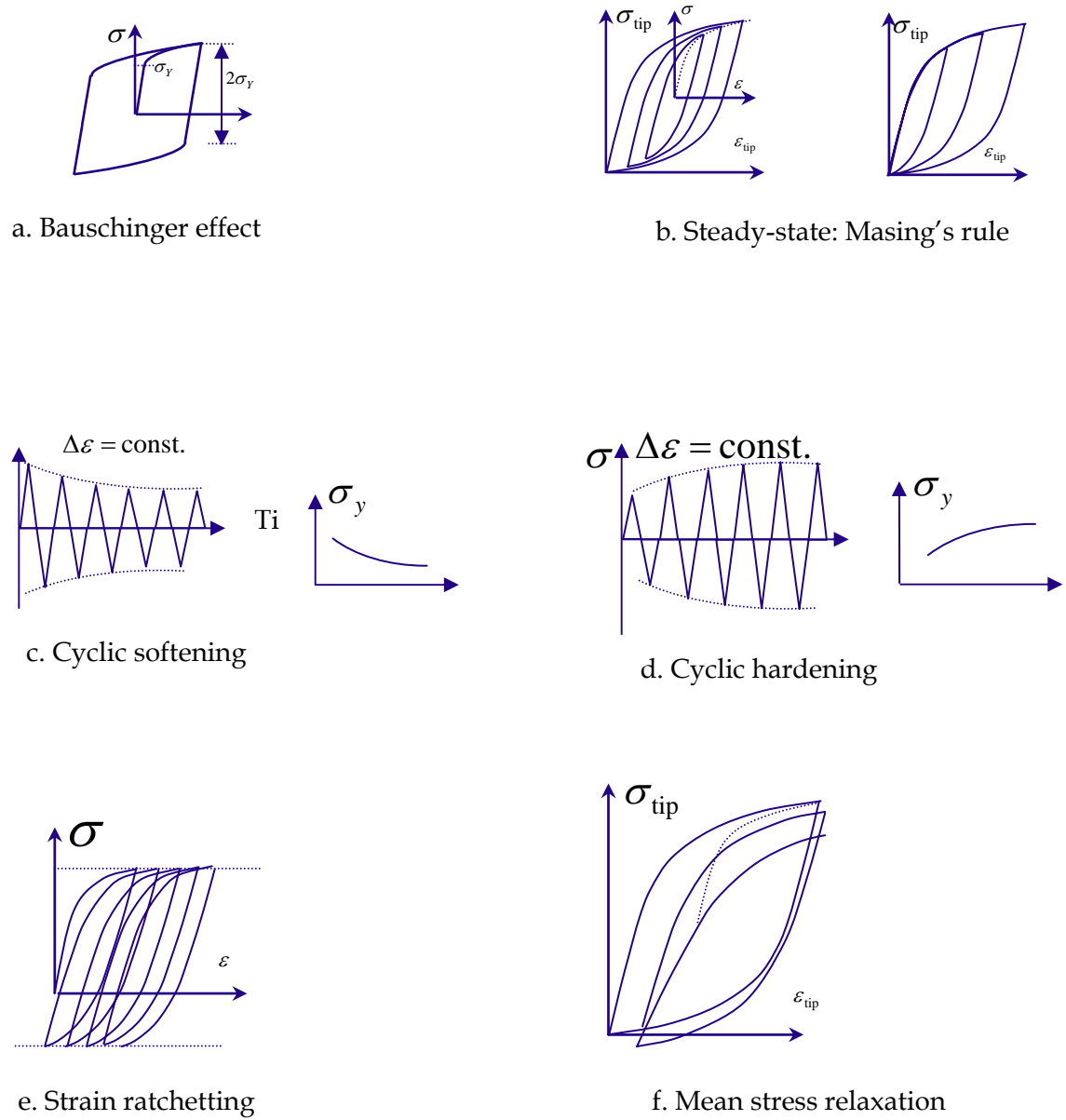


Figure 5 Transient and steady-state cyclic elastic-plastic stress-strain response at a notch root

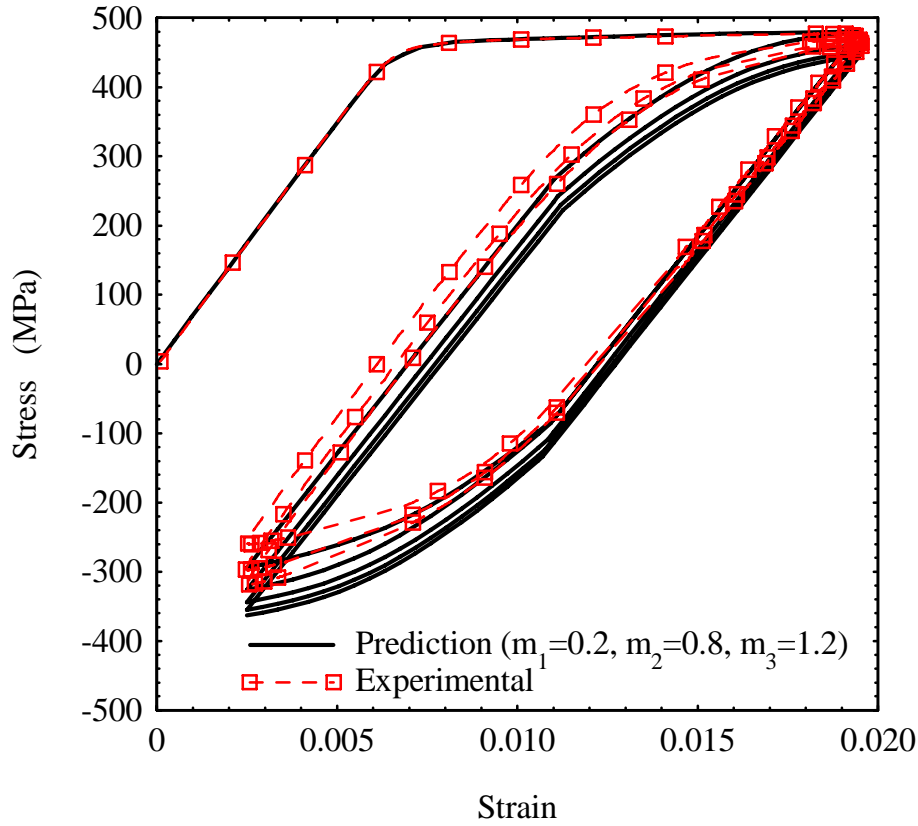


Figure 6 Cyclic stress-strain response of aluminium 7050 under strain-controlled test, demonstrating the gradual relaxation of mean stress (Hu and Wang 2000)

2.2.2 Strain-Life Curves

Strain-life curves are usually generated under strain-controlled fatigue tests conducted on smooth specimens, as illustrated in Figure 7, in which the amplitude of the total strain ε_a is plotted against the number of cycles to failure, N_f , on a log-log scale. A standard strain-controlled test consists of constant amplitude, completely reversed straining at a constant or almost constant strain rate. As the strain limits are controlled, the stress may vary in a fashion similar to that shown in Figure 6. Under such test conditions, the relationship between the controlling parameter $\Delta\varepsilon$ and the response stress range $\Delta\sigma$ and the plastic strain range $\Delta\varepsilon_p$ is simply

$$\Delta\varepsilon = \Delta\varepsilon_e + \Delta\varepsilon_p = \frac{\Delta\sigma}{E} + \Delta\varepsilon_p. \quad (3)$$

With both the total strain range and the stress range recorded, Equation (3) can be used to calculate the corresponding plastic strain range. The elastic strain amplitude and the plastic strain amplitude are related to the fatigue life through (Basquin 1910)

$$\frac{\Delta \varepsilon_e}{2} = \frac{\sigma_f'}{E} (2N_f)^{b'}$$

$$\frac{\Delta \varepsilon_p}{2} = \varepsilon_f' (2N_f)^{c'}$$
(4)

where σ_f' and ε_f' are known as the fatigue strength coefficient and fatigue ductility coefficient, respectively, and b' and c' are the fatigue strength exponent and fatigue ductility exponent, respectively. For a given total strain range $\Delta \varepsilon$, Equations (3) and (4) need to be solved iteratively for the corresponding fatigue life.

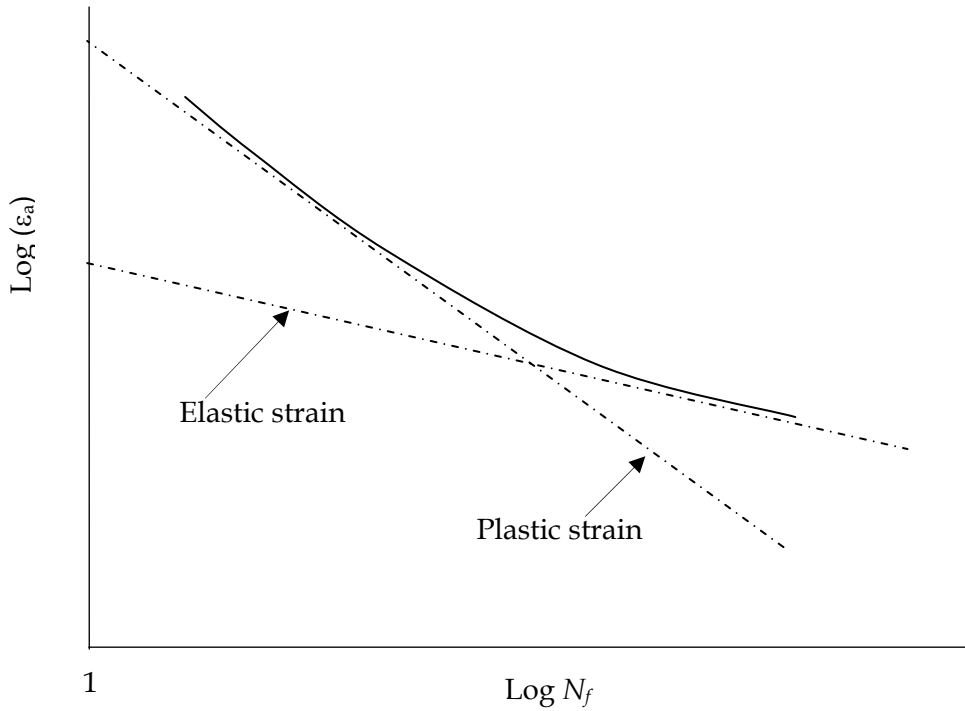


Figure 7 Schematic of strain-life curve

2.2.3 Equivalent Strain Equations

Since the strain-life data are generated under strain ratio of -1, it is necessary to convert a general strain cycle to an equivalent fully-reversed strain cycle before it can be used to calculate fatigue damage. This conversion mainly accounts for the effect of mean stress on fatigue damage, but in more general cases, the maximum stress is also taken into consideration. The general form of equivalent strain equation can be cast as

$$\varepsilon_{eq,a} = f(\varepsilon_a, \sigma_{mean}, \sigma_{max}, \dots)$$
(5)

where ε_a is the actual strain range calculated by $\varepsilon_a = (\varepsilon_{max} - \varepsilon_{min}) / 2$.

Table 1 shows some important strain equations which are implemented in the fatigue life prediction tools CI89 and FAMS.

Table 1 Examples of equivalent strain equations implemented in CI89 and FAMS (Shah 2004)

Equivalent Strain Equation	If, $\sigma_{\text{mean}} \geq 0$.	If, $\sigma_{\text{mean}} < 0$.
Modified Morrow's (FAMS)	$\epsilon_{\text{eq}, a} = \epsilon_a / (1 - \sigma_{\text{mean}} / \sigma_F)$	$\epsilon_{\text{eq}, a} = \epsilon_a / (1 - \sigma_{\text{mean}} / \sigma_F)$
Loopin	$\epsilon_{\text{eq}, a} = \epsilon_a * (1 + \sigma_{\text{mean}} / \sigma_a)^\beta$	$\epsilon_{\text{eq}, a} = \epsilon_a * (1 - \sigma_{\text{mean}} / \sigma_a)^{-\beta}$
Walker	$\epsilon_{\text{eq}, a} = \epsilon_a^{(m)} * (\sigma_{\text{max}} / E)^{(1-m)}$	$\epsilon_{\text{eq}, a} = \epsilon_a^{(m)} * (\sigma_{\text{max}} / E)^{(1-m)}$
Smith Watson Topper (SWT)	$\epsilon_{\text{eq}, a} = (\epsilon_a * \sigma_{\text{max}} / E)^{(m)}$	$\epsilon_{\text{eq}, a} = 0.0$
F-18 (DSTO-TR-0381)	$\epsilon_{\text{eq}, a} = \epsilon_a + (\sigma_{\text{max}} / E)^{(m)}$	$\epsilon_{\text{eq}, a} = 0.0$
Modified Loopin	$\epsilon_{\text{eq}, a} = \epsilon_a * (1 + \sigma_{\text{mean}} / \sigma_a)^\beta$	$\epsilon_{\text{eq}, a} = \epsilon_a * (1 - \sigma_{\text{mean}} / \sigma_a)^{-\alpha/\beta}$
LM-Aero Mod # 1	$\epsilon_{\text{eq}, a} = \epsilon_a^{(m)} * (\sigma_{\text{max}} / E)^{(1-m)}$	$\epsilon_{\text{eq}, a} = \epsilon_a * (1 - \sigma_{\text{mean}} / \sigma_a)^{-\alpha/m}$
LM-Aero Mod # 2	$\epsilon_{\text{eq}, a} = \epsilon_a^{(m)} * (\sigma_{\text{max}} / E)^{(1-m)} * [(1-R)/2]^\alpha$	$\left\{ \begin{array}{l} R < -1, R = -1; \\ R > 1, R = 1 \end{array} \right\}$

2.2.4 Notch Root Stress and Strain Response

To apply the strain-based approach to notched components, it is necessary to determine the notch root stress and strain from the applied load, the stress-strain equation, the stress concentration factor K_t , and an extra equation linking the remote stress and strain to the local stress and strain. Two of the most commonly used equations are Neuber's rule (Neuber 1961) and Glinka's equivalent strain energy method (Glinka 1985; Glinka 1985a). Neuber analysed notches with various flank angles subjected to shear loading, with a non-linear material response. He noted the now famous Neuber's rule

$$K_t^2 = K_\sigma K_\epsilon. \quad (6)$$

Under monotonic loading, $K_t = S_N / S$ is the theoretical stress concentration factor, and for uniaxial loading, the actual stress concentration factor $K_\sigma = \sigma / S$ and the actual strain concentration factor $K_\epsilon = \epsilon / e$, where S and e are remote stress and strain, σ and ϵ are the local stress and strain, and S_N is the elastic stress at the notch root. If the applied stress does not cause yield at the notch root, $S_N = \sigma$ is the actual response stress; otherwise, $S_N > \sigma$ is a hypothetical elastic stress. Hence

$$\sigma \epsilon = \frac{K_t^2 S^2}{E} \quad (7)$$

Using this equation with the stress-strain equation

$$\epsilon = f(\sigma), \quad (8)$$

the two unknowns, local strain ϵ and stress σ can be calculated. The stress-strain relation of the material may be represented by a Ramberg-Osgood equation

$$\epsilon = \epsilon_e + \epsilon_p = \frac{\sigma}{E} + \left(\frac{\sigma}{K'} \right)^{1/n'}, \quad (9)$$

where K' and n' are material constants to be determined from experimental data.

Glinka (1985a) calculated the stress and strain at a notch root based on a concept of equivalence of strain energy densities from the remote load system and the notch root stress system. He showed that the theoretical notch-tip strain calculations can be improved if the stress redistribution due to the plastic yielding around the notch-tip is taken into account. In the simplest case of plane stress loading, the equivalent strain energy density method can be stated as

$$\frac{1}{2} S_e = \int \sigma d\varepsilon \quad (10)$$

Figure 8 gives a graphical comparison and contrast of Neuber's rule and the equivalent strain energy density method. In both cases, the hypothetical local elastic stress and strain is represented by point B, and the local stress and strain are given by point A. The point A is determined by equating the dotted area to the shaded area. Sharpe and Wang (1991) and Sharpe et al (1992) conducted a detailed evaluation of the Neuber and the Glinka methods and their variants under monotonic loading by comparing the numerical predictions to experimental data, and concluded that if the state at the notch root is closer to plane stress, the Neuber rule gives a better prediction, while Glinka method gives an upper bound solution; on the other hand if the state at the notch root is closer to plane strain, Neuber's rule is inadequate, while Glinka's model gives a better prediction.

Under cyclic loading, the corresponding equations for determining the notch root stress and strain using Neuber rule are

$$\Delta\sigma\Delta\varepsilon = \frac{K_t^2 \Delta S^2}{E} \quad (11)$$

$$\Delta\varepsilon = \Delta\varepsilon_e + \Delta\varepsilon_p = \frac{\Delta\sigma}{E} + \left(\frac{\Delta\sigma}{2K'} \right)^{1/n'} \quad (12)$$

CI89 (McDonnell Douglas 1991b) implements both Neuber rule and Glinka's method while FAMS uses only Neuber's rule.

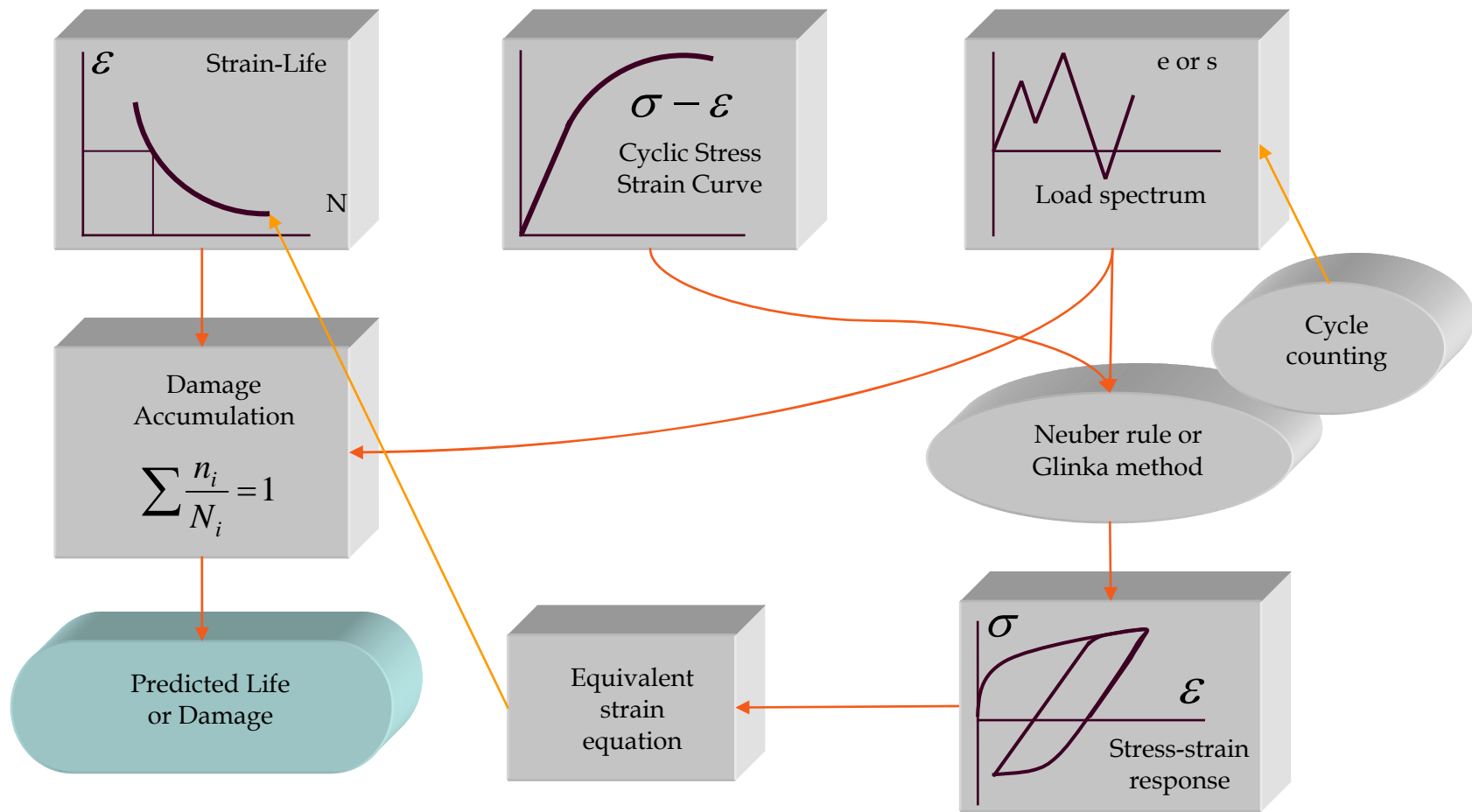


Figure 9 A generic flow chart for strain-based fatigue life analysis program

3. Software Tools for Fatigue Life Prediction

Two of the more frequently used software tools within Structures Branch of AVD for fatigue life prediction are CI89 for F/A-18 and FAMS for P3-C. They both implement the strain-life approach, and the main differences are in the number of equivalent strain equations available, the capability in dealing with residual stresses, and the output formats.

3.1 CI89

CI89 (McDonnell Douglas 1991b) is a FORTRAN program that predicts the time to crack initiation for a given material and load sequence. It was developed by McDonnell Douglas (now Boeing Aircraft) based largely on the Northrop crack initiation program LOOPIN8. One of the aims in developing CI89 was to make the tool more comprehensive than LOOPIN8.

The program was the primary fatigue prediction tool used on the F/A-18 International Follow-On Structural Test Project (IFOSTP). It has been used extensively on the IFOSTP to predict the fatigue life of components under RAAF usage, evaluate spectrum severity and determine the life of repaired components. It has also been used to create the unit damage matrices in the F/A-18 fatigue tracking program MSMP2. It should be noted that CI89 is limited for use for F/A-18 tasks only due to an understanding of the restrictions placed on DSTO's use of the code by Boeing as part of the transfer of the software.

CI89 performs fatigue crack initiation analysis on a spectrum of load points. This spectrum must be normalised by the maximum peak stress of the spectrum before being run through the program's life calculation algorithm. This allows CI89 to process a sequence of loads, stresses or strains, as desired. The reference condition (which may represent a peak stress, strain or load) facilitates the convenient comparison of multiple sequences.

Once the spectrum is read in, Neuber's rule and the cyclic stress-strain curve of the material are used to determine the stress and strain at the notch root. The crack initiation life for various stress levels is calculated by the program using material strain-life data and the Miner-Palmgren hypothesis of cumulative damage. There is no intrinsic definition of crack initiation life, although for USN F/A-18 structures it is defined as the time to development a crack of 0.01 inch. This is represented by the strain-life data, independent of the program. CI89 implements a number of equivalent strain equations which relate the strain range for any particular cycle to a strain range for $R = -1$.

Some of the key options/components of CI89 are:

- Spectrum starting position – CI89 allows the user to determine which load point to put at the beginning of the sequence (i.e., maximum peak, minimum valley, maximum load or no change). It was normal to start the analysis at the maximum peak as this ensures that there will be no unclosed loops or half cycles.
- Hysteresis loop counting – With each run the user has the option to choose if the hysteresis loops should be rain-flow counted. Analyses have shown that not counting the hysteresis loops results in a non-conservative life prediction.

Counting the hysteresis loops have generated lives that agree better with experimental data.

- Equivalent strain equations – CI89 has 8 built in equivalent strain equations. These are: F15, Morrow, Modified Goodman, Gerber, Soderberg, Smith-Watson-Topper, F-18, and a hybrid F18-Morrow equation. The default equivalent strain equation for the aft fuselage and empennage of the F/A-18 is the Smith-Watson-Topper. For the centre fuselage, the modified F-18 equation is utilised. Some analyses have been performed to investigate the impact of the different equivalent strain equations on life predictions.
- Allowance for different elastic modulus in tension and compression – This is to improve the predictability for materials such as aluminium 7050 forging which has a difference in modulus of about 3 to 5% between tension and compression. This is also used to model lugs which may experience different loads in tension and compression.
- Second material life curve – This option is used for cases in which there is a transition between pre-strain and no pre-strain conditions.
- CI89 has the ability to calculate and output line-by-line damage and a peak-valley damage table.
- Residual stress – a residual stress may be provided to account for the effects of cold worked holes or other application where residual stresses are present.

CI89 Version 4.0 was used for most of the analysis performed by the IFOSTP fatigue group. This version differed from the original code provided by McDonnell Douglas in that an equivalence factor was included which allowed different spectra to be conveniently compared. The function of the equivalence factor was to scale a spectrum to a common reference condition. Further additions included a modified output file which contained the program inputs and outputs and the inclusion of the LOOPIN8 equivalent strain equation.

3.2 FAMS

The Naval Air Warfare Center (NAWC) of the United States Navy (USN) originally sponsored the development of a software code called FAMS (Naval Air Warfare Center 1995). FAMS is an acronym for Fatigue Analysis of Metallic Structures. FAMS has primarily been used at DSTO on the P-3C SLAP task and has been used for test interpretation activities where results from the USN fatigue tests were converted into equivalent RAAF hours. It has also been used in sequence comparison and evaluation studies and in the development of unit damage matrices which are to be used in the RAAF P3-C aircraft tracking system.

FAMS accepts a number of different input sequence file types. All files types, however, must be in peak-valley format and begin with a peak greater than or equal to zero and end with a valley. Unlike CI89, only stress sequences can be used since FAMS does not normalise the sequence. A conversion factor allows these stress sequences to be in metric or imperial units. The sequence file may be in block (i.e., peak, valley, number of cycles) or cycle (i.e., peak, valley) format and can be processed on a flight-by-flight basis. Processing a sequence on a flight-by-flight basis can lead to different results compared to processing as a complete spectrum. This is because the hysteresis loops formed within a flight will be different to those formed within the complete spectrum. Flight-by-flight processing should not have a

significant effect on fighter type spectra which are short (F/A-18 spectra typically 300 hours) as opposed to transport aircraft spectra (P3-C spectra typically 15,000 hours).

FAMS follows a similar algorithm as CI89. Neuber's rule in conjunction with a cyclic stress-strain curve is used to convert the remote stresses in the input sequence file into notch stresses and strains. The input spectrum is automatically hysteresis loop counted. FAMS then checks each peak-valley pair for the following conditions:

1. Global stress exceeds material yield stress,
2. Notch stress exceeds material fracture stress,
3. Notch strain exceeds fracture strain.
4. The accumulated damage equals 1.

FAMS stops execution if any of the above conditions is met.

The crack initiation lives for various K_n values are then calculated by the program using material strain-life data and the Miner-Palmgren hypothesis of cumulative damage. The original version of FAMS used the Morrow equivalent strain equation to convert the peak-valley strain cycle into its equivalent cycle at $R = -1$.

Some of the key components of FAMS are:

- Multiple passes of analysis – The FAMS analysis can be run with either the option of taking the first-pass results or the second-pass result. The first-pass analysis assumes a zero residual stress at the commencement of the damage calculation, while the second-pass analysis uses the residual stresses attained at the end of the first pass;
- Multiple K_n values – One of the most useful options is the ability to run FAMS with up to ten different notch factors. This feature is not available in CI89;
- Material data formats – The material data can be stored either as a series of points or as a function. One of the main advantages of the material data in a function format is the ability to calculate the material properties for a wide range of stresses. In the case of the tabular data if the data does not span the full range of the stress then the damage due to that load must be extrapolated.
- Equivalent strain equations – The default equivalent strain equation for the program is the Morrow equation. Initially this was the only equivalent strain equation available; however, the current modifications to the program by LM and DSTO have resulted in the inclusion of a number of other equivalent strain equations. These are: Loopin, modified Loopin, Walker, Smith-Watson-Topper, F-18, LM-Aero Mod #1, and LM-Aero Mod #2.

A number of versions of FAMS exist at DSTO. The first was obtained from the USN and is the baseline version. Later, Lockheed Martin for the P-3 SLAP modified FAMS to output damage per load source (i.e., manoeuvre, gust, landing etc). This version of FAMS was known as FAMS-Bailey. DSTO then modified FAMS to account for the different load sources produced by the spectrum generation program. DSTO also modified the format of the output file to

make plotting of the results easier. This version of FAMS became known as famsh, the latest being version 1.42.

3.3 Comparison of FAMS and CI89

A comparison between FAMS and CI89 was performed in (Ayling and Molent 1998). The results have been reproduced in Table 2 using a number of F/A-18 spectra.

Table 2 Comparison of FAMS and CI89

SEQUENCE DETAILS			FATIGUE LIFE (HOURS)					
Sequence Name	Flight Hours	K_t xDLS MPa (ksi)	Morrow Equation			F/A-18 Equation		
			FAMS	CI89	FAMS/CI89	FAMS	CI89	FAMS/CI89
SPEC6g	302.9	408.7 (59.28)	13452	17228	0.78	7819	7794	1.00
IARPO2	323.4	403.6 (58.54)	14977	19235	0.78	8940	9027	0.99
IARPO4	323.4	403.6 (58.54)	13454	17353	0.78	8030	8093	0.99
ST16	300.0	432.7 (62.76)	18491	23562	0.78	12507	12359	1.01
A21-103	255.4	389.7 (56.52)	10863	12623	0.86	6459	6496	0.99

Using the Morrow equivalent strain equation, it can be seen that FAMS is more conservative than CI89 by about 22%. (Ayling and Molent 1998) determined that the main reason for this was the version of the Morrow equation that was used in FAMS was more conservative than the one used in CI89.

In order to test the F/A-18 equation it was necessary to incorporate the equation into FAMS. Once incorporated, the analysis was conducted using the same spectra. In this case it can be seen that the predictions between the two programs are very similar and it can be expected that, given consistent input options and data, the same results can be obtained from either software.

One of the main benefits of FAMS over CI89, apart from the fact that there are no restrictions imposed on its use in DSTO, is that the program will halt if the gross area stress at any turning point of the loading spectrum exceeds the material ultimate strength. This is the major difference between CI89 and FAMS. As CI89 cannot detect this condition it may invalidate the assumption of elastic gross area stresses and strains used in the Neuber relationship. In terms of modelling capabilities, "famsh" (DSTO-modified FAMS for the DSTO P-3 SLAP analysis, see Teunisse, Phillips, Jackson, Matricciani, Weiping Hu, Amaratunga, Hartley and Mongru 2006) has incorporated the strengths of the both the original FAMS and CI89 for example, expanded Equivalent Strain Equation options, and expanded input and output file format options. It also has CI89's advantage of cross-platform (Windows, UNIX) accessibility.

4. Modelling of Fatigue Crack Growth

There are three basic modes of crack growth, the opening mode, edge sliding mode and the tearing mode (Anderson 1995, for example). The discussion in this report is restricted to the opening mode crack, which is the most frequently encountered mode in aircraft structures such as wing and fuselage skins.

The modelling of fatigue crack growth takes place at several levels. At the microstructure level, the cyclic load may affect the material properties, such as the occurrence of persistent slip bands, as manifested by cyclic hardening or softening of materials; at mesoscopic level involving many grains, there is trans-granular and inter-granular crack propagation, the blockage of cracks by grain boundaries, etc; crack tip plastic zone, reverse yielding, material inhomogeneity, anisotropy; at macroscopic level, there are different shapes of cracks, through-thickness cracks, corner cracks, surface cracks, in addition to different specimen thicknesses, etc.

On one hand, the engineering fatigue problems have to be expressed in terms of mechanical concepts, such as load spectra, stress and strain, stress concentration factors K_t and stress intensity factors K . On the other hand, the fatigue mechanisms are expressed in terms of material concepts such as crystal, grains, persistent slip bands, and micro cracks. The task of modelling is to relate those two sets of data so that a mathematical model could be established on the basis of a mechanical model that reasonably represents the physical mechanisms. This requires an accurate reflection of the micro activities with a rational set of parameters and rules. Numerical tools are then used to implement the mathematical models efficiently and robustly.

To appropriately analyse a structural component, it is necessary to first establish a mechanical model of the component, by either isolating the component from the structure or cut part of the component out. The effects of the surrounding structure on the “model” need to be accurately represented through boundary conditions which could be prescribed displacement or surface traction. The quality of the analysis hinges on the quality of the input data, including the applied spectrum and simplified geometry.

4.1 The Fundamental Principle for Crack Growth Analysis-LEFM

The fatigue crack growth modelling codes in use at AVD, DSTO are mostly based on the concepts of LEFM. A very good overview of LEFM is provided in (Anderson 1995; Grandt 2004). The main concept is that SIF, K , is able to be used as a unique correlating parameter to characterise critical and sub-critical crack propagation. K is a parameter which characterises the stress field singularity at the crack tip, and is defined as follows

$$K = \beta S \sqrt{\pi a} \quad (13)$$

where

S is the remote applied stress,

a is the crack length¹, and

β is a dimensionless geometry factor which is a function of crack size and component geometry. It accounts for such effects as boundary condition (e.g., the crack emanating from a hole), finite width, and whether the crack is through thickness, a part through surface crack, or a corner crack.

The use of K as a correlating parameter is in large due to the work of people such as Paris et al (Paris and Erdogan 1963; Paris 1964). The key discovery was that under fatigue loading, the cyclic range in stress intensity factor, ΔK , controls the rate of fatigue crack growth. The most compelling part is that it was shown to be independent of the geometry, i.e., for different geometries, for the same value of ΔK they observed a consistent crack growth rate da/dN . It was, therefore, suggested that the relationship between the crack growth rate and SIF range is a material property. This discovery paved the way for ΔK to be used to relate what would happen in a complex aircraft structural component based on material data collected from simple coupons subjected to constant amplitude loading. This postulation is known as similitude, see Section 4.2 below.

Paris and others observed that if the crack growth rate under constant amplitude loading is plotted on a log scale on the vertical axis, and the SIF range ΔK is plotted on a log scale on the horizontal axis, the data follow approximately a straight line, as schematically shown in the mid-section of Figure 10. Paris fitted a simple power law equation to model the data, and this has become known as the Paris law

$$\frac{da}{dN} = C \Delta K^m \quad (14)$$

where C and m are empirical constants, obtained for a particular set of data (i.e., for a particular material).

¹ For surface cracks and corner cracks, a is the crack depth in thickness direction and c is the crack length in width direction.

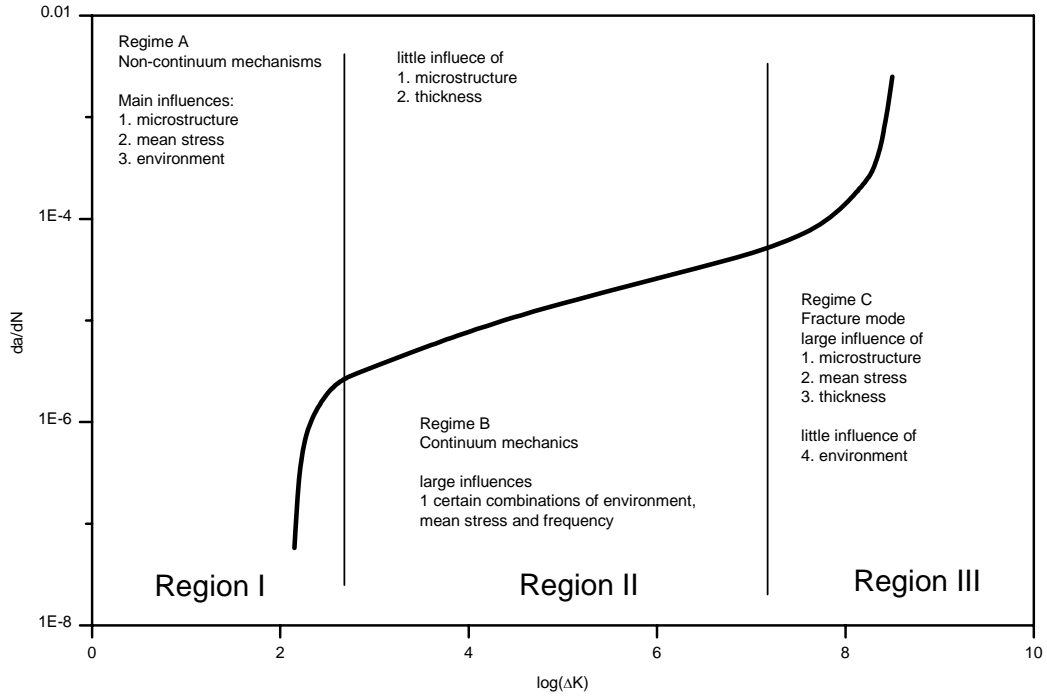


Figure 10 Schematic illustration of da/dN versus ΔK curve. The crack growth may be divided into three regions; the threshold region, the stable growth region and fast fracture region. The growth rates in these regions are influenced, to different extent, by the microstructure, mean stress, thickness and environment. Adapted from (Ritchie 1979)

Modelling the crack growth rate data is crucial for the analysis of fatigue crack growth. Based on the Paris law the crack growth life may be calculated by integrating the rate equation

$$N_f = \int_{a_i}^{a_f} \frac{da}{C \Delta K^m}, \quad (15)$$

where

N_f is the life (for example in cycles or flight hours),

a_i is the initial crack size, and

a_f is the final crack size.

If the geometry factor β is independent of crack size (for example a centre crack in an infinite width sheet, or an edge crack in a semi-infinite width sheet), then a closed form of the integration is possible. This is usually not the case, and some form of numerical integration is employed. All the numerical tools based on LEFM implement some form of integration algorithm of the Equation (15).

4.2 Similitude Principle

In simple words, the similitude principle states that two different cracks of different sizes will grow at the same rate if they are subjected to the same driving force, such as SIF range ΔK . This principle provides a theoretical justification for the use of crack growth rate data obtained from laboratory specimens, which are typically much smaller than aircraft structures, to predict the crack growth in real structures. It essentially states that the effects of size, etc., are all encapsulated in the quantity ΔK .

However, it was soon found that the similitude principle breaks down for short cracks whose lengths are comparable to either the size of microstructures such as the grain size or the size of its own plastic zone (Suresh and Ritchie 1984). More detailed discussion on short crack effect is given in Section 4.4.

4.3 Crack Growth Rate Curve and the Factors that Influence Crack Growth

Equation (14) was established on the basis of constant amplitude loading and long crack data. It was further assumed that, when the above equation was used for life prediction, only the tensile part of the load cycle contributes to fatigue damage and that the crack tip surfaces close at zero load. Since the stress intensity range could be expressed as $\Delta K = \beta \Delta S \sqrt{\pi a}$, the right hand side of Equation (14) may be re-arranged as an explicit expression of the crack length

$$da / dN = C_1 a^{m/2}$$

with $C_1 = C(\beta \Delta S \sqrt{\pi})^m$. In practical cases, C_1 does not only depend on the stress range ΔS but also varies with the crack length (through the geometry factor $\beta = \beta(a)$), but if the variation of β with the crack length is small, we may treat it as a constant and integrate the above rate equation to obtain an explicit relation between the stress range ΔS and the crack growth life N in terms of the number of cycles, for a given initial crack size c_i (Latzko, Turner, Landes, McCabe and Hellen 1979) (assuming $m \neq 2$. For $m = 2$, Equation (14) integrates to a simple exponential function)

$$N = \frac{1}{C_2} \left[a^{(2-m)/2} - a_i^{(2-m)/2} \right] \quad (16)$$

Or in terms of the final crack length

$$a = \left[a_i^{(2-m)/2} + C_2 N \right]^{2/(2-m)} \quad (17)$$

Here the constant

$$C_2 = C(\beta \Delta S \sqrt{\pi})^m \frac{2-m}{m}. \quad (18)$$

Some crack growth curves are plotted in Figure 11, according to Equation (16), to demonstrate the sensitivities of various factors on crack growth. The baseline parameters are $C = 10^{-9}$, $\beta = 1.0$, $m = 3.0$, $\Delta S = 30$ and $a_i = 0.5$, and the result is represented by the solid black line. Then each of the parameters was reduced by 20% to show their effect on crack growth. The

dashed (blue) line shows the most pronounced effect of the Paris exponent m , with a decrease of m from 3 to 2.4 leading in an increase of the crack growth life at $a = 10$ by a factor of 6. The next most significant factor is the load level ΔS , shown by the dotted green curve, followed by the Paris coefficient C , represented by the double-dotted cyan curve. The effect of initial crack size is demonstrated by the dotted red curve.

The curves in Figure 11 demonstrate the relative importance of each parameter on crack growth within the Paris regime. It clearly highlights the importance of the Paris exponent m . A small variation in m may lead to a large difference in crack growth rate. Hence, every effort should be made to obtain an accurate value of the exponent from experimental data.

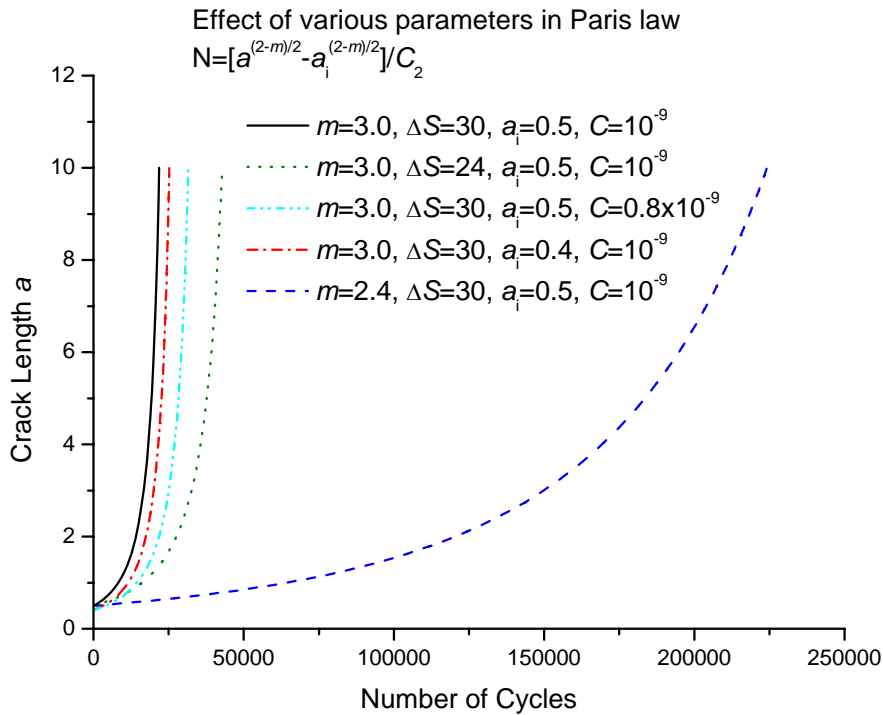


Figure 11 Crack growth curves predicted using Paris law, illustrating the effect of different parameters on crack growth

Although Equations (16) and (17) can rarely be directly used for crack growth analysis, they do help to reveal the relationships between the stress range, initial crack size and the final crack size, as well as the effect of the material constants C and m on crack growth.

It should be pointed out that Equation (14) is an approximate representation of the crack growth rate in Region II, Figure 10. The full range of the experimental $da/dN - \Delta K$ curve, actually exhibits a sigmoidal shape, as shown in Figure 10, which can be divided into three regions: the slow growth threshold Region I, the stable growth Region II and the fast growth and fracture Region III. Experimental studies have shown that the crack growth rate may be affected by the microstructure, the environment, the mean stress, in addition to the stress

intensity range ΔK , but as shown in Figure 10, the influence of these factors are different for different regions (Ritchie 1979).

4.3.1 Region I: Threshold Growth

For long cracks subjected to ΔK within Region I, a threshold is often observed below which no noticeable crack growth takes place. In practice, the threshold rate is defined as 10^{-10} m/cycle, i.e., if the growth rate is below 10^{-10} m/cycle the crack is considered non-propagating. It should be emphasised that the threshold refers to long cracks, not short cracks. For long cracks to attain a low SIF range, the load level is necessarily low, according to Equation (13). The crack growth behaviour for short cracks subjected to similar levels of stress intensity factor range is very different from the long crack threshold behaviour. Short cracks typically exhibit a higher growth rate than the corresponding long crack, as discussed in more detail in Section 4.4.

The techniques and procedures for determining the threshold stress intensity range ΔK_0 can be found in (Scott, Newman and Forman 2002) and the references therein.

Threshold growth has been taken into consideration in some crack growth codes, e.g., FASTRAN (Newman 1981a) and METLIFE (Ball 2005a).

4.3.2 Region II: Stable Growth

This region is also known as the Paris region in which the macroscopic crack growth is mainly influenced by a combination of environment, mean stress and load frequency (Blom and Holm 1985). The microstructure and specimen thickness have little influence on the crack growth. The growth rate is described by the Paris law (14). By taking the logarithm on both sides of the Paris equation (14), we have

$$\log\left(\frac{da}{dN}\right) = m \log \Delta K + \log C,$$

which represents a straight line on a log-log scale. Geometrically, the Paris exponent m represents the slope, and $\log C$ is the intercept on the vertical line at $\Delta K = 1$ (hence, $\log \Delta K = 0$), respectively. Hence, C and m can be determined by curve-fitting experimental crack growth rate data.

It should be emphasised that the applicability of the Paris law is in Region II. Extrapolation of the Paris law into Region I will shield the threshold growth, hence over predict the crack growth rate, and extrapolating it into Region III will grossly under estimate the crack growth rate. However, attempts have been made to establish a Paris-type relation in Region I and III, notably by Newman (1981a). See Section 5.6.3 on p. 53 for more detail.

4.3.3 Region III Growth: Fast Fracture

Fatigue crack growth in Region III is typically fast, and approaches unstable fracture quickly. Hence, the crack growth life in this region is short. The crack growth is mainly influenced by microstructures, mean stress and the thickness of the structure, with little influence from the environment due to the short life represented by this region. Newman (1981a) also proposed

an extension of the Paris law to cover the crack growth rate in this region, see Section 5.6.3 on p. 53.

4.3.4 Stress Ratio Effect

Experimental evidence shows that the SIF range ΔK is not the only factor which controls crack growth rate. As shown in Figure 12, da/dN at a given ΔK often increases with stress ratio

$R = \frac{S_{\min}}{S_{\max}}$. The effect of stress ratio may be modelled by Walker equation (Walker 1970) and

Forman equation (Forman, Kearney and Engle 1967), for example. The details of these equations are also available in the METLIFE technical manual (Ball 2005a). FASTRAN (Newman 1992b) deals the effect of stress ratio through the crack closure model.

4.3.5 Sequence Effect, Crack Growth Acceleration and Retardation

It is well documented (Blom 1988) that crack growth rate decreases after an overload (retardation) and increases after an underload (acceleration). Further, it has been observed that the effect of retardation following an overload is more significant for materials with lower strength, smaller thickness (plane stress), higher baseline SIF range, or higher overload. Initially, all these effects were attributed to the size of the plastic zone at the crack tip, and a number of models were proposed based on this assumption, among them the more commonly known Wheeler (1970; 1972) and Willenborg (1971) models. However, these models were not able to account for other sequence effects, notably the initial increase in growth rate immediately after an overload before decrease takes place, i.e., the so-called delayed retardation effect; nor were they able to explain why under repeated overloads, steels with higher strength exhibited more retardation effect than those with lower strength (Blom 1988). This latter observation is contrary to the case of a single overload, and cannot be explained by the crack tip plastic zone size as the material with higher strength develops a smaller plastic zone, hence should have less retardation.

In order to rationalise these observed data, other mechanisms were studied, such as the plasticity-induced crack closure concept, which is detailed in Section 4.5 on p. 39. At DSTO, Clayton (1989) analysed the elastic-plastic stresses imposed on a crack during growth through a fatigue overload plastic zone using the basic Dugdale theory. Good correlation was obtained between the experimental crack growth data for 2024-T3 aluminium alloy and the numerical results based on the crack closure model (Clayton 1989). Finney (1994) reviewed the models for load sequence effect in fatigue crack growth in the context of military aircraft, and classified the models based on crack tip plastic zone as the first-generation models and those based on crack closure as the second generation ones.

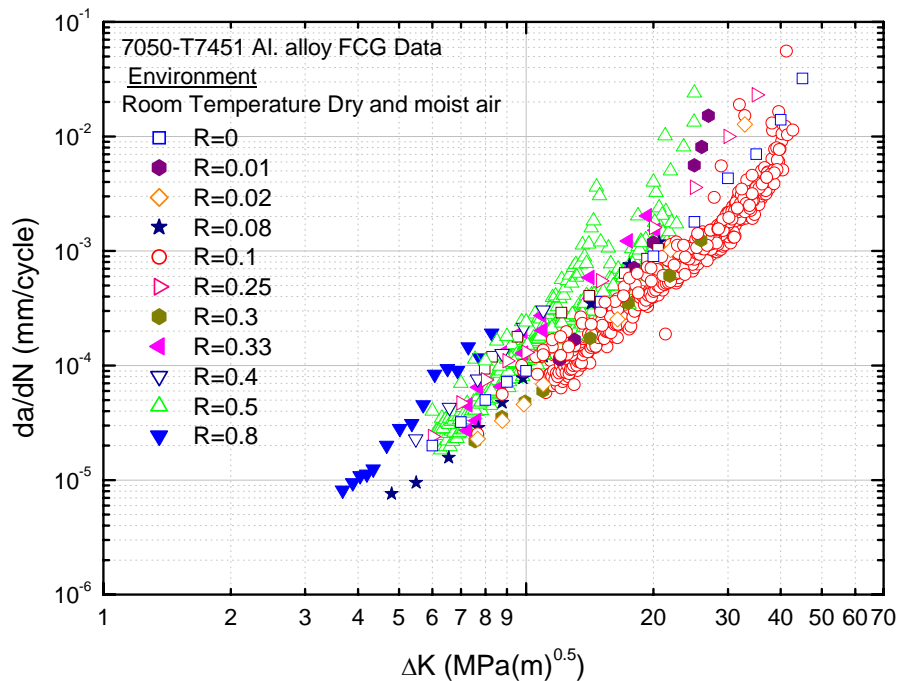


Figure 12 Fatigue crack growth rate for 7050-T7451 aluminium alloy tested at a variety of R ratio values correlated on ΔK (compiled from (Sharp, Byrnes and Clark 1998))

4.4 Short Cracks

There are several definitions for short cracks, and in this report short cracks refer to those cracks which are of a length comparable to the scale of the microstructure, or comparable to the scale of local plasticity, following (Suresh and Ritchie 1984). For these cracks, it has been found that they (1) continue to grow below the long crack threshold SIF range; (2) grow faster than long cracks under the same SIF range. These phenomena are commonly referred to as short crack effects, and they have practical engineering significance because the predictions based on LEFM methodology usually lead to non-conservative crack growth rate, inspection intervals or possibly critical crack size (Leis, Hopper, Ahmad, Broek and Kanninen 1986). The technical issue for the analysis of short crack growth is to establish models that can use long crack growth rate data to predict short crack growth, as short crack growth rate data are difficult and expensive to obtain experimentally.

4.4.1 Experimental Evidence

While LEFM gained recognition in analysing fatigue crack growth in the form of Paris law, it was eventually realised that short cracks do not follow the same “law” as the long ones do. Typically, short cracks grow faster than long cracks when subjected to the same ΔK , and they continue to grow below the long crack threshold. The growth rate for short cracks may decelerate and then accelerate to merge with that of long cracks, or they may stop growing, as illustrated in Figure 13. These phenomena are collectively referred to as short crack effects, or short crack anomalies. From the viewpoint of LEFM, short crack effects demonstrate a break

down of the similitude principle, i.e., the SIF range is no longer a valid correlating parameter for crack growth rate.

The technical relevance of short crack growth is manifested in the fact that the major part of the life for components managed according the philosophy of damage tolerance is generally spent on growing micro- and small cracks, hence a significant amount of research work has been conducted to understand it and to model it. In a classical paper on short crack growth by Suresh and Ritchie (1984), a comprehensive review was given to the then state-of-the-art in the research of short crack effects, including the different techniques used for measuring short cracks, the generation of short cracks, the measurement of short crack thresholds and crack closure, and the breakdown of similitude for three types of short cracks.

4.4.2 Modelling Technique

Attempts have been made to model the anomalous growth behaviour of short cracks, from both the viewpoints of micro-mechanics and continuum mechanics. Within the framework of LEFM, the short crack effect may be modelled by adopting an artificial crack length of $a + a_0$ for stress intensity range calculation (El Haddad, Smith and Topper 1979), where a is the physical crack length and a_0 a material parameter. Thus

$$\Delta K_{\text{eff}} = \beta \Delta S_{\text{eff}} \sqrt{\pi(a + a_0)} \quad (19)$$

which significantly increases the effective stress intensity range when the crack length is comparable to a_0 , but its effect diminishes for long cracks.

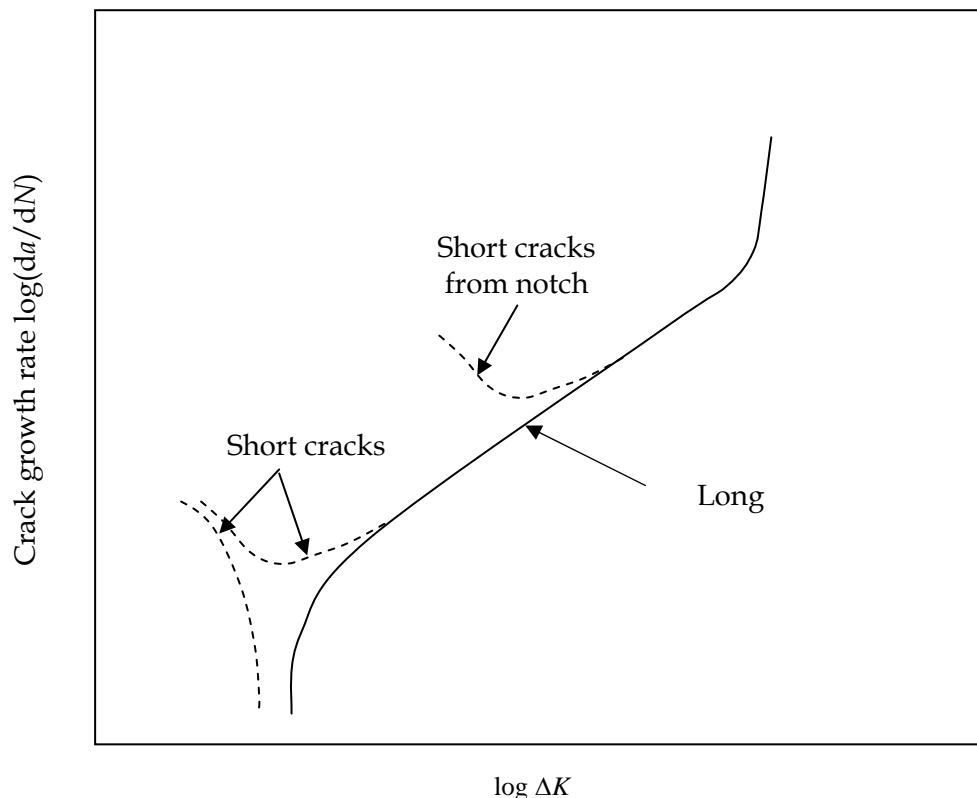


Figure 13 Illustration of typical long and short crack growth rates as a function of stress intensity factor range, under constant amplitude loading. Short cracks grow at ΔK below the threshold value. They may either develop into long cracks or arrest. Short cracks emanating from notches usually develop into long cracks (adapted from (Suresh and Ritchie 1984))

4.5 Crack Closure Concept

Elber (1971) observed that even under tension-tension cyclic loading, the crack tip remains closed during part of the cycle. This was attributed to the plastic deformation left in the wake of the advancing crack tip which causes the crack tip to be closed before the remote load reaches zero. Based on this observation, it was proposed that instead of using the full SIF range ΔK as a crack driving force, an effective SIF range ΔK_{eff} should be used. Further studies by other researchers have found that crack closure may be caused by factors other than plasticity, such as oxides and surface roughness, but plasticity-induced closure is by far the more intensively studied phenomenon. Although recently there have been questions on the level of plasticity-induced crack closure, or the existence of it at all, by a number of researchers (Sadananda and Vasudevan 1995, for example), the plasticity-induced crack closure remains an important mechanism for the interpretation and modelling of a number of crack growth features such as stress ratio effect, sequence effect, retardation and acceleration due to overload and underload, etc.

The plasticity-induced crack closure model developed by Newman and Armen (1975) and Fühling and Seeger (1979a; 1979b) can be summarised as follows. As a crack progresses, the material at the crack tip experiences severe plastic deformation, which eventually causes fracture. After separation, the residual plastic deformation is left behind the advancing crack tip. During subsequent unloading, the crack faces come into contact before the external load is reduced to zero. And once the external load is reduced to zero, a compressive stress field is developed between the closed crack faces. Upon subsequent loading, the crack faces will remain in contact for part of the load cycle until the external load reaches a certain level, which is known as the crack opening load and the corresponding remote uniform stress is known as the crack opening stress. It is reasoned that the crack will not grow unless the crack tip is open, hence, the stress below the crack opening stress should not be included in the calculation of the crack driving force. Instead, an effective SIF range should be calculated based on the stress range defined by the crack opening stress and the maximum stress, i.e.

$$\Delta K_{eff} = \beta(S_{max} - S_{open})\sqrt{\pi a} .$$

4.5.1 Crack Opening Stress under Constant Amplitude Loading

Central to the analytical modelling of plasticity-induced crack closure is the determination of the crack opening stress. Most models for crack closure are based on a modified strip-yield model or Dugdale model (Dugdale 1960), by leaving plastically deformed material in the wake of the advancing crack tip. Based on the results from FE analysis, Newman (1984) developed equations for crack opening stresses under constant amplitude loading. More details are given in Section 5.6.1 on p. 49.

4.5.2 Crack Opening Stress under Spectrum Loading

The crack opening stress under spectrum loading is more difficult to determine because of the history effect. Several methods were developed such as the contact stress model and the strip yield model. More details on the strip yield model are presented in Section 5.6.1 on p. 49.

4.6 Constraint or Thickness Effects

4.6.1 Fracture Toughness

Experimental data show that the fracture toughness K_C for a given material is dependent on specimen thickness. The observed K_C decreases with increasing thickness until a minimum value is reached. The minimum fracture toughness is given the special designation K_{IC} and is called the plane strain fracture toughness. This behaviour has been explained by the state of stress at the crack tip. Thinner sheets exhibit conditions closer to plane stress, while plane strain conditions dominate for thick plates. The state of stress affects the plastic zone size, with plane stress having a larger plastic zone and higher fracture toughness. These effects need to be considered when modelling the final failure/fracture aspects of crack growth.

4.6.2 Crack Growth

Crack tip plasticity also seems to affect crack growth. Although constant amplitude fatigue crack growth data do not usually exhibit a strong dependence on specimen thickness, variable amplitude spectrum load histories may lead to significantly longer lives for thinner specimens

than for thicker ones. This has been related to the plastic zone size which depends on the state of stress: plane stress, plane strain or in between. These effects need to be considered by a crack growth analysis programs. In the context of crack closure modelling, less thickness constraint leads to larger crack tip plastic deformation and hence more residual plastic deformation in the crack face. This causes a higher crack closure load and slower crack growth rate, consistent with experimental observations.

5. Software Tools for Fatigue Crack Growth Analysis

A number of software codes are used and/or have been developed by AVD, DSTO for fatigue crack growth analysis. Some of them are OEM provided platform-specific, such as ADAMSys and METLIFE, while others are generic codes, such as AFGROW, FASTRAN and CGAP. The following subsections present an evaluation of the capabilities of each code.

5.1 AFGROW

AFGROW (Harter 2004) is a user friendly, PC based computer program freely available over the internet. The program is produced by the United States Air Force at the Air Force Research Laboratories, Wright Patterson Air Force Base, Ohio, USA. The program is LEFM based, and as such it should produce similar results (given the equivalent input data and assumptions) as any other LEFM-based code. This has indeed been shown to be true for some cases, but in other cases inconsistent results have been obtained (see (Swanton 2005) and (Walker 1997)). In particular, it seems that inconsistencies can arise when retardation modelling is turned on. The most recent version of the program includes the analytical crack closure model as per FASTRAN, but this has not been evaluated and tested at DSTO. Since the analytical crack closure model is considered superior to the empirical retardation models (Wheeler, Willenborg etc.), it is considered appropriate to concentrate future efforts on it.

5.2 Broek

The Broek software was developed by Dr D. Broek from Ohio, USA (Broek 1998). It is also a user friendly PC based software for performing LEFM-based crack growth analysis. The software is now quite old and is not actively updated and supported. AFGROW seems to have taken up that role. However there are at least two unique modules within the Broek software which are potentially useful in the future. They are as follows:

- a. GEOFAC. GEOFAC offers a method to develop geometry factors using compounding and superposition methods. The code also allows the user to develop a geometry factor solution using any arbitrary applied stress distribution. This is done using a Green's function technique. A similar, but more sophisticated, feature is available in METLIFE. AFGROW and CGAP also offer the capability, but again they are not as comprehensive, refined and powerful as the METLIFE version.
- b. IPOCRE. IPOCRE calculates the cumulative probability of crack detection as a function of the inspection interval for a variety of inspection methods. The program requires the single inspection probability of detection and the crack growth curve as inputs. Some inspection characteristic data is built in. Adjustments are made according to factors such as the specificity and accessibility. The IPOCRE methodology is based on Chapter 11 of (Broek 1988).

5.3 ADAMSys

ADAMSys is a UNIX based proprietary code used by Lockheed Martin to perform LEFM based crack growth analysis for the F-111 (Lockheed Martin not-dated). ADAMSys was used

extensively in the F-111 DADTA program (see (Ball 1997a)). An evaluation of AFGROW in comparison to ADAMSys was performed by Ball of Lockheed (Ball 1997a) and it was found that AFGROW could do everything that ADAMSys could do and more. Similarly, it was shown by Walker (1998) that ADAMSys and AFGROW (and indeed METLIFE) produce very similar results for a given case. The case referred to here is a location known as DADTA Item 86 – cracking at fuel flow vent hole (FFVH) 58 in the Wing Pivot Fitting (WPF) lower plate of the F-111. This is one of the example cases in Section D.2. ADAMSys has not been changed or improved for many years, and it is unlikely that it ever will be in the future. DSTO has the executable code only and not the source code. It therefore seems appropriate to concentrate on AFGROW for standard LEFM type analysis.

5.4 METLIFE

METLIFE is a Unix based suite of software for the analysis of “metallic components and structure subjected to isothermal, quasi-static, cyclic mechanical loading” (Ball 2005a). Using notch strain and fatigue crack growth analysis techniques, its biggest advertised feature is the ability to estimate crack growth behaviour in the presence of notch plasticity effects (caused by a combination of severe loads and structural detail). Traditional linear-elastic crack growth problems are also supported by METLIFE.

Elastic-plastic behaviour of metallic structure results in a non-linear stress-strain response to the applied loading. In the case of such elastic-plastic analyses, METLIFE assumes that yield occurs locally, and uses a generalised form of Neuber’s rule to estimate the response stresses by tracking the hysteresis behaviour of the material on a cycle-by-cycle basis². Also, this material behaviour is assumed to follow a non-linear kinematic hardening³ rule. However, it would not be practical to make such calculations formally in the context of fatigue life prediction where hundreds of thousands of cycles may be involved, so a number of simplifying assumptions are made to the cyclic plasticity algorithm as follows:

- Stresses are explicitly addressed on a single, two-dimensional cross-section through the component, coincident with the anticipated plane of crack growth (the description of component geometry is a simplification of the actual aircraft component).
- This plane of crack growth is a principal plane, i.e., there is no shear stress on the plane. As a result, the crack remains (flat) in the plane and grows in Mode I only.
- The response stress calculations are made for an *uncracked* section, assuming that the presence of a crack causes only a local perturbation in the stress field (no load redistribution due to the presence of the crack).
- Masing’s hypothesis for reversed cyclic yielding is implied. This means that the stress-strain curve for reversed straining, or the hysteresis loop, measured from the reversal point, is the cyclic curve scaled by a factor of two.

² METLIFE analyses for F-111 DADTA work typically use the Ramberg-Osgood equation to model the material cyclic stress-strain curve.

³ In a physical sense, (strain) hardening is the increased resistance of a solid to plastic flow, after being initially plastically deformed, unloaded, then reloaded in an attempt to induce further plastic deformation.

The calculation of response stress after each cycle in the load history then establishes the initial conditions for the response at the next pass. *(It has been the implementation of METLIFE's cyclic plasticity algorithm that has caused the most concern, as discussed later).* It should be noted that elastic constraint effects are also considered in METLIFE - the response calculations (state of stress) and fracture (crack tip plastic zone size) are both influenced by these effects.

METLIFE can also estimate residual stress and strain. This is achieved by unloading the component after the application of prior non-zero loads that has caused local plasticity. It should be noted that this calculation assumes that there is sufficient surrounding elastic material engulfing the plastic zone.

METLIFE uses classical LEFM concepts to perform the actual fatigue crack growth analysis, i.e., using the SIF range ΔK to be the correlating fracture parameter. However, for elastic-plastic analyses, the SIF is calculated using Green's function or weight function approach, based on the local response stress, with a K_{\max} , K_{\min} and ΔK determined for both the a and c crack growth directions⁴. The ΔK is used in conjunction with a crack growth rate equation (e.g., Forman's equation with acceleration⁵) in a standard cycle-by-cycle algorithm which increments the crack length until failure. The program is terminated when at least one of the following criteria is satisfied: the final crack size is reached, instability occurs, the number of load blocks is completed, or no crack growth occurs after one full application of the spectrum. Note that short crack effects and crack closure effects have not been addressed in the versions of METLIFE received so far.

The assumptions presented above impose certain limitations on the types of analyses that can be performed using METLIFE. Specifically it is limited to flat, Mode I cracks which are small with respect to the overall dimensions of the cross-section. Nevertheless, the types of cracking seen at F-111 DADTA locations can be categorised as such, and the coupon test experiments are even more representative of these assumptions. A full technical description of METLIFE (including the cyclic plasticity algorithm) can be found in (Ball 2005a), while its operation is described in (Ball 2005b) and its applicability to the RAAF F-111 DADTA program is found in (Lockheed Martin 2001).

METLIFE has been shown in (Lockheed Martin Aeronautics Company 2001) to produce results very similar to AFGROW and ADAMSys for standard LEFM cases. The feature of using a Green's function approach to determine the geometry factors for an arbitrary stress distribution was used to good effect in (Walker 2004) where a good correlation between the analysis and test was achieved.

The problem with METLIFE occurs when the notch plasticity feature is used. As detailed in (Swanton 2005) an arbitrary load sequence involving a "sawtooth" pattern of cyclic compression-compression cycles produced an erroneous stress-strain response in METLIFE. Some sequences did not produce the error, but it was clear that a problem exists in the code.

⁴ The 'c' dimension is measured along the width of the specimen (coincident with the x -axis in METLIFE), whilst the 'a' dimension is measured across the depth, or thickness, of the specimen (coincident with the z -axis in METLIFE). Also see footnote 1 on 31.

⁵ This takes the form of the Forman equation except has an acceleration factor term included.

These problems have been conveyed to Dr Ball at Lockheed. An updated version of the program (METLIFE V1.3.17) was obtained in August 2005, but it has not yet been checked to confirm if the problems have been resolved.

5.5 CG90

CG90 (McDonnell Douglas 1991a) is a crack growth analysis program that calculates crack growth life starting from a given initial flaw size through to failure of the component. This software was developed by McDonnell Douglas (now Boeing) during the time when it was conducting a damage tolerance analysis for the Swiss F/A-18 fleet. CG90 was not created as a new program but rather it was the evolution of the original crack growth software CNTKM8 which was also developed by McDonnell Douglas. CNTKM8 was the original program provided to Australia for use in 1985. Since then the program has gone through a number of different modifications and name changes as it evolved into the software that is now known as CG90. One of the major additions that differentiate CG90 from its predecessors was the incorporation of the Newman-Raju (Newman and Raju 1983) stress intensity solution for part-through crack configurations. The crack growth model used in this software to determine the crack growth is known as the contact stress model (Leist and Saff 1981) which was also developed by McDonnell Douglas specifically for predicting crack growth in metallic structure.

The contact stress model is based on the assumption that load interaction effects in spectrum crack growth are controlled by crack surface contact as the crack grows through prior plastic zones. The effect of crack surface contact during a load cycle is to restrict the change in crack opening displacements during the cycle, reducing the portion of the load cycle effective in propagating the crack. After overloads, larger residual displacements are left on the crack surface, further reducing the load range effective in propagating the crack and thus retarding crack growth.

From an analysis of crack surface displacements during loading and unloading, the potential interference of the crack surface is determined. By performing an elastic-plastic analysis of the stresses, the contact stress behind the crack tip is found⁶. The effective stress intensity is determined and this information is used to calculate the crack growth behaviour for each cycle. The incremental effects of growth are then summed up to define the crack growth for an entire spectrum.

The software implementing the contact stress model accounts for retardation effects, including delayed retardation, effects of single and multiple overloads on retardation, the effect of stress ratio on constant amplitude crack growth and the effect of compressive loads. It is capable of predicting crack growth under random loads spectra because the model accounts for the history of prior load cycles as preserved in the distribution of yielded material behind the advancing crack tip. Many crack geometries may be included through the use of different SIF solutions.

⁶ Crack surface contact effects are accounted for through implementation of a K_{eff} versus K_{app} curve, where K_{app} is the total applied stress intensity and K_{eff} is the corresponding effective stress intensity.

There are several common solution types built into CG90 for crack growth analysis. The geometry, flaw and loading types associated with these solution types are listed below:

In-built geometry types:

1. Hole in a plate
2. Plate without a hole
3. Cylinder

Flaw types:

1. Single corner from hole (different a and c)
2. Double corner from hole (different a and c)
3. Single embedded from hole (different a and c)
4. Double embedded from hole (different a and c)
5. Single through-thickness crack from hole
6. Double through-thickness crack from hole
7. Surface flaw in plate
8. Centre crack in plate
9. Single corner crack in plate (different a and c)
10. Single embedded crack in plate (different a and c)
11. Single through-thickness crack in plate
12. Surface flaw in cylinder (different a and c)
13. Single through-thickness flaw in cylinder

Loading Types:

1. Thru stress
2. Bearing stress
3. Thru plus bearing stress
4. User defined stress
5. Bending stress
6. Thru plus bending stress

CG90 checks for failure after each load level application. It is possible that a crack could grow to the edge of a part without the critical SIF value being exceeded; this is considered one form of failure. Usually however, failure occurs when the applied SIF K exceeds the critical value.

CG90 was used on a very limited basis by the F/A-18 IFOSTP fatigue group to calculate the crack growth of defects found during the F/A-18 aft fuselage and empennage fatigue test. CG90 is limited for use with F/A-18 tasks only.

5.6 FASTRAN

FASTRAN was developed by Newman when he was with NASA (Newman 1981a). It implements a plasticity-induced crack closure model. The closure model was based on the Dugdale strip yield model (Dugdale 1960), but the model was modified to leave residual deformation in the wake of the crack. The crack opening stress was calculated using an analytical model that was applied to discretised elements in front of the crack tip (Newman 1981a). The plane stress and plane strain conditions were simulated by using a constraint

factor on tensile yielding to account for the three-dimensional effect. FASTRAN also accounts for the short crack effect (Newman and Phillips 1999), through the evolution of the residual plastic deformation in the crack surface behind and the crack tip. For short cracks there is little residual plastic deformation, which means the crack closure effect is less pronounced. As a result, the crack opening stress will be lower, leading to a higher effective SIF range and a higher crack growth rate. Another approach adopted in FASTRAN to account for the short crack effect was to implement a variant of a model proposed by El Haddad et al (1979).

Figure 14 shows a flowchart of FASTRAN implementation. Central to the algorithms is the module for the calculation of the crack opening stress S_o . Once that is determined, the effective SIF range is calculated and used to compute the crack growth rate. As this module is computation-intensive, the crack opening stress is not calculated for each cycle; instead, it is only calculated (i) for the first cycle; (ii) for every predetermined number of cycles; (iii) if an overload or underload is encountered; and (iv) if the accumulated crack growth since the previous calculation of the opening stress exceeds a certain value. The actual calculation of the crack opening stress involves the determination of the plastic deformation for the material in the crack tip plastic zone and that in the crack wake, as well as the stresses in those regions.

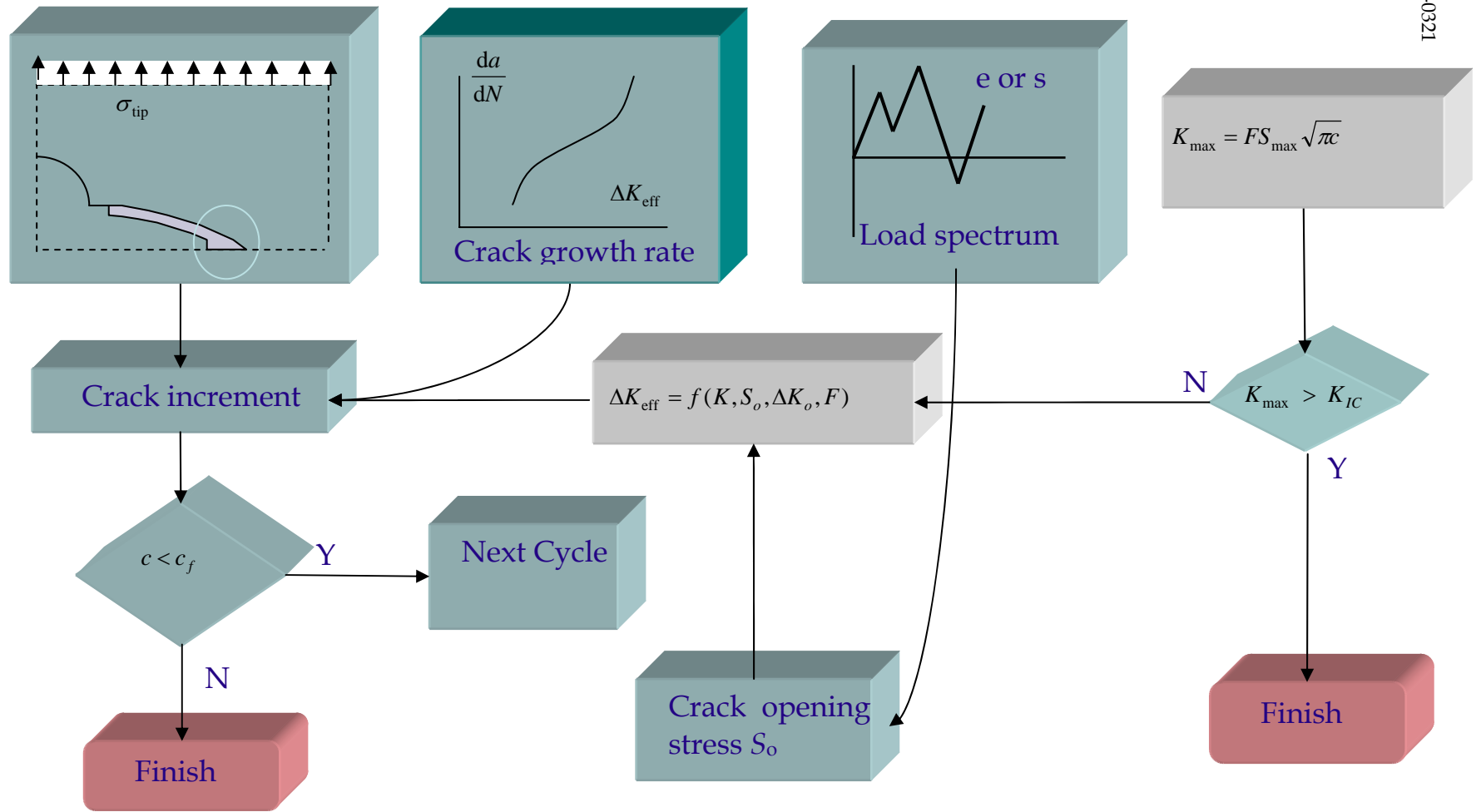


Figure 14 A flow chart for fatigue crack growth analysis using the plasticity-induced crack closure model

5.6.1 Crack Opening Stress under Constant Amplitude Load

Based on numerical results, Newman (1984) developed the following equation for crack opening stress under constant amplitude loading defined by S_{\min} and S_{\max}

$$S_o / S_{\max} = \begin{cases} A_0 + A_1 R + A_2 R^2 + A_3 R^3, & \text{for } R \geq 0, \\ A_0 + A_1 R, & \text{for } R \leq 0. \end{cases} \quad (20)$$

Thus, the crack opening stress is defined as a function of the maximum stress and the load ratio. If the opening stress calculated from this equation is smaller than the minimum stress S_{\min} , then $S_o = S_{\min}$. The coefficients in Equation (20) are given as

$$A_0 = (0.825 - 0.34\alpha + 0.05\alpha^2) [\cos(\pi S_{\max} / 2\sigma_0)]^{1/\alpha}$$

$$A_1 = (0.415 - 0.071\alpha) S_{\max} / \sigma_0$$

$$A_2 = 1 - A_0 - A_1 - A_3$$

$$A_3 = 2A_0 + A_1 - 1$$

where α is a constraint factor representing the stress state at the crack tip, and σ_0 is the flow stress, which is the average of the uniaxial yield stress σ_y and the ultimate stress σ_u .

Figure 15 and Figure 16 plot normalised crack opening stress calculated from Equation (20) for simulated plane stress condition ($\alpha = 1$) and plane strain condition ($\alpha = 3$), respectively. It can be seen clearly that the effect of R on the opening stress is more pronounced when $R \geq 0$ where there is an almost linear relationship between the normalised opening stress and R . At negative stress ratios, the opening stress has a weaker dependence on the stress ratio, especially when the loading level is low.

Figure 17 shows the influence of constraint factor on the crack-opening stress, for a stress level of $S_{\max} / \sigma_0 = 0.4$. Clearly it shows that under plane strain condition the crack-opening stress is much lower than that under plane stress condition, which is consistent with the experimental observation that the size of the crack tip plastic zone size for plane strain is only one third of that for plane stress.

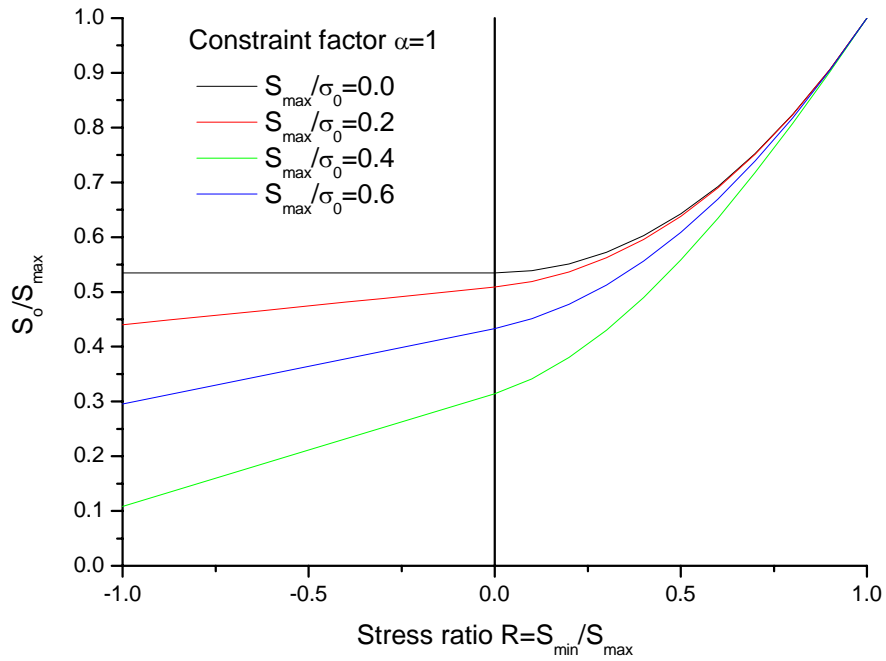


Figure 15 Normalised crack opening stress under constant amplitude loading and simulated plane stress condition. ($\alpha = 1$)

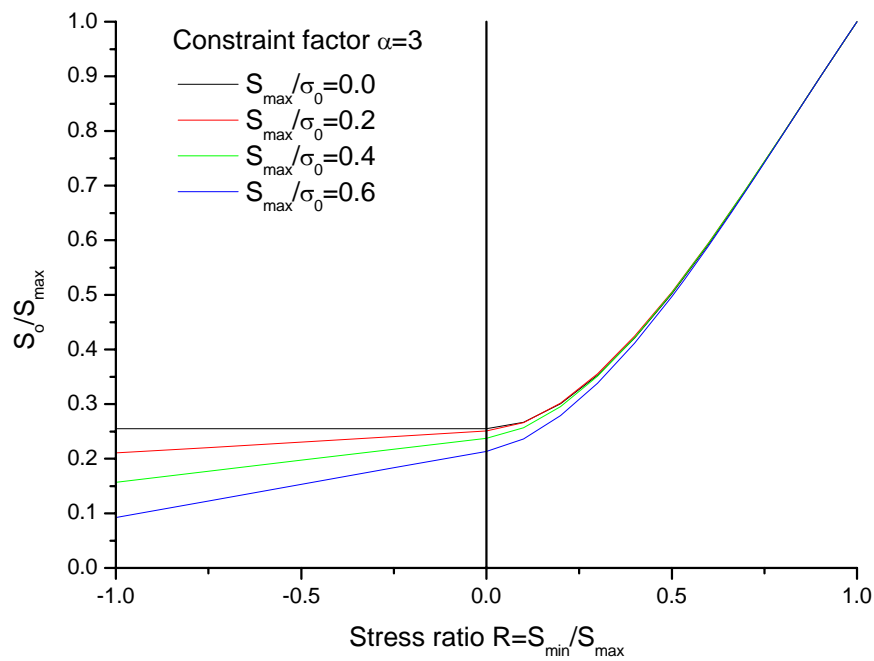


Figure 16 Normalised crack opening stress under constant amplitude loading and simulated plane strain condition. ($\alpha = 3$)

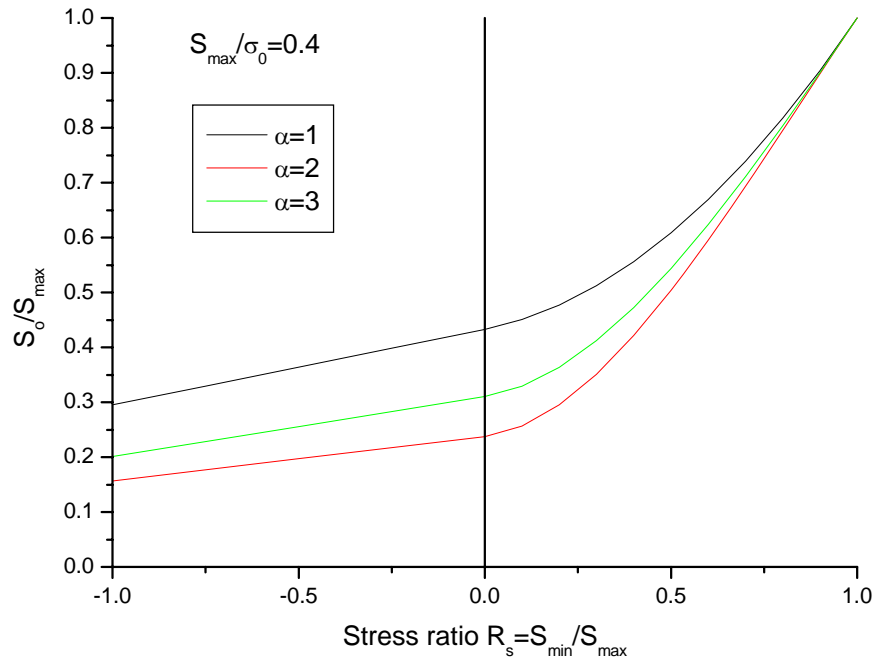


Figure 17 The influence of constraint factor on crack-opening stress. $S_{\max} / \sigma_0 = 0.4$.

For variable amplitude loading, FASTRAN implements an analytical crack closure model as developed in (Newman 1981b) which is based on the Dugdale strip yield model (Dugdale 1960). The Dugdale model was modified to leave plastically deformed material in the wake of the crack.

5.6.2 Crack Opening Stress under Variable Amplitude Load

A detailed description of the model used for the calculation of the crack opening stress under variable amplitude load can be found in (Newman 1981a), but the salient points may be outline here in terms of a central-crack tensile (CCT) specimen:

- There is residual deformation in the crack wake;
- This residual deformation causes premature crack closure during the subsequent unloading;
- Upon reloading, the crack tip remains closed until the tensile load reaches a certain value, the opening load.

Based on the assumptions that (1) the bulk of the specimen is linearly elastic; (2) the material that undergoes plastic deformation is rigid-perfectly plastic (this includes the material in the crack tip plastic zone and that in the crack wake), the plastic zone near the crack tip and the crack wake was divided into N_e elements, each behaving rigid-plastically. As schematically illustrated in Figure 18, if the length of the element, L_j , is greater than or equal to the current crack surface displacement V_j , then the element is in contact, meaning the crack is closed at

that point; otherwise that element is open. If the element is in contact, a stress σ_j is applied to it to enforce the compatibility $V_j = L_j$, to avoid the impossible condition of $V_j < L_j$. Using the principle of superposition, the crack surface displacement at any point i is the resultant displacements caused by the external stress S and the internal stresses σ_j , i.e.

$$V_i = Sf(x_i) - \sum_{j=1}^{N_e} \sigma_j g(x_i, x_j), \quad (21)$$

where $f(x_i)$ and $g(x_i, x_j)$ are the influence functions for the applied stress S and the internal induced stress σ_j , respectively. Physically, $f(x_i)$ represents the displacement caused at point i by a unit external stress and $g(x_i, x_j)$ represents the displacement caused at point i by a unit internal stress acting at point j . By imposing the compatibility condition $V_j = L_j$, we get the following system of equations for the unknown stresses σ_j

$$\sum_{j=1}^{N_e} \sigma_j g(x_i, x_j) = Sf(x_i) - V_i \quad (22)$$

Once the contact stresses corresponding to the applied minimum stress is thus determined by setting $S = S_{\min}$ in the above equation, the crack opening stress S_{open} may be calculated by setting the stress intensity factor due to $S_{\text{open}} - S_{\min}$ equal to that due to the contact stresses $K(\sigma_i)$, i.e.

$$K(S_{\text{open}} - S_{\min}) = K(\sigma_i),$$

in which the brackets mean "function of".

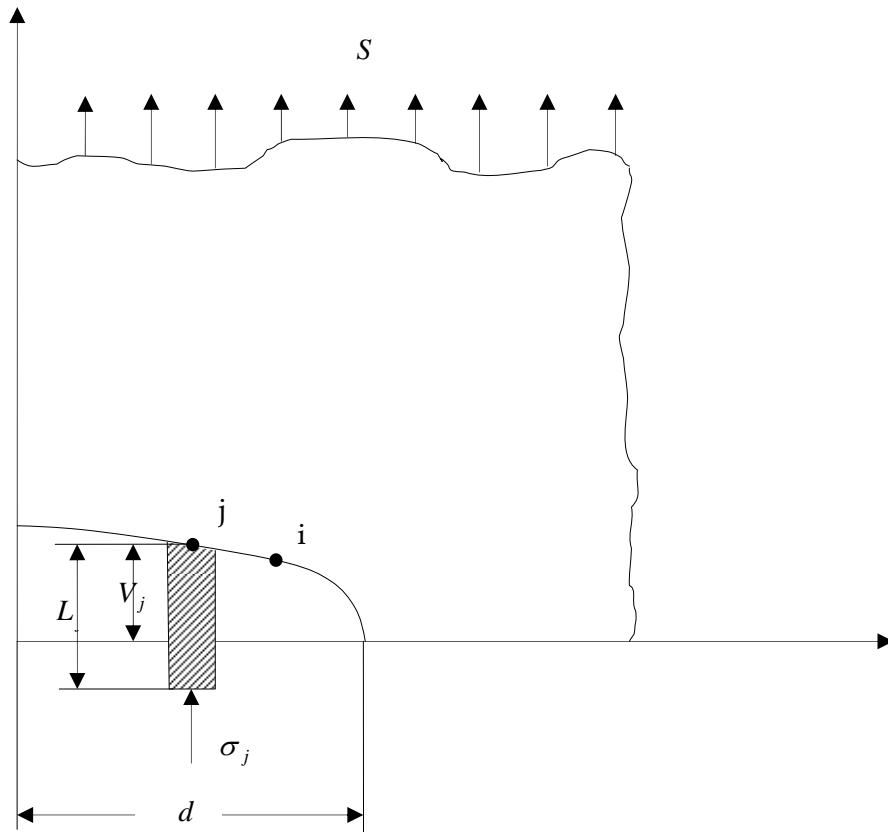


Figure 18 Schematic of loading and coordinate system for the analytical plasticity-induced crack closure model (after Newman 1981a)

5.6.3 Crack Growth Rate Equation

Newman modified Paris law to account for the threshold range where long cracks stop growing and the limit range when fracture is about to take place. The crack growth rate equation implemented in FASTRAN 3.8 is as follows

$$da / dN = C(\Delta K_{\text{eff}})^n G / H \quad (23)$$

where C and n are two material constants, e.g., $C = 1.65 \times 10^{-9}$, $n = 3.045$ for D6ac steel. G is a function of the threshold stress-intensity factor range and the effective stress-intensity factor range

$$G = 1 - (\Delta K_0 / \Delta K_{\text{eff}})^p \quad (24)$$

where p is a material constant, and ΔK_0 is the (long crack) threshold SIF range. If the applied SIF range is below the threshold SIF range, no crack growth takes place; hence it is a parameter to be determined experimentally, and depends on the material and the stress-ratio. If the applied effective SIF range approaches the threshold, the function G diminishes, thus reducing the crack growth rate to zero, simulating the threshold phenomenon. On the other

hand, H is a function of the maximum stress-intensity factor and the cyclic fracture toughness, defined as

$$H = 1 - (K_{\max} / C_5)^q. \quad (25)$$

Here, q is a material constant and K_{\max} is the maximum applied SIF. C_5 is the cyclic fracture toughness of the material. Under normal fatigue load, $K_{\max} < C_5$, and when K_{\max} approaches C_5 , the function H diminishes, thus causing the crack growth rate to approach infinity, simulating the fracture process.

With functions G and H thus defined, it is possible to use the crack growth rate equation (23) to simulate the well known sigmoidal shape often observed in fatigue crack growth rate data plotted against SIF range.

5.6.4 Crack-Tip Plastic Zone

Under fatigue load, plastic deformation takes place at the crack tip. In FASTRAN, the plastic zone size is determined by the assumption that stress singularity disappears at the fictitious crack tip $a + \rho$, where ρ is the plastic zone size. Hence the SIF due to applied maximum stress is equated to the SIF due to the distributed stress in the plastic zone ahead of the fictitious crack tip. Once this is determined, the fictitious crack length is used for the calculation of the stress intensity factor, i.e.

$$\Delta K_{\text{eff}} = \beta \Delta S_{\text{eff}} \sqrt{\pi(a + \rho)}, \quad (26)$$

where $\Delta S_{\text{eff}} = S_{\max} - S_{\text{open}}$ is the effective stress range, and S_{open} is the crack opening stress.

5.6.5 Constraint Factor α for Three-Dimensional Effect

The flow stress σ_0 used in FASTRAN is an average of the yield stress and the ultimate strength, $\sigma_0 = (\sigma_y + \sigma_u) / 2$, but the effective flow stress used for the calculation of plastic zone size is raised by a factor of α , in order to account for the effect of the state of stress on the plastic-zone size. Based on finite element analyses performed on an elastic, perfectly plastic material, the constraint factor α was determined to be 3 for simulated plane strain, and 1 for plane stress condition (Fleck and Newman 1988), but essentially, the constraint factor is a scaling factor to account for the differences in shape and size of the plastic zone in plane stress and plane strain. In practice, this factor is adjusted to correlate the experimental crack growth rate data to the crack growth rate equation (23), and the same factor is then used for the prediction of crack growth for specimens of the same thickness as that from which the growth rate are obtained.

5.6.6 Short Crack Model

In FASTRAN3.8, the short crack effects, i.e., that observation that short cracks grow faster under the same applied stress intensity factor range and they may grow below the long crack

threshold, are modelled using the approach proposed by El Haddad and co-workers. The basic concept is to modify the SIF by increasing the physical crack size by a_0 , where a_0 is considered a material-dependent constant, and may be estimated from the limiting conditions of crack length where the nominal stress approaches the fatigue limit when $a \rightarrow 0$ and $\Delta K = \Delta K_0$ (Suresh and Ritchie 1984)

$$a_0 \approx \frac{1}{\pi} \left(\frac{\Delta K_0}{\Delta \sigma_e} \right)^2. \quad (27)$$

With this modification of the crack length, the SIF range can be calculated as

$$\Delta K = \beta \Delta S \sqrt{\pi(a + a_0)}.$$

Here a_0 could be interpreted as the smallest crack size that can be characterised at the threshold in terms of LEFM. In El Haddad's model, it was explicitly stated that the geometry factor β in this case should be calculated using the physical crack size c instead of the fictitious crack length $a + a_0$.

A similar approach was implemented in FASTRAN. Instead of c_0 defined in Equation (27), a portion of the Dugdale cyclic-plastic-zone size ω is added to the crack length (Newman and Phillips 1999). Hence the plastic zone size corrected effective SIF range becomes

$$\Delta K_{\text{eff}} = (S_{\text{max}} - S_0) \beta (d/w) \sqrt{\pi(c + \omega/4)} \quad (28)$$

where $\beta = \beta((c + \omega/4)/w)$ is the plastic zone corrected geometry factor. It should be noted that this treatment differs from El Haddad's proposal in which the usual geometry factor is used. Since ω is only significant in the short crack regime, its effect on long crack is negligible. In FASTRAN implementation, Equation (28) is used uniformly for short cracks and long cracks. An evaluation together with comparison to the experimental data is available in (Newman and Phillips 1999).

5.7 CGAP

In the structural integrity management of F111 aircraft, cold proof load tests (CPLT) are conducted periodically. During these severely loaded tests, plastic deformation may occur in components such as the WPF. Initially, this type of damage tolerance analyses involving notch plasticity were carried out using the software METLIFE from Lockheed Martin, but the following three factors has motivated the development of CGAP within AVD: (1) a serious numerical problem was uncovered in METLIFE which incorrectly modelled the stress-strain response under certain loading conditions. As DSTO does not have the source code, the correction of the error depends on the good will and priority of Lockheed Martin. CGAP would address this issue; (2) the plasticity model in METLIFE, when correctly implemented, does not capture the transient behaviours such as plastic strain ratchetting and mean stress relaxation as shown in Figure 5e and f (p. 19), which may lead to a shift up or down of the hysteresis loops subsequent to a severe load cycle such as those in CPLT. CGAP would implement a more advanced cyclic plasticity model; (3) It was judged that the plasticity-induced crack closure model would provide a better and more robust mechanism for accounting the effect of load sequence, over- and under-load, etc, than the Willenborg or

Wheeler model implemented in METLIFE. As an added benefit, CGAP was developed with a graphical user interface for ease of use and case management.

To date, all three issues have been address in CGAP (Hu and Walker 2006b; Hu and Walker 2006a). A numerical capability has been developed for the analysis of crack growth involving notch plasticity. Preliminary results from CGAP show an encouraging trend compared to experimental data, but further work needs to be carried out to validate the stress distribution against test data or FE results, to assess the effectiveness of CGAP in dealing with various over- and under-loading conditions, and to validate the model results against test data.

CGAP is MS Windows-based, and it provides a database capability for the management of geometry, material, load and solution information. Apart from the deterministic crack growth, it also provides a capability in probabilistic crack growth analysis based on the Monte Carlo method, with randomised initial crack size, crack growth rate and the peak spectrum stress. In addition, CGAP also interfaces seamlessly with FASTRAN3.8.

Compared with FASTRAN, the key technical issues addressed in CGAP were the determination of the stress distribution ahead of a notch root, based on Neuber's rule and an Armstrong-Chaboche constitutive model and the implementation of Green's function solution for several crack configurations.

5.7.1 Cyclic Plasticity Model

To model the transient as well as the steady state elastic-plastic response as shown in Figure 5, an Armstrong-Chaboche (1986) type constitutive model was implemented in CGAP to describe the notch root stress-strain response. In summary, the model may be described by the following set of equations, representing the yield surface, the evolution rule for the back stress, which reflects kinematic hardening, and the equation for isotropic hardening

$$f = J_2(S_{ij} - X_{ij}) - R(p) - \sigma_y = 0 \quad (29)$$

$$\dot{X}_{ij} = k_1 \dot{\epsilon}_{ij}^p - k_2 X_{ij} \dot{p} \quad (30)$$

$$R = R_s (1 - e^{-bp}) \quad (31)$$

where f represents the yield surface, and S_{ij} is the deviatoric stress tensor, i.e.

$$S_{ij} = \sigma_{ij} - \sigma_{kk} / 3.$$

Here and henceforth, the convention of summation over repeated indices is assumed, e.g.

$$\sigma_{kk} = \sigma_{11} + \sigma_{22} + \sigma_{33}.$$

Geometrically, the back stress tensor X_{ij} represents the centre of the yield surface in the stress space, and physically it represents the effect of dislocation pile-up at grain boundaries on the subsequent yield strength of the material. The internal stresses created by the pile-up in one loading direction reduce the stress required to cause yield in the opposition loading direction, hence kinetically harden or soften the material. The uniaxial yield stress of the material is σ_y ,

and R is a function of the equivalent plastic strain p representing the effect of isotropic hardening. J_2 is the function defining the equivalent stress

$$J_2 = \sqrt{\frac{3}{2}(S_{ij} - X_{ij})(S_{ij} - X_{ij})}$$

The superposed dot “.” signifies the differentiation with respect to time. The total strain rate $\dot{\epsilon}_{ij}$ may be decomposed into an elastic part and a plastic part

$$\dot{\epsilon}_{ij} = \dot{\epsilon}_{ij}^e + \dot{\epsilon}_{ij}^p$$

k_1, k_2, b and R_s are parameters to be derived from experimental data. It should be pointed out that isotropic hardening can be turned off by setting $R_s = 0$.

To determine these parameters from the steady-state cyclic stress-strain curve, the constitutive equations need to be recast for uniaxial loading. The conditions for uniaxial loading are $\sigma_{ij} = 0$ except $\sigma_{11} = \sigma \neq 0$; $\dot{\epsilon}_{22}^p = \dot{\epsilon}_{33}^p = -\frac{1}{2}\dot{\epsilon}_{11}^p$, $X_{22} = X_{33} = -\frac{1}{2}X_{11}$, and $S_{22} = S_{33} = -\frac{1}{2}S_{11}$ (Chaboche 1986; Hu, Wang and Barter 1999), by considering plastic incompressibility. Let $X_{11} \equiv X$, $\dot{\epsilon}_{11}^p = \dot{\epsilon}^p$, the evolution rule of the back stress, Equation (30), can be rewritten as

$$\dot{X} = \frac{2}{3}k_1\dot{\epsilon}^p - k_2X\dot{p} = C\dot{\epsilon}^p - \nu g X \dot{\epsilon}^p \quad (32)$$

where the relation $\dot{p} = \nu \dot{\epsilon}^p \sqrt{\frac{2}{3}\dot{\epsilon}_{ij}^p \dot{\epsilon}_{ij}^p} = |\dot{\epsilon}^p| = \nu \dot{\epsilon}^p$ was introduced, with $\nu = \pm 1$ depending on the loading direction. The parameters C and g are used for clarity and

$$k_1 = \frac{3}{2}C$$

$$k_2 = g$$

If the expected strain is large, e.g., ≈ 0.02 , then multiple back stresses need to be introduced to obtain an accurate representation of the stress-strain curve. Taking three back stresses, the evolution rule can be written as

$$\dot{X}_i = \frac{2}{3}k_{1i}\dot{\epsilon}^p - k_{2i}X_i\dot{p} = C_i\dot{\epsilon}^p - \nu g_i X_i \dot{\epsilon}^p \quad (i=1,2,3),$$

And the effective back stress is given by the summation of the components

$$X = X_1 + X_2 + X_3$$

With these developments, the relationship between the amplitude of cyclic stress and the parameters defining the model can be derived as (Hu, Wang and Barter 1999)

$$\sigma_a = \sum_{i=1}^3 \frac{C_i}{g_i} \tanh(g_i \epsilon_a^p) + \sigma_y.$$

Figure 20 illustrates the difference between the one-back stress and three-back stress models in representing the same set of experimental data. Clearly, the single back stress model was not able to capture the hardening characteristics of the 7050 aluminium alloy.

In CGAP, this model is used in combination with Neuber's rule to determine the notch root stress and strain.

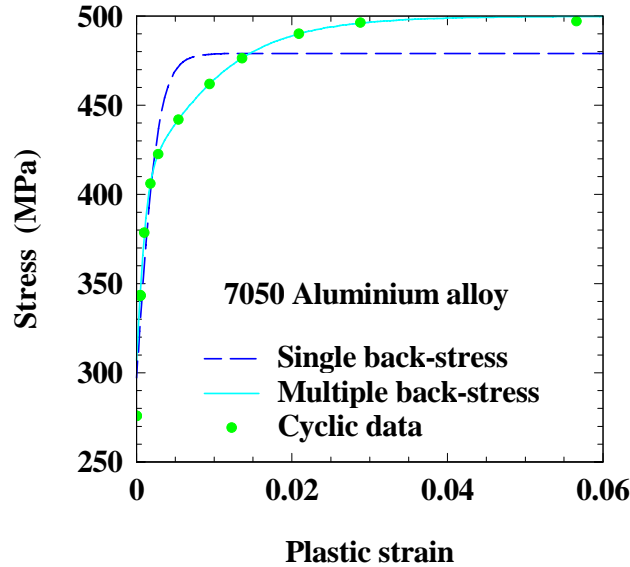


Figure 19 The determination of material constants for the cyclic plasticity model. A single back stress is only suitable for modelling a small strain range

5.7.2 Stress Distribution Ahead of a Notch Root

There are two approaches to determining the elastic-plastic stress distribution ahead of a notch root, that of single load path and multiple load path (Ball 2005a). With single load path, the structure being analysed is isolated from the surrounding structures, and the load applied to it remains unchanged as crack progresses. Hence, if the material yields at the notch root, load carried by the yield zone is reduced and it is shifted to the material ahead of the yield zone, thus cause further yielding. The concept of multiple load path is based on the understanding that when a component within a structure weakens, either through yielding or crack growth, the external load tends to be picked up by the surrounding components. As an approximation, the load shedding from yielding is not redistributed to the material ahead of the plastic zone. This assumption greatly simplifies the procedure for determining the stress distribution ahead of a notch root, but its validity needs to be investigated further. The procedure used in multiple load paths is detailed below.

For a given component with a generic notch, the crack plane may be divided into $N - 1$ segments, where N is the number nodal points, as shown in Figure 20. The segments do not need to be uniform. In fact, in order to accurately represent the stress distribution, finer grids should be used in the area where the stress variation is significant, i.e., near the notch root. The hypothetical elastic stress distribution is assumed to be known, either from experimental measurement or the finite element analyses. Each grid point is then treated as a point at notch root, so that the response stress-strain may be determined using the constitutive equations and Neuber's rule. Figure 22 shows the stress-strain response of D6ac material subjected to the CPLT sequence shown in Figure 21. In CGAP, the stress-strain response at each grid point is

computed for each applied stress, and the local stresses are used to compute the SIF range using Green's function approach.

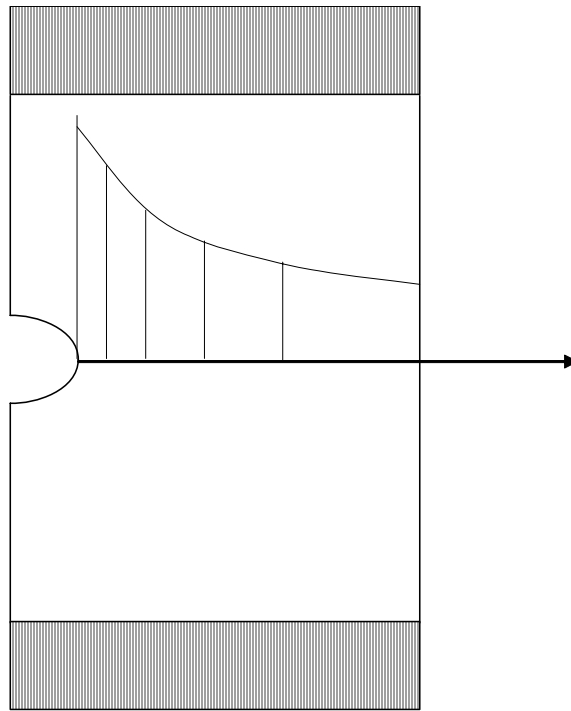


Figure 20 A plate component containing a generic notch subjected to remote tensile loading

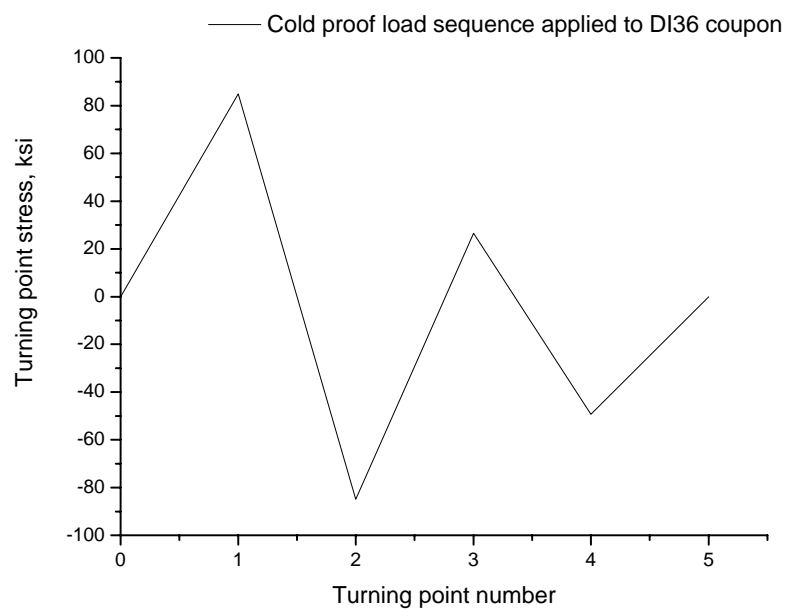


Figure 21 The cold proof load sequence applied to Damage Item 36 (DI36) coupon

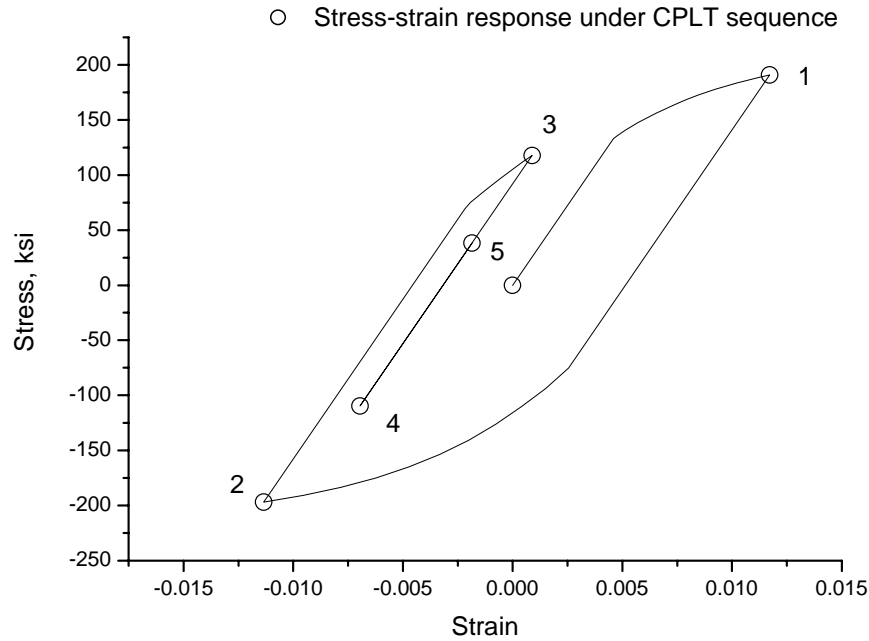


Figure 22 Cyclic stress-strain response under CPLT sequence shown in Figure 21

5.7.3 Weight Function/Green's Function Approach

The maximum stress-intensity factor is calculated using the Green's function approach. Based on an analytical function representation of elastic fields for isotropic materials, Bueckner (1970) showed that the stress intensity factor due to an arbitrary set of applied loads can be obtained by integrating over the crack length a product of these loads and an appropriate Green function, i.e.

$$K_{\max} = \int_0^a \sigma_{yy}(x)W(x)dx \quad (33)$$

where $\sigma_{yy}(x)$ is the local (possibly elastic-plastic) stress distribution over the crack length obtained *without* considering the existence of the crack. Hence, for a given geometry, a hole in a plate, for instance, the stress distribution will be the same irrespective of the type of crack emanating from the hole. The effect of the crack type is reflected through the corresponding Green's function $W(x)$, i.e., the Green's function will be different for a through-thickness crack, a corner crack or a surface crack emanating from the edge of the same hole in the same plate.

Therefore, for a given geometry, the stress distribution corresponding to each maximum load is determined, and it is then used in combination with the Green's function corresponding to the type of crack to determine the maximum stress-intensity factor.

Equation (33) may be re-written to give the more familiar format of stress-intensity factor formula

$$K_{\max} = \int_0^a \sigma_{yy}(x)W(x)dx = \beta S_{\max} \sqrt{\pi a}$$

with

$$\beta = \frac{1}{S_{\max}} \int_0^a \sigma_{yy}(x)W(x)dx \quad (34)$$

The exact form for β depends on the actual crack type, e.g., for corner cracks and surface cracks, the integration will be over the crack surface instead of the length, but the concept is exactly the same.

Figure 23 shows a comparison of crack growth curves for a through-thickness crack emanating from the edge of a hole in a plate, subjected to constant amplitude loading, at different stress levels. The load ratio is 0.1 in all cases, and the notch stresses are below yield stress. The comparisons demonstrate the capability of CGAP in predicting the crack growth behaviour in the limiting case of LEFM (Hu and Walker 2006b).

Figure 24 plots the experimental and the numerical result for a single through-thickness crack subjected to a spectrum loading. Due to the severity of the CPLT sequence, plastic deformation takes place at the notch root and in its vicinity. The notch root stress-strain response, as calculated by CGAP, is plotted in Figure 22, where the maximum stress is 183.78 ksi. In contrast, the hypothetical elastic stress at the notch root is about $3 \times 84.9 = 254.7$ ksi. Therefore, if notch plasticity is ignored, a much higher stress is seen at the crack tip, hence results in a faster crack growth. Figure 24 also compares the results from CGAP to those obtained from FASTRAN3.8 and METLIFE, and it appears that CGAP was able to produce a better prediction than the other codes, although it should be noted that the version of METLIFE used for this prediction still has the implementation error in the calculation of notch stress and strain, while FASTRAN3.8 does not model notch plasticity explicitly.

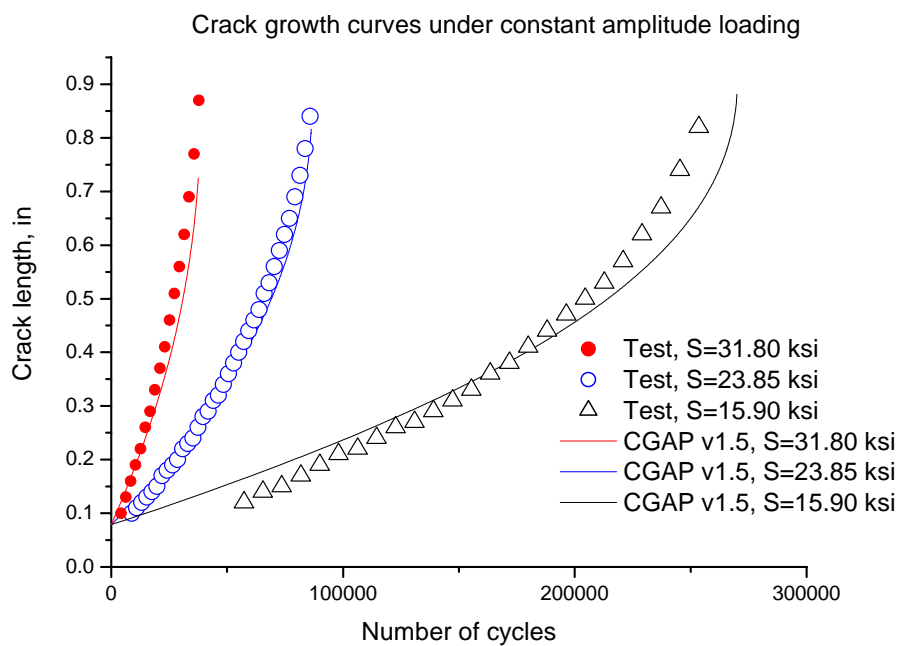


Figure 23 Crack growth curves for a single through-thickness crack emanating from the edge of a central hole in a plate subjected to constant amplitude loading

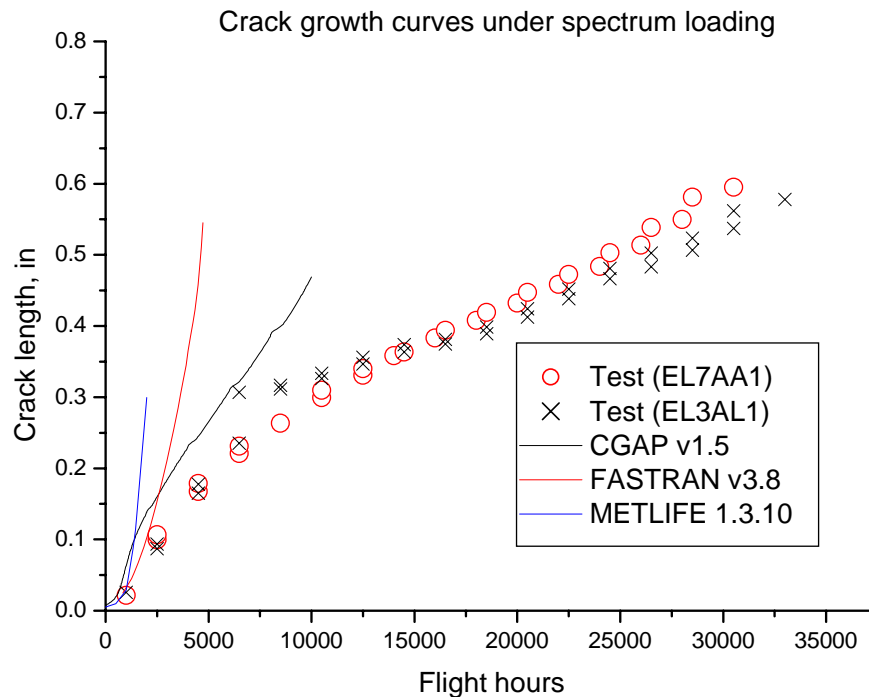


Figure 24 Crack growth curves for a single through-thickness crack emanating from the edge of a central hole in a plate subjected to CPLT sequence and four blocks of service spectrum, each block representing 500 flight hours

5.8 Other Developments in Fatigue Crack Growth Modelling

In addition to the above methods and tools based on classical fracture mechanics, other approaches have been explored within AVD for the assessment of fatigue crack growth in aircraft structures, noticeably the work of Molent and Jones et al. (Molent, Jones, Barter and Pitt 2006). The log-linear approach, or the exponential growth law, is based on the assumption that the crack growth rate (per cycle or per block of loading) is directly proportional to the crack length; on the other hand, the effective block approach treats each block of the load spectrum as an equivalent single cycle, so the spectrum loading is reduced to equivalent constant amplitude loading. These approaches are briefly summarised below, but additional work needs to be carried out to independently verify the methodology and validate the predictive capability.

5.8.1 Modelling Crack Growth under Spectrum Loading

5.8.1.1 Modelling Crack Growth by an Exponential Function

Researchers at AVD-DSTO (Barter, Athinotis and Lambianidis 1990; Barter, Bishop and Clark 1991; Barter 1998; Athinotis, Barter and Clark 1999; Barter 2003; Barter, Molent, Goldsmith and Jones 2005; Molent, Jones, Barter and Pitt 2006) have suggested that fatigue cracks

subjected to service spectrum loads of fighter aircraft grow at approximately a constant exponential rate, i.e.

$$a = a_i e^{\beta_L N} \quad (35)$$

where a is the crack depth, a_i is the initial crack depth, N is the crack growth life in cycles and β_L a regression parameter. Similar findings have been reported for constant amplitude data, see (Head 1953; Frost and Dugdale 1958; Liu 1963; Frost, Marsh and Pook 1974; Rose and Wang 2001). Fitting of Equation (35) to fatigue data determines a_i and β_L that produces the least squared-of-error fit to the data. The regression parameter β_L is a function of material properties, crack and component geometry, and load spectrum.

An example is shown here using the fatigue tests result from (Barter 2003). These tests were carried out on 7050-T7451 aluminium alloy specimens subjected to variable amplitude loading of the IARPO3a spectrum with various peak stress levels S_{peak} . These data, as plotted in Figure 25, have been reassessed here based on the assumption that the crack length versus the number of programs of loading follows an exponential law.

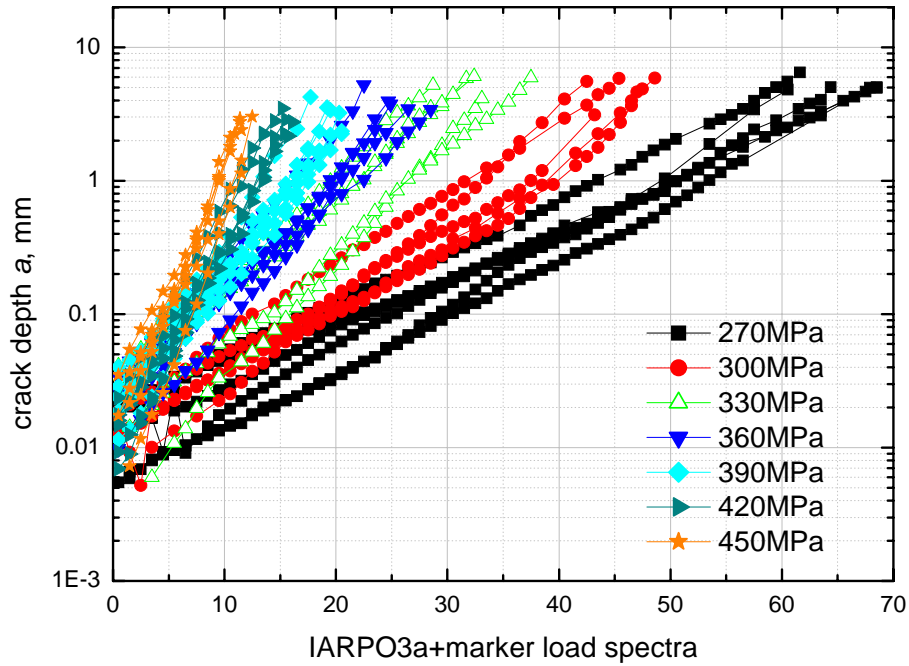


Figure 25 Experimental fatigue crack growth curves for 7050-T7451 aluminium alloy specimens subjected to IARPO3a + marker load spectrum, crack depth a versus blocks of spectrum loading

For a given load spectrum, β_L was found to be related to the peak stress S_{peak} through

$$\beta_L = A_L S_{\text{peak}}^{q_L} \quad (36)$$

where A_L and q_L are regression parameters. The relation between β_L and S_{peak} is plotted in Figure 26 for the results in Figure 25. A variation in the fit of a single line based on regressed

values of β_L and A_L at a given S_{peak} can be observed, and can be modelled statistically by modelling the statistical variation in A_L .

Based on this finding, Equation (35) can be extended by replacing β_L using Equation (36), so that a for various S_{peak} can be correlated by $S_{\text{peak}}^{q_L} N$

$$\ln(a) = \ln(a_i) + A_L (S_{\text{peak}}^{q_L} N) \quad (37)$$

The fatigue test data are re-plotted in Figure 27, using Equation (37). This equation can then be used to predict the crack length for a scaled spectrum which has not been tested. The advantage of the log-linear model is its simplicity. The classical complex problem of fatigue crack growth is reduced to one determining one model parameters: β_L or A_L , and once this parameter is determined, the crack growth curves for this crack configuration and load spectrum (may have different peak stress) will be determined. With this appealing simplicity comes a number of uncertainties and one of them is the applicability of β_L determined from one spectrum to a completely different spectrum.

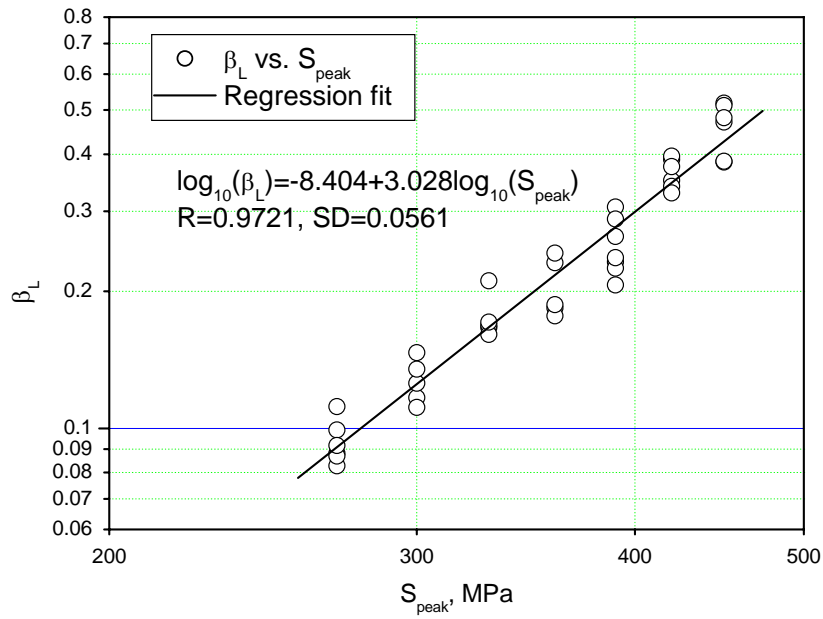


Figure 26 The dependence of β_L on the peak stress of the spectrum, according to Equation (36).

$$A_L = 10^{-8.404}, q_L = 3.028$$

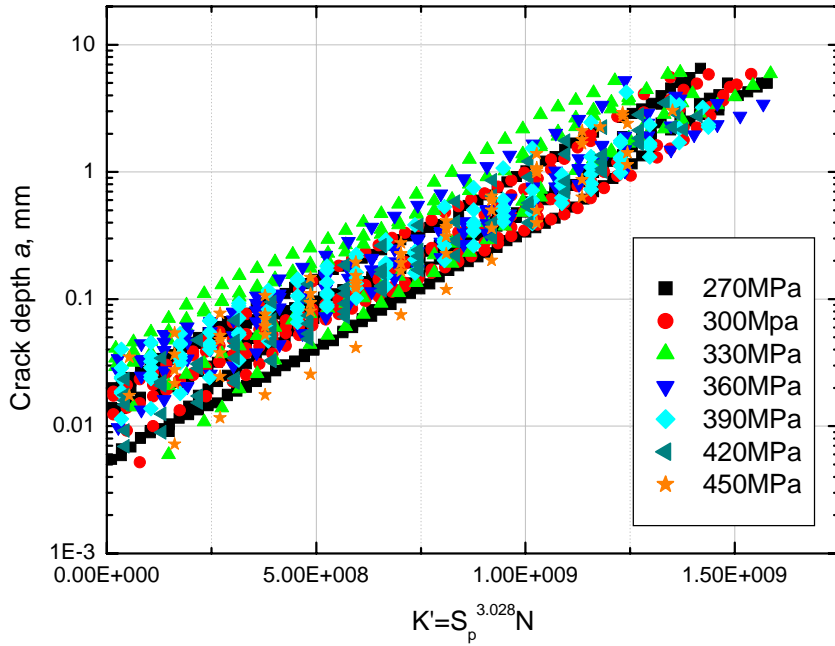


Figure 27 Fatigue test data for various peak stress factors correlated using Equation (3)

5.8.2 Effective Block Approach

An alternative approach known as the Effective Block Approach (EBA) has been developed by McDonald et al (McDonald, Molent and Green 2006). The key aspect of the EBA is to treat a block of spectrum loading as a constant amplitude cycle and to model the growth rate of a fatigue crack as a power function of the crack length, i.e., instead of $\frac{da}{dN}$ the crack growth rate is defined as

$$\frac{da}{dB} = C_B K_{\text{ref}}^{n_B} = C_B \left(S_{\text{ref}} \beta \sqrt{\pi a} \right)^{n_B} \quad (38)$$

where da/dB is the crack growth rate, which is given as the crack increment per block or per spectrum, a the crack size, and C_B and n_B are regression parameters. Equation (38) is exactly the same as the Paris law provided each block of spectrum is interpreted as an equivalent cycle, and K_{ref} is a SIF characterising the loading spectrum, and S_{ref} is the corresponding reference stress. Hence, this approach is not restricted to an exponential crack growth, and it inherits some of the advantages and limitations of the Paris law. The most important gain over the Paris law is the lumping of the sequence effect into the growth rate data, but this will also become the biggest obstacle for the application of the approach, i.e., the theoretical justification and experimental validation of taking C_B and n_B obtained from one spectrum and then applying them to another spectrum.

The same fatigue test data used previously in Figure 25 are used here to demonstrate the capability of the EBA. The plots of da/dB versus a are shown in Figure 28.

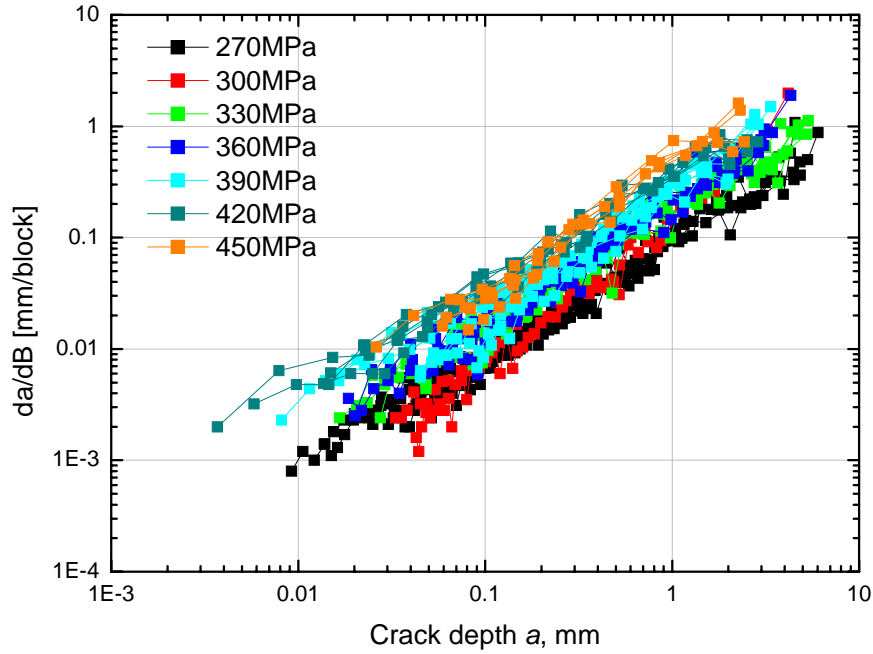


Figure 28 Crack growth rate curves for 7050-T7451 aluminium alloy specimens subjected to IARPO3a + marker load spectrum

Unsurprisingly, the results showed that the crack growth rate intercept, C_B , is dependent on the peak stress, and further assessment found that C_B is a function of S_{peak} , and is best described by the same relationship as given in Equation (36), by substituting β_L there with C_B . Thus, by re-arranging Equation (38) and taking S_{peak} as the reference stress, the crack growth rate for various S_{peak} can be expressed as (denoting $A = C_B \pi^{n_B/2}$)

$$\frac{1}{S_{\text{peak}}^{n_B}} \frac{da}{dB} = A \beta^{n_B} a^{n_B/2}. \quad (39)$$

Figure 29 re-plots the fatigue crack growth rate data in Figure 28 using Equation (39). It shows the crack growth rate data for various peak stress level have collapsed reasonably well onto a single curve. This is shown in Figure 29. The variation in crack growth rate as observed in Figure 29 can be taken into account using statistical or probabilistic methods.

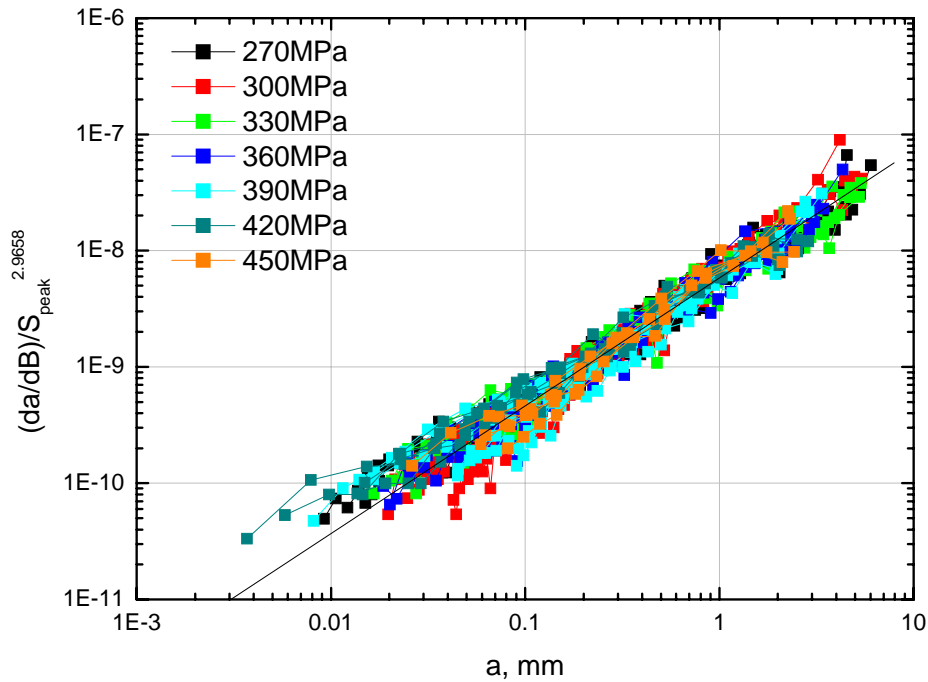


Figure 29 The collapse of the crack growth rate curves on to a single curve using Equation (39) for 7050-T7451 aluminium alloy specimens subjected to IARPO3a + marker load spectrum

The EBA can be used to predict crack growth (no restriction on it being exponential or log-linear) for spectra which may or may not have been subjected to coupon testing. For a more complete explanation of the approach, see (McDonald, Molent and Green 2006).

5.8.3 Discussion

In the absence of a reliable fatigue crack growth prediction model for making accurate fatigue life prediction, the log-linear and the EBA approach provide two simple approaches for assessing crack growth behaviours in a realistic structure based on specimen fatigue tests tested under the identical loading spectrum and crack configuration. The disadvantage of this method is that a large number of tests, which needs to simulate the real structure and loading spectra, are required to be carried out. The use of test results obtained under one spectrum for the prediction under another spectrum needs further verification and justification.

The equivalent initial crack size is essentially a regression parameter of the crack growth data based on a sensible crack size-time or crack growth rate function. It should be noted that a_0 generally does not reflect the actual flaw size at which the fatigue crack began its growth, instead, it is a measure of the crack-like characteristic of the initiation site due to the initial flaw and local material properties that best fitted to the crack growth model employed. Further verification work needs to be conducted to test the validity of the models using a physical initial flaw size. Alternatively, given the same normalised loading spectrum, material type, and surface finish and treatment, a consistent extrapolation model must be used if the equivalent initial flaw sizes are to be compared or used for subsequent assessment.

At this stage, it is not entirely clear whether the distribution of equivalent initial crack size obtained in such a way is suitable or transferable for use on the same material and same surface treatment but under different loading conditions, such as different spectra, constant amplitude or variable amplitude loading. Evidences have shown that the mechanisms of fatigue crack initiation are different for high and low stress levels under constant amplitude loading. Under variable amplitude loading, however, the effect of stress levels on crack initiation can be envisaged to be less remarkable since fatigue cracks are generally initiated with a good mix of low and high stress levels. This is certainly the case for the fatigue data examined above, where the plot of a_0 versus S_{peak} , shown in Figure 30, demonstrated a_0 and S_p has an extremely weak correlation, which may suggest a_0 and S_{peak} are independent.

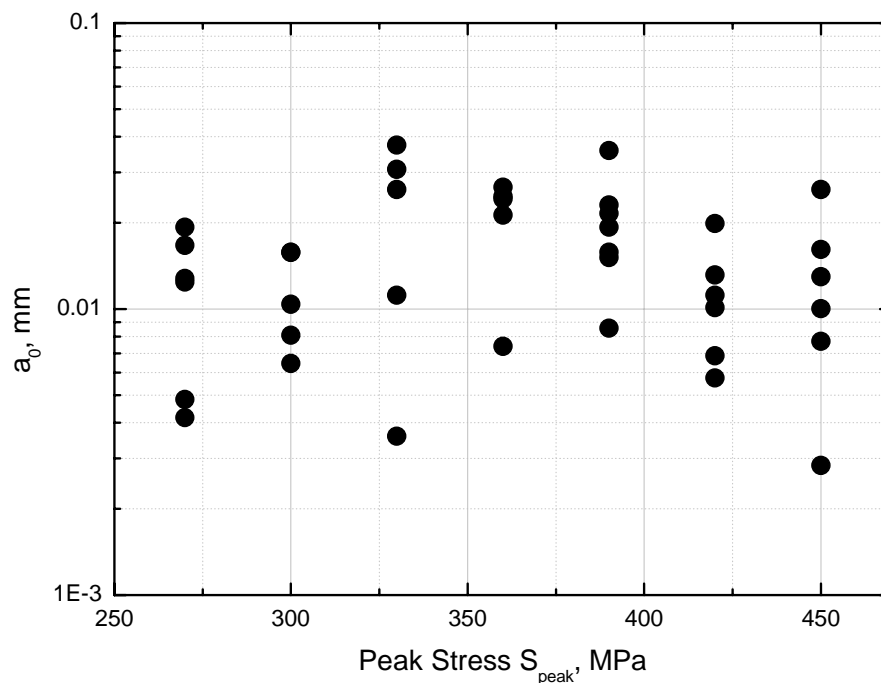


Figure 30 The relationship between the equivalent initial crack size and the stress level of a spectrum

6. Probabilistic Approach

Fatigue is by nature a stochastic process that exhibits a great deal of variability and uncertainty. To assure the safe operation of engineering structures under fatigue loading, it is paramount that this variability is accounted for in fatigue life prediction. To do this, a conservative deterministic approach that utilises safety factors to scale down the result of fatigue test and life prediction has been employed in airworthiness standards. However, the safety provided by this approach has been based mainly on service experience, where the level of safety it provides is uncertain. In today's environment, however, there is continuous pressure on cost reduction, and the term conservative is becoming increasingly unacceptable. Hence, the over-conservatism in the deterministic approach is now becoming a target area for allowing potential fatigue life extension and cost reduction.

In order to quantify the level of safety associated with the conservative deterministic approach and to permit the retirement life of fatigue critical components to be defined on risk levels, a risk-based approach has been gaining significant interest over the past decades. It has been envisaged that this approach not only provides tools to quantify the risk of failure, but also permits more efficient management of the aircraft structure by, for example, minimising maintenance cost and maximising availability. Due to these potential advantages, it makes good sense to migrate the traditional deterministic requirements to probability-based ones, for maintaining safe operation of structures, components and even repairs of future aerospace systems.

In the context of fatigue, the failure event of interest is the structural failure due to fatigue damage, which may be expressed as the time to fracture (or fatigue life N) of the structure. The aim of a probabilistic fatigue life assessment is thus to determine the probability distribution of fatigue life, so that the component retirement time or inspection schedules could be justified by the probability of failure occurring. In addition to the cumulative distribution function (cdf), the variation in fatigue life N can be characterised by the *probability density function* (pdf), a *survival function* (sf) or a *hazard function* (hf). Although the cdf and pdf are the most commonly used, all of these functions are useful for one purpose (or perspective) or another for assessing and managing the risk of failure. The definitions of these functions are as follows:

- The cdf of N , expressed as $F(N') = P(N \leq N')$, gives the probability of a component failing before time N' .
- The pdf is the relative frequency of failure times as a function of time. For continuous random variables, it is defined as the derivative of the cdf, i.e.,

$$f_p(N) = \frac{dF(N)}{dN}.$$
- The sf is the complement of the cdf, i.e., $S_p(N) = 1 - F(N)$
- The hf is the instantaneous failure rate function, and it is given by, $h(N) = \frac{f(N)}{1 - F(N)}.$

It should be noted that these functions are related to one another, i.e., if one function is known, the others can be derived from it.

There are two general approaches, namely the statistical approach and the probabilistic approach, for determining the variation and estimating the probability of failure. These two approaches are presented in the following sections.

6.1 Statistical approach

Traditionally, fatigue life risk assessments were mostly carried out using the statistical approach on failure-time (fatigue life) data. This approach involves the statistical analysis of fatigue test data collected from coupons representing the structure or component to estimate the fatigue life distribution for the general population and its confidence levels. Depending on the data types in the dataset, several different methods are available for determining the fatigue life distribution, and they are as follows.

6.1.1 Failure-Time Data Analysis

In the case where all of the data in the dataset are known fatigue life data, the analysis could be as simple as examining the data, followed by fitting an appropriate continuous probability distribution to characterise the variation of the data. The fatigue life data previously shown in Figure 25 on p. 64 are plotted in Figure 31 to illustrate the idea. Since all the coupons have been tested to failure under laboratory conditions, so the fatigue life of each specimen is known exactly. The fatigue life data for the various applied peak stress values have been normalised based on the regression fit shown in this figure.

Two simple methods for modelling the variation in the logarithm of fatigue life are:

- (1) the constant coefficient of variation (cov) method; and
- (2) the constant standard deviation (σ) method.

It may not be obvious, but the constant-cov method assumes that the ratio of the standard deviation over the mean of the logarithm of fatigue life at any peak stress level is constant. i.e., $\text{cov} \equiv \sigma(S_p)/\mu(S_p) = \text{constant}$. On the other hand, the constant- σ method assumes that the standard deviation σ of the logarithm of fatigue life is constant and independent of the applied peak stress level. The differences between these two methods in modelling the variation (0.1% and 99.9% bound) in fatigue life for the data are also displayed in Figure 31. It can be seen that the spread in the logarithm of fatigue life increases with increasing mean fatigue life for the constant-cov method, but it remains constant for the constant- σ method. For this example, the constant- σ method appears to provide a better overall representation of the variation in fatigue life. The distribution in fatigue life based on the constant- σ and the constant-cov methods are displayed in Figure 32 and Figure 33, respectively, for comparison.

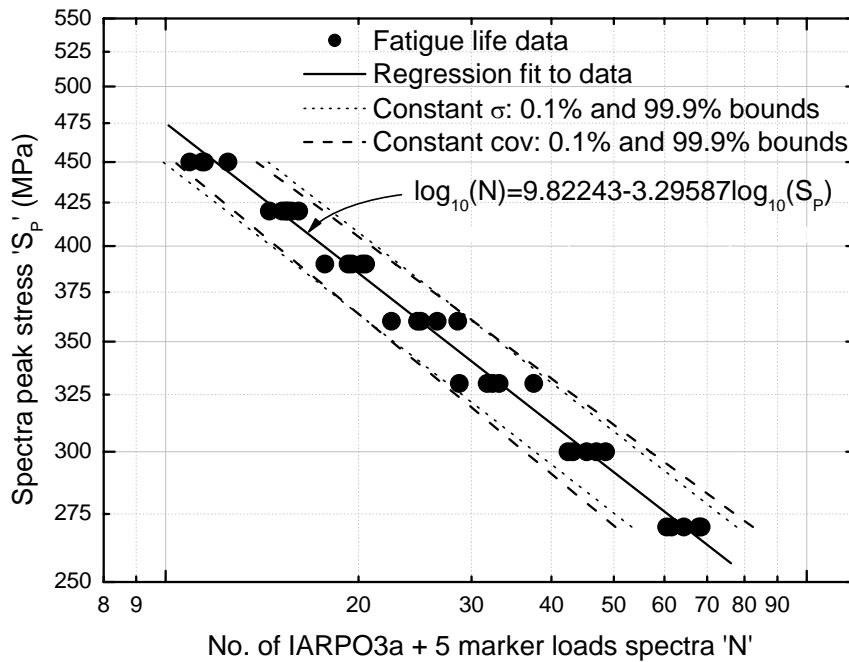


Figure 31 Variation in fatigue life data for aluminium 7050 alloy specimens tested under a normalised fighter aircraft spectrum with various peak stress levels, life versus blocks of spectrum loading

Both the normal distribution and the 3-parameter Weibull distribution were fitted to the data, and the parameters of the distributions were obtained using the least square method. However, an alternative and a more general fitting technique for the determination of the distribution parameters is the maximum likelihood method. Figure 32 and Figure 33 show that for both the constant- σ and constant-cov methods, the 3-parameter Weibull distribution provides a better fit to the data than the normal distribution.

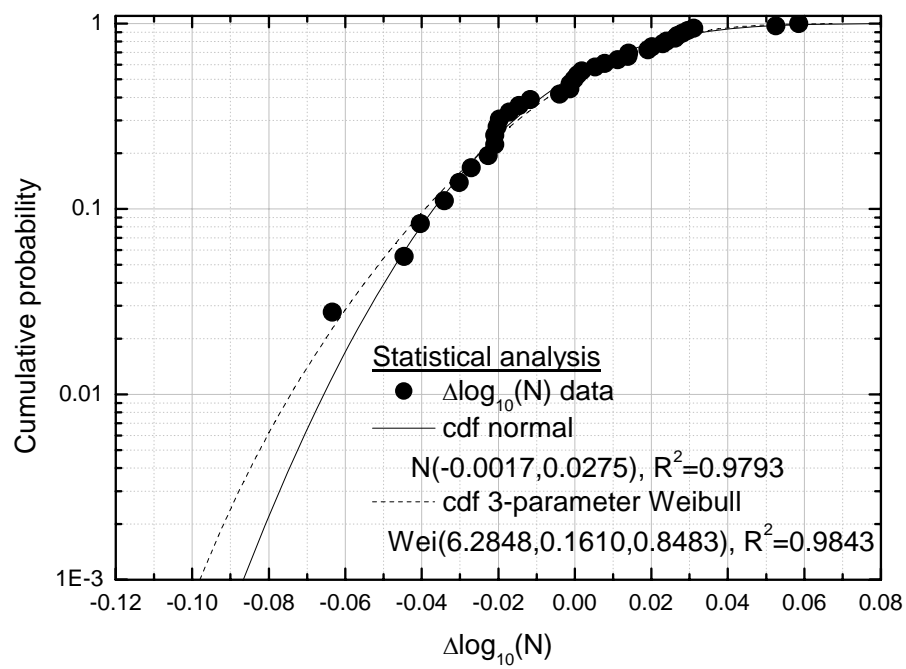


Figure 32 Statistical analysis of the variation in fatigue life data shown in Figure 31 using the constant standard deviation (σ) method

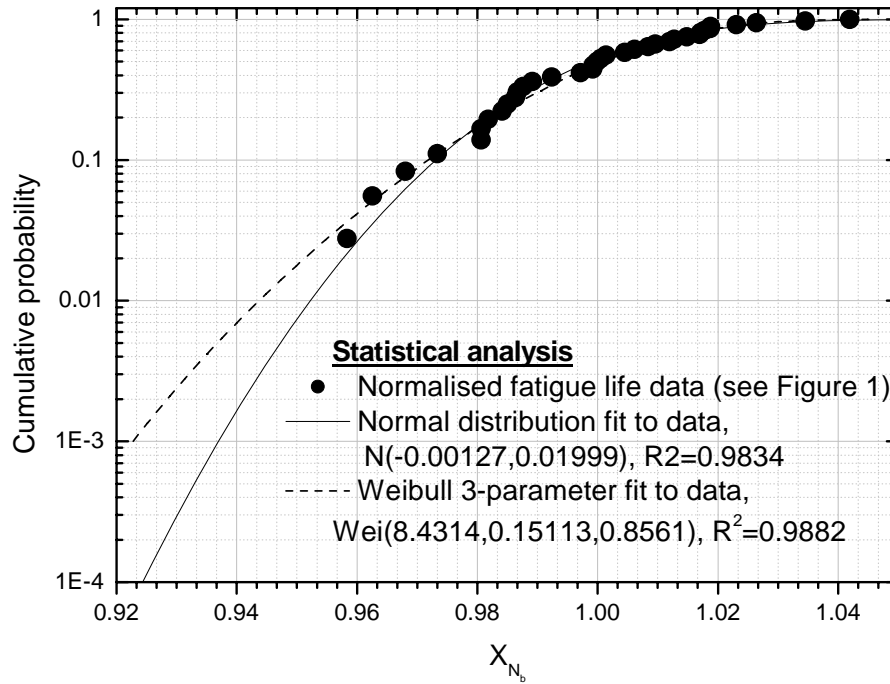


Figure 33 Statistical analysis of the variation in fatigue life data shown in Figure 31 using the constant coefficient of variation (cov) method

6.1.2 Failure-Time with Censored Data Analysis

The above presents the case where the exact failure times are known for all the specimens tested or data collected, but generally not all the data in the dataset would have their exact failure-time recorded. This may be due to failure not occurring within a given test time frame, for instance. The test specimens that have not failed after a given time frame are called *right-censored data* in statistics or *run-outs* in fatigue testing. Such data must also be incorporated into the statistical analysis, as they are a part of the population of data. In such a case, the maximum likelihood method needs to be employed instead of the least square method.

The maximum likelihood method is capable of taking censored data into account for determining the distribution parameters for a selected statistical distribution. For data containing both exact failure-time and some right censored data, the likelihood equation is generally expressed as

$$Lh(X, \theta) = \prod_{i=1}^I f_p(x_i, \theta)^{\delta_i} [1 - F(x_i, \theta)]^{(1-\delta_i)} \quad (40)$$

where δ_i is a parameter that has a value of 1 for failed data, and 0 for right-censored data. The symbol θ denotes the vector of distribution parameters, and X is the vector of length I of all of the failure-time and right-censored data. The maximum likelihood estimate of θ is obtained by determining the value of θ that maximises Equation (40).

Figure 34 shows the cumulative probability of the same data as shown in Figure 31, using Equation (40). In this plot, comparison has been made between the two cases with different amount of right-censored data. In the first case, fatigue lives greater than 45 blocks (cdf shown as open circular symbols) were taken as right-censored data, and in the second case, those greater than 35 blocks (cdf shown as open triangular symbols) were taken as right-censored data. For demonstration purposes, it has been assumed that the variation in the logarithm of fatigue life is modelled by the constant- σ method and normal distribution. As shown in Figure 34, although 8 and 11 data points (out of a total of 36 points) were censored in the first and the second case, respectively, the maximum likelihood method provided highly consistent parameters compared with the case without any censored data (cdf shown as filled square symbols). However, this demonstration of the small influence of censored data is based on the censoring of the high life data, and could be misleading. The service case recently studied has the low life service data as the censored data and the high life full-scale test life data as the precise data. In that instance there is a significant effect on the low probability end (Tong, White, Watters and Antoniou 2006).

In addition to right-censored data, there are another two types of censored data: interval-censored data and left-censor data. The left-censored type is used if the exact failure time is not known, but it is known that the specimen or component failed some time between now (the first inspection) and time zero. Interval-censored type is used if the exact failure time is not known, but it is known that the specimen or component failed some time between the previous and present inspections. Both of these censored data types can also be taken into account by the maximum likelihood method for estimating the failure distribution. It should be pointed out that although the maximum likelihood method can account for various types of limited or imprecise missing information in the collected dataset, unreliable data do significantly penalise the reliability or confidence of the statistical assessment.

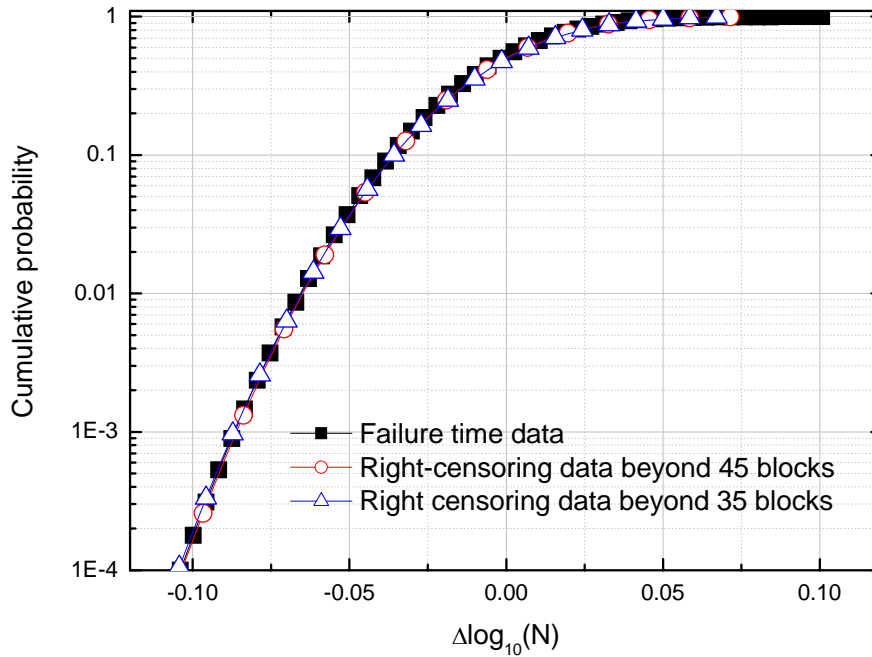


Figure 34 Example demonstrating maximum likelihood estimate of the distributions with and without right censored data for fatigue life data shown in Figure 31 using the constant standard deviation (σ) method

6.1.3 Zero Failure Data (Weibayes) Analysis

In some extreme cases, the available fatigue life data are only those collected from service experience, and hence the failure-time statistical data is generally exceptionally scarce, as we cannot allow structures to fail for data recording. If there are only a couple of failure data points available and the remainder is right-censored data, the maximum likelihood method cannot generally be used to determine the model parameters. Instead, the Weibayes analysis (Meeker and Escobar 1998) should be used. With only a couple or even no failure time data, the results of a Weibayes analysis would provide an exceptionally conservative estimate of the failure probability distribution of the component or system based on service time data. This method is, therefore, not recommended for fatigue lifing purposes as the results generally do not provide a mean fatigue life estimate. They simply represent a lower bound to the probability of failure. However, this approach could be valuable in situations where risk management information is urgently needed and further testing obtain more reliable data is not feasible.

A simple example is presented in Figure 35. Consider some specimens whose median fatigue life at any applied peak stress is given by the result in Figure 31, and the variation in logarithm of fatigue life is characterised by the constant standard deviation method and the normal distribution. Then the fatigue life distribution at an applied peak stress of 325 MPa with a standard deviation $\sigma_{\log N}$ of 0.0276 is shown in Figure 35 by the curve with

filled black squared symbols. The median life at this applied peak stress level is approximately 35 spectrum block loadings.

Now consider a different test program in which 15 nominally identical specimens were tested at the same applied peak stress, but due to economical reasons, these tests could only be carried out up to 25 spectrum blocks of loadings. Upon completion it has been found that no specimens failed after 25 spectrum blocks of loading. Based on these 15 right censored data and assuming fatigue life is characterised by the lognormal distribution and $\sigma_{\log N}$ is known to be 0.0275, the fatigue life distributions at 50%, 90% and 95% confidence levels 'CL' can be predicted using the Weibayes analysis, as shown in Figure 35. This example clearly demonstrates the conservatism in using the Weibayes analysis and hence in performing statistical analysis when there is no failure data available. However, if a life factor approach, as per the airworthiness standards, is applied to this same test data, then an even lower life results at a typical failure probability of 0.001. In the above example, it was assumed that the scale parameter, $\sigma_{\log N}$ in this case, is known, but it is not the general case. In the latter case, it is common to use the scale parameter values based on past experiences and/or other test data (such as for this example). Therefore, the uncertainty in the results of zero failure data analysis or the Weibayes analysis can be large. However, in the absence of failure data, it appears no better alternatives are presently available. Some assessments have been carried out by AVD in recent time to support the management of some ADF air platform components (Tong and Antoniou 2005; Wood and Antoniou 2005).

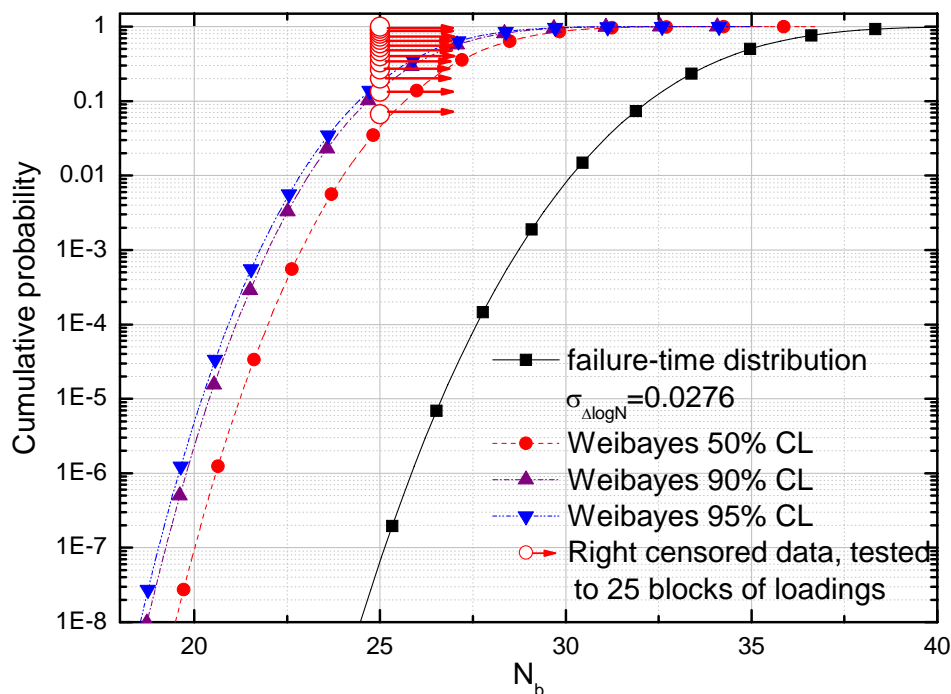


Figure 35 Zero failure reliability or the Weibayes analysis example

6.2 Statistical Analysis Software Tools

Numerous specialised software tools are now available for statistical analysis of failure-time data, and two with which the authors have had experience with are MINITAB (a product of MINITAB INC., State College, PA, USA) and Weibull++ (a product of ReliaSoft Corp., Tuscon, AZ, USA). While most of these software tools utilise standard techniques, methods and formulae that are found in reliability texts, they differ in the graphical user interfaces, presentation and graphical capability. These features are becoming increasingly the key reasons for one statistical analysis package to be preferred over another.

6.3 Probabilistic Approach

Probabilistic analysis tools may be used to quantify the probability of an event $Y(X)$, or events, occurring as a function of the variations (statistical distributions) of a fundamental random variable X . Since in the context of fatigue crack growth and life prediction, the event of interest is commonly the time to fracture, i.e., fatigue life N of a component, the probabilistic analysis focuses on the numerical determination of the variation or probability distribution of fatigue life N based on the influence and variation of the fundamental variable X . As presented in the earlier sections, the variables affecting fatigue may include the initial crack size a_i , material properties, geometry, and loading.

Since it is generally not feasible to carry out a large number of full scale fatigue tests to determine the distribution of fatigue life with high reliability, probabilistic fatigue life analysis that combines life prediction methodologies with statistical methods may be used as an alternative for the determination of the fatigue life distribution. Provided that the fatigue life model is capable of simulating the fatigue life of the component or structure under a combination of loading, initial flaw size, and environmental conditions, this approach would eliminate the need for carrying out expensive fatigue tests.

For this reason, the accurate mathematical prediction model giving the relationship of fatigue life N to its influential variables a_i, C, m, K_{cr}, \dots , say

$$N(X) = N(a_i, C, m, K_{cr}, \dots) \quad (41)$$

is the pre-requisite of a probabilistic fatigue life assessment. The fatigue life prediction model selected defines the variables that can be taken into consideration in a probabilistic assessment, and it also defines the region of integration (i.e., limit-state boundary) in a reliability problem.

Given an adequate fatigue life prediction model and the pdf of the influential variables a_i, C, m, K_{cr}, \dots , the probability distribution of the fatigue life N can be mathematically computed. In general, the cdf is computed by evaluating the integration

$$P(N(X) \leq N) = \int_{\Omega=(N(X) \leq N)} f_X(X) dX \quad (42)$$

where $P(N(X) \leq N)$ denotes the probability of $N(X)$ being less than or equal to N , $f_X(X)$ is the joint pdf (or Jpdf) of X , and X is a vector of the variables. The region of integration Ω is the region $N(X) \leq N$, and the hyper-plane $N(X) = N$ is known as the limit-state boundary.

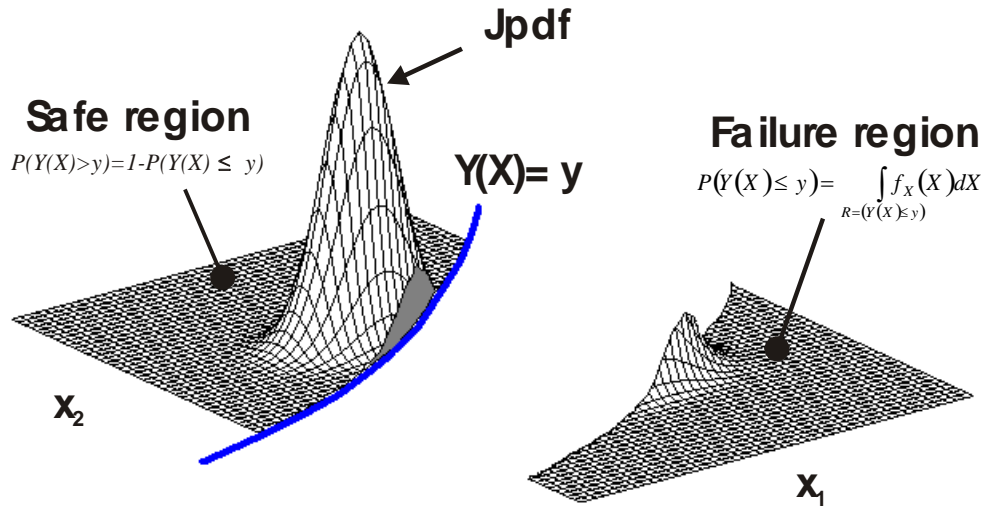


Figure 36 Probability of failure is the hyper volume under the joint pdf bounded by $Y(X) \leq y$

From a geometrical point of view, in the general case of $Y(X) \leq y$, the probability of failure simply equals to the part of the multi-dimensional volume of the joint pdf that lies inside the failure region bounded by Ω , as shown in Figure 36. In this sense, probabilistic analysis simply means the formulation and evaluation of Equation (42) for a particular problem. However, the evaluation of this generally complex multidimensional integration is often not possible. Even with numerical techniques implemented in special mathematical software, the integration of three non-normally distributed random variables with a simple limit state function may be the limit of evaluation.

The difficulty in evaluating Equation (42) has consequently led to the development of alternative methods for obtaining probabilities, and has been a major thrust in probabilistic methods over the past two decades (Breitung 1984; Wu 1985; Southwest Research Institute 1991; Grooteman 1999; Wang 2000; Orisamolu 2001). As a result, a variety of methods are now available, such as the first-order second-moment, first-order reliability, second-order reliability, fast probability integration, Monte Carlo simulation (MCS), the classic load-strength interference or response-surface, limit-state surface element (LSSE), and the discrete-element methods (Tong 2006).

6.4 Probabilistic Fatigue Life Assessment Software Tools

The increasing interest in utilising the probabilistic approach for determining the safe fatigue life and for the management of aircraft structures has led to the emergence of a number of probabilistic fatigue life assessment software tools over the recent decades. These tools were designed to reduce the burden of detailed technicalities on the user, but the effective use of

these tools does require the user to have a general understanding of the probabilistic analysis method implemented and the underlying assumptions made. Two of the probabilistic fatigue life assessment software tools, PROF and CGAP, available to AVD-DSTO are discussed below. A more detailed comparison of DARWIN (Wu, Enright and Millwater 2002), PROF and AVD developed NERF (Graham and Mallinson 1984) in the context of fatigue life management of titanium aircraft engine rotor disks is given in (Tong, Hou and Antoniou 2005).

6.4.1 PROF

PRobability Of Fracture (PROF) (Hovey, Berens and Skinn 1991; Hovey, Berens and Loomis 1998) is a probabilistic fatigue life assessment software tool tailored for the USAF damage tolerant program in the 1990s. The major output by PROF is the probability of failure of the critical location under consideration and the crack size distribution, with or without consideration for the effect of a maintenance program.

A major assumption made in PROF is that it models the fatigue crack growth rate as deterministic. As a result, it does not take into account the variability in fatigue life due to the variation in material properties. This assumption is now recognised as a major limitation in PROF, as the variability in fatigue crack growth rate is one of the most influential variables affecting the fatigue crack growth. White et al addressed this issue in a recent paper, which considered the effect of the initial crack sizes, crack growth rate, crack growth rate variability, fracture toughness and the accuracy of the fleet-wide fatigue damage estimation tool (White, Molent and Barter 2005).

PROF models five variables statistically. They are the equivalent initial flaw sizes (EIFS), the applied stress, the critical SIF, the probability of detection and the equivalent repair flaw sizes (ERFS), which accounts for the machining marks and flaws caused by repair.

Based on the assumption that the fatigue crack size versus time curve is deterministic and given the distribution of EIFS, the crack size distribution at any service time can be determined by extrapolating from the deterministic crack size function. The probability of failure computed by PROF considers two failure events, (1) probability of exceeding a pre-defined critical crack length, and (2) probability that the critical SIF is exceeded. The first event may not constitute actual failure of the structure, for exceeding the defined critical crack length does not mean the structure has fractured.

In the examination of the deterministic fatigue crack size versus time curve assumption, a number of inadequacies may be identified. Firstly, the distribution of EIFS must be obtained using the same deterministic crack size versus time function that will be use in PROF, and EIFS needs to be extrapolated back to time zero from failure cracks (i.e., not un-failed cracks). It is only by doing this that the EIFS distribution could adequately capture both the variation effects of the initial crack size and the fatigue crack growth. The EIFS distribution is, hence, not a realistic distribution of the flaw sizes or crack sizes existing in the structure, and realistic crack sizes would only be obtained as crack sizes approaches failure. The prediction of crack sizes, particularly at low service life, and the detection of crack size when inspection/repair is involved is thus unlikely to be reliable, again, because EIFS are artificial crack sizes that only approach the real crack size at failure.

6.4.2 CGAP

CGAP (Hu and Walker 2006b; Hu and Walker 2006a) is an in-house program based on FASTRAN developed by Newman (1992b). In addition to the major development in the modelling of crack growth in a notch-plasticity affected zone as detailed in Section 5.7, CGAP also added a module for probabilistic fatigue crack growth life assessment (Hu and Walker 2006a; Tong 2006). The probabilistic method implemented in CGAP is the Monte Carlo simulation (MCS) method with optional use of the Importance Sampling Technique (Melchers 1999). The Importance Sampling technique allows probabilistic assessment to be carried out by the MCS method with much greater computational efficiency.

Presently, CGAP allows a maximum of six variables to be modelled statistically for probabilistic crack growth analysis. These are the initial crack size, the peak stress of the spectrum, the crack growth rate exponent, the crack growth rate coefficient, the critical SIF and the threshold SIF. The initial crack size, the peak stress of the spectrum and the threshold SIF variable are modelled as independent random variables in CGAP, but correlated statistical models were developed and used in CGAP to allow the correlations (or dependencies) of the crack growth rate exponent, the crack growth rate coefficient and the critical SIF to be modelled.

To allow the dependency of the crack growth rate coefficient on the crack growth rate exponent to be modelled, CGAP assumed that

$$\log_{10}(C) = X_{\log C} [A_p + P_p \log_{10}(m)] \quad (43)$$

where A_p and P_p are regression parameters that correlates the dependency of $\log_{10}(C)$ with $\log_{10}(m)$. The independent random variable $X_{\log C}$ was introduced to capture the statistical variation of $\log_{10}(C)$ with $\log_{10}(m)$. Unlike PROF, and a number of other probabilistic fatigue life assessment software codes currently available, CGAP has taken on a highly robust, correlated statistical model based on the Monte Carlo method to simulate the variability in fatigue crack growth rate.

Similarly, to allow the dependency of the critical SIF on the crack growth rate exponent to be modelled, CGAP assumed that

$$\log_{10}(K_{cr}) = X_{\log K_{cr}} [B_p + Q_p m] \quad (44)$$

where B_p and Q_p are regression parameters that correlates the dependency of $\log_{10}(K_{cr})$ with m . The independent random variable $X_{\log K_{cr}}$ was introduced to simulate the statistical variation of $\log_{10}(K_{cr})$ with m .

The regression parameters A_p , P_p , B_p and Q_p are therefore additional parameters required in CGAP for carrying out a probabilistic assessment. Note that the crack growth rate coefficient C can be made independent of m by setting $P_p = 0$, and similarly, the critical SIF K_{cr} can also be made independent of m by setting $Q_p = 0$. It has been demonstrated in reference (Tong 2006) that treating correlated variables as independent random variables can

be detrimental to the result of the probabilistic fatigue life assessments. It is, therefore, crucial that any correlation between variables be simulated accurately. From this point of view, it is also desirable to correlate the threshold SIF with other crack growth variables, which is currently treated as an independent random variable in CGAP. Further work needs to be carried out to ascertain the relationship between the threshold SIF and the crack growth rate before this correlation could be implemented.

CGAP assumes that there are four independent groups of variables, namely, initial condition variables, material property variables, stress variables, and maintenance and inspection variables. Although this assumption is theoretically and logically sound, statistical analyses have shown, for example, that the equivalent crack size of an initial flaw could affect the material crack growth variables due to short crack effect. A better understanding of the transition and growth behaviour of an initial flaw to a fatigue crack appears to be the key to model this behaviour, and hence more accurate fatigue life and reliability predictions. To this end, increasing the research effort on fatigue crack initiation and on the short crack effect is required.

CGAP allows any and all of the variables to be modelled as deterministic, or as random variables with normal, lognormal base 10, and the Weibull distributions. Note that with a shape parameter of unity, the Weibull distribution reduces to the exponential distribution.

6.5 Probabilistic Certification Requirement

In the literature and some certification documents, probability-based certification requirements have been proposed, (e.g., (Lincoln 1985; UK DEFSTAN 1987; Hovey, Berens and Skinn 1991; Zion 1996; Hovey, Berens and Loomis 1998). A collection of some of the probabilistic acceptance requirements found in the literature for various categories of aerospace structures and systems is given in Table 3.

Table 3 Examples of some typical probabilistic requirements assigned for certification of aerospace structures and components

	Cumulative probability	Risk (per hour)
Airframe	$10^{-6} \leftrightarrow 10^{-3}$	10^{-6}
Composite repair	10^{-6}	----
Engine component	10^{-4}	$5 \times 10^{-8} \leftrightarrow 10^{-6}$
Dynamic component	10^{-6}	----
Space vehicle	$10^{-3} \leftrightarrow 10^{-2}$	----

Probabilistic-based certification requirements, and particularly the standards where they can be found, do not state explicitly how the required level of probability of failure should be maintained. However, it should be noted that the value of the acceptable level of probability of failure generally reflects the consequence of a failure event, and implicitly defines the efforts required for probabilistic assessment. The reason for the former is quite obvious, and the reason for the latter is that as the acceptable level of probability of failure decreases, an increasing amount of data would be needed to adequately characterise the variation of the variables, particularly at the tails of the distribution, so that reliable probabilistic fatigue life

assessments could be made. What constitutes a sufficient amount of statistical data is dependent on the target level of probability of failure and the influence of a particular variable on the probability of failure. This can be determined using sensitivity analysis of the probability of failure with respect to each of the variables (Tong 2006). Collecting a large, or sufficient, amount of data for probabilistic assessment is a tedious and an expensive exercise. This is one of the major barriers confronting the probabilistic approach to structural integrity.

7. Discussions and Compendium of Problems

DSTO develops, maintains and uses a wide set of software tools for fatigue life and fatigue crack growth analyses of aircraft structural integrity. In order to make effective, efficient and intelligent use of these tools, it is important to understand the differences and similarities between the underlying methodologies and the implementation details. It is even more important to understand their capabilities and limitations. This knowledge is also important for making incremental improvement for the software tools where desirable and possible. In this section, we highlight some of the known limitations and caveats in various tools, and make some recommendations on the selection of tools and methods for a given problem.

7.1 Comparison of Fatigue Life Approaches

Both the stress-life and strain life based methods remain valid approaches to modelling fatigue life or crack initiation life for aircraft metallic structures. It is expected that the two strain-life based software models available in AVD, CI89 and FAMS, will produce equivalent results given identical input data and a limited case has shown this to be true. Ci89 has been mostly successful in its use on the F/A-18. Appendix A shows data from the P-3 SLAP where the strain-life approach produced superior results to the stress-life approach for a number of typical P-3 type wing spectra. This is to be expected as the Neuber based equations in the strain-life approach allow for non-linear stress-strain response above the yield point. Nevertheless, whilst the strain based approach is recognised as most suitable for notches with low to medium levels of K_t or K_n , high K_t features such as lugs present a more challenging case and may well be better suited to the more traditional stress-life approach using data from coupons that explicitly represent the feature being analysed. There is not much literature in this area and further evaluation of the strain-life approach for high K_t features is warranted.

7.2 Challenging Issues in Modelling Fatigue Crack Growth

7.2.1 Short Crack Behaviour

With the advancement in experimental and computational capabilities, the current trend in fatigue life assessment is to expand and extend the capabilities of crack growth models to the realm of traditional crack initiation, by improving the models for short crack growth. However, research in the last few decades has shown that the SIF concept for small cracks may be questionable and alternative correlating parameters and models need to be investigated.

Crack closure has, however, been proposed as the responsible mechanism for the physically short crack phenomenon, and the use of the effective crack-tip stress intensity range, ΔK_{eff} , helps to explain the 'anomalous' short crack behaviour. Also, the use of correlating parameters such as ΔJ and the crack-tip opening displacement, CTOD, have been used along with crack closure as potential solutions in explaining and predicting the behaviour of mechanically small cracks which are physically short but greater than the microstructure features, $a \approx 1$ mm (Ritchie and Lankford 1986).

Navarro and de los Rios (1988) developed a model for short crack growth based on micro-mechanics. Briefly, the growth of a crack is analysed in terms of the successive blocking of the plastic zone by slip barriers such as grain boundaries and the subsequent initiation of slip in the next grain. The discontinuous character of the slip process (slip jumps) plays a fundamental role in the model. The factor governing the transfer of slip across a grain boundary is considered to be the stress concentration ahead of the plastic zone which, for a constant applied stress, is found to be dependent only on a parameter defining the position of the crack tip relative to the grain boundary. The discrete behaviour of the slip has a strong influence in the short-crack period and hence cannot be neglected in the analysis of the crack growth rate. By making the crack extension per cycle proportional to the crack-tip plastic displacement, the intermittent pattern of decelerating and accelerating behaviour of short cracks and the existence of non-propagating cracks may be explained. For long cracks, a linear relationship in log coordinates holds between the plastic displacement and the SIF range. The reasons why short cracks grow at rates higher than those predicted by the straightforward application of fracture mechanics long-crack data are explicit in the analysis. The fatigue limit is equated to the stress below which a crack is unable to transfer slip to the next grain. The application of this criterion leads to the representation of a Kitagawa-like plot, Figure 37. The deviations and the large scatter of data in the short-crack regime are apparently explained.

The implementation of a short crack model in FASTRAN is different from those specified in Suresh and Ritchie (1984) and McClung and Feiger (not dated) in the treatment of the geometry correction factor. In FASTRAN, the fictitious crack length was used to calculate the correction factor, while in Suresh and Ritchie (1984) and McClung and Feiger (not dated) it was stated that the physical crack length should be used. It is worth investigating the effect of the difference.

7.2.2 Threshold Growth

In McClung and Feiger (not dated) a short crack model based on the El Haddad model (El Haddad, Smith and Topper 1979) was assessed. The model implemented in FASTRAN is similar to this, but a_0 was chosen to be the reverse plastic zone size ω (Newman and Phillips 1999), which is dependent on the geometry and the load level. In McClung and Feiger (not dated) a_0 was calculated for 2124-T851 and 7475-T7351 aluminium alloy and it appears that a_0 only depends on the material and the load ratio. Further literature review and numerical analysis need to be carried out to evaluate these different models.

The short crack growth anomaly indicates that the threshold stress intensities for long cracks and short cracks are different. Further work needs to be done to evaluate and implement the El Haddad model. This may improve the long crack regime prediction while maintaining a reasonable estimation for the short crack regime.

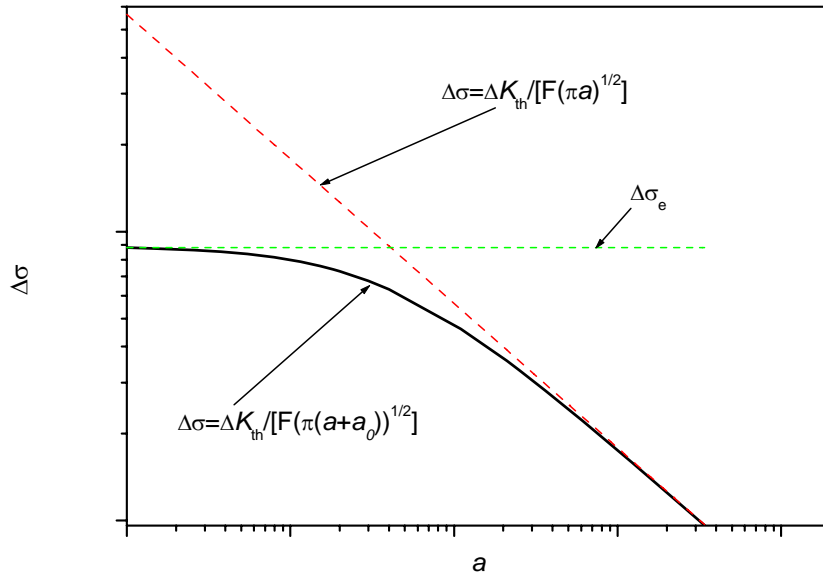


Figure 37 Kitagawa diagram and the threshold stress prediction by El Haddad model. ΔK_{th} is the long crack threshold stress intensity factor range, $\Delta\sigma_e$ is the endurance limit, and F is the geometry factor

Kitagawa and Takahashi first showed that below a critical crack size the threshold ΔK_{th} for short cracks appears to decrease with decreasing crack length (Kitagawa and Takahashi 1976), where the threshold stress approached that of the smooth bar fatigue limit at very short crack length. In FASTRAN, the threshold stress intensity factor range was calculated as

$$\Delta K_{th} = C_3 + C_4 R$$

where R is the stress ratio and C_3 and C_4 are material constants. A natural question to ask is how the above equation compares with the normalised SIF range versus the normalised crack length given in Figure 38. Therefore, it is recommended that the relation between $\Delta K_{th} / \Delta K_0$ and a/a_0 as given in Kitagawa diagram be implemented in a life assessment code to evaluate its effectiveness on short crack modelling and the threshold growth.

As discussed by Suresh and Ritchie (1984), a_0 effectively represent the limiting crack size for valid LEFM analysis, and its value depends on the strength of the material. For ultrahigh strength materials (with a yield strength of about 2000 MPa) it varies between 1~10 μm and for low strength materials (with a yield strength of about 200 MPa) it varies between 0.1~1 mm in. Therefore, it is recommended that experimental data for a_0 be collected and compiled, and its effect numerically investigated.

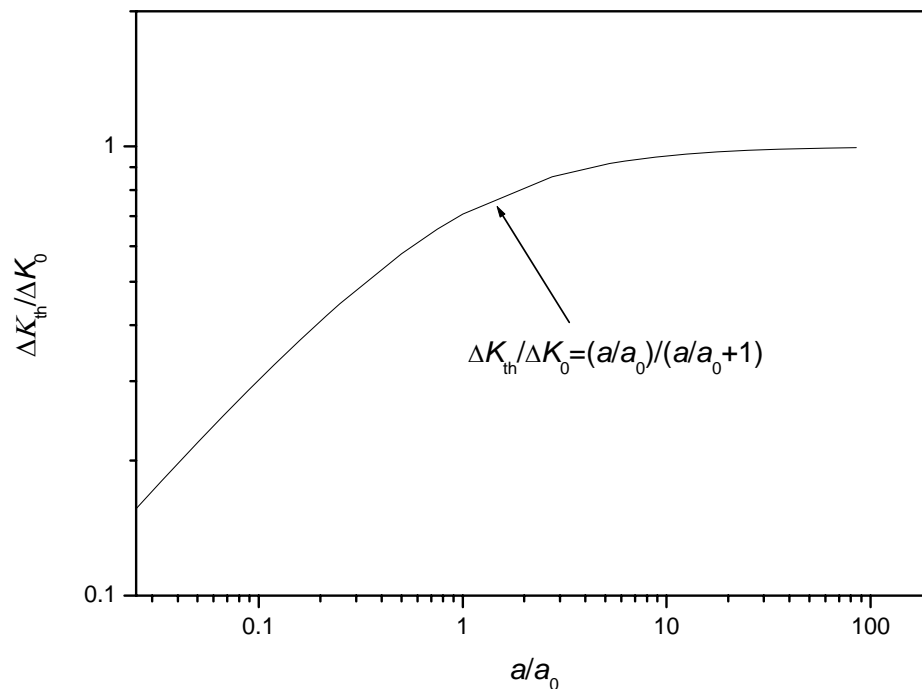


Figure 38 Normalised threshold stress intensity factor range for short cracks. ΔK_0 is the long crack threshold and is considered to be a constant (Suresh and Ritchie 1984; McClung and Feiger not dated)

7.2.3 Sequence Effect

In spite of the success of crack closure model in explaining the retardation and acceleration of overload and underload, the sequence effect remains an unresolved technical issue.

McDonald and Molent et al attempt to solve the problem of sequence effect with a synthetic approach, analogous to the relative Miner's rule approach for fatigue life prediction (Rose and Preston 1999). Rather than developing complicated models that use constant amplitude crack growth data and analyse the contribution of individual factor to the observed sequence effect, it is proposed that the sequence crack growth data be used (McDonald, Molent and Green 2006). It has been suggested that cracks grow differently under constant amplitude loading and variable amplitude loading. The key technical difficulty in this approach is to establish a rational procedure to obtain the crack growth rate constants from the data obtained from one spectrum test to another spectrum.

7.2.4 Tensile Growth and Shear Growth

The Paris law is an approximate description of the relationship between the crack growth rate and the SIF range. Even within the traditional Paris region there are consistent variations in

the shape of the $da/dN - \Delta K$ curve, known as transition regions (Zuidema, Veer and Van Kranenburg 2005) related to the changes in geometry of the crack surfaces from flat to slant .

7.3 Limitations and Caveats for FASTRAN and CGAP

7.3.1 Negative Stress Ratio

It is known that the calculation of crack opening stress is not accurate enough under negative stress ratios, as discussed in (Silva 2004). Silva conducted crack-growth experiments, with a stress ratio of $R = -1$, to study the influence of different maximum load levels on crack closure and fatigue crack growth. The studied focused on the effects of crack tip plasticity and roughness on crack closure. Measurements of roughness and o crack opening loads are made to verify their influence on crack propagation rate. It is confirmed that, at negative stress ratios, crack closure changes with S_{\max} for the same R ratio. It is also confirmed that roughness is not a relevant mechanism at negative stress ratios. It is demonstrated that the crack closure concept is not adequate to explain crack propagation rate as a function of S_{\max} at $R = -1$. In its place, a concept based on plasticity and cyclic plastic properties, or on internal stresses, should be used to explain fatigue crack propagation (Silva 2004).

7.3.2 The Geometry Factor β

In FASTRAN and CGAP, the length of a crack emanating from a semi-circular notch is measured from the centre of circle rather than from the edge of the notch. Therefore, when the user-defined crack configuration is used, and the β -factors are calculated using third party tools such as FE analyses, care should be take to ensure that the β -factors are properly defined. Usually, the β -factors extracted from FE analyses are defined against the crack length l measured from the edge of the notch, as illustrated in Figure 39. Accordingly, we have

$$K = \beta_l S \sqrt{\pi l} .$$

However, in FASTRAN it is the nominal crack length a in Figure 39 that is used to computer the SIF. Consequently, we have

$$K = \beta_a S \sqrt{\pi a} .$$

where β_l and β_a are the corresponding β -factors. Since under the same external load, the SIF at the crack tip should be identical irrespective the crack length measure taken, we obtain the relationship between β_l and β_a

$$\beta_a = \beta_l \sqrt{\frac{l}{a}} = \beta_l \sqrt{\frac{l}{R + a}} ,$$

where R is the notch length. The thin red curve in Figure 39 represented the appropriate β -factors to be used in FASTRAN.

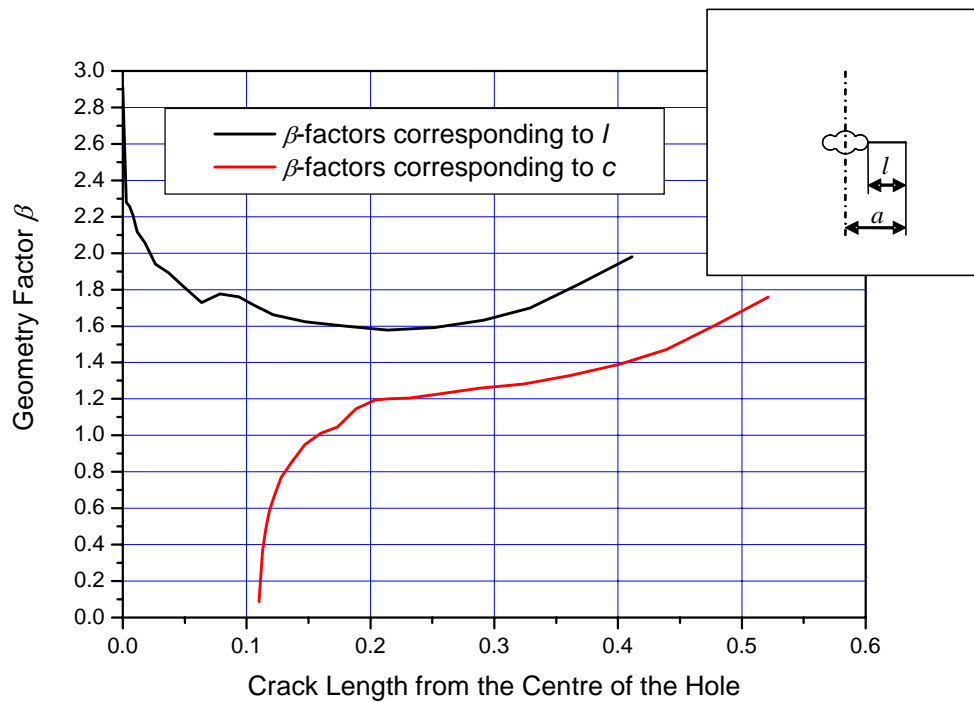


Figure 39 Beta factors defined against different crack measurements

7.3.3 The Shifting of Crack Growth Curves

In crack growth analysis, there is a practice of shifting the crack growth curve to match the actual measured initial flaw size. For the results obtained from FASTRAN or CGAP, this shifting introduces some inherent error. The error may not be significant in some cases, but it is consistent. This is because FASTRAN or CGAP results are history dependent, hence, the segment of the curve beyond $a = 0.8$ mm on a crack growth curve with an initial crack length of $c_0 = 0.3$ mm is different from the curve obtained with $a_0 = 0.7$ mm, as demonstrated in Figure 40. This difference is innate to the crack closure model, and its significance may be dependent on the spectrum applied. Hence, *it is recommended that sensitivity studies be conducted when it is required to shift the crack growth curves obtained from software tools based on the concept of crack closure.*

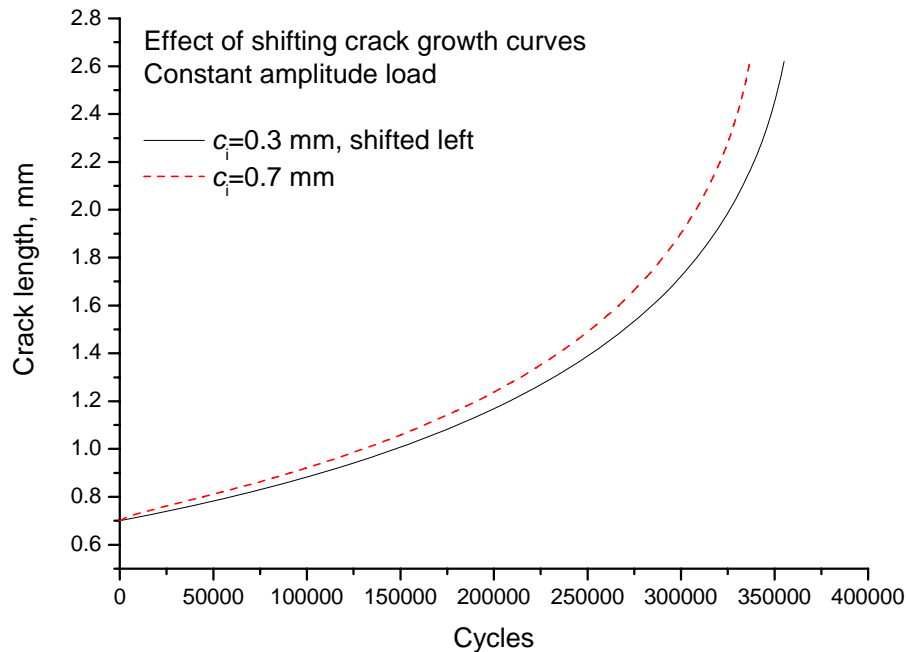


Figure 40 Effect of shifting crack growth curves. The red, dashed line represents the crack growth curve obtained using a smaller initial crack size, and it was shifted leftward to align up with the black solid line, which was obtained using a larger initial crack size

7.4 Compendium of Problems

The previous Sections for this report provided a review of the development of the theories describing fatigue of metallic structures as well as reviewing the methods and software tools used in Structures branch of AVD that implement these theories for fatigue life prediction and crack growth analyses. The emphasis was on the strain-life method for fatigue life modelling and the crack closure model on crack growth modelling. The recent developments on crack growth modelling within DSTO was summarised and flagged for further evaluation and assessment. In this section, we attempt to begin the process of compiling a compendium of problems for fatigue life and crack growth analyses. The problems are categorised as “benchmark problems” for which we can obtain reasonable predictions and “challenging problems” for which we cannot obtain reasonable predictions using existing tools. For each problem, detailed description of the geometry, material, loading and test conditions are given, followed by experimental and numerical data, as shown in Appendix B through Appendix D. All the input data files, the software used for the analysis are also listed in the appendices for easy reproduction of the numerical results in the future.

8. Recommendations and Concluding Remarks

8.1 Concluding Remarks

As part of DSTO's research on fatigue of materials and structures, and in the conduct of test and analysis programs to support the structural integrity of ADF aircraft, DSTO uses a number of software tools and associated approaches to calculate fatigue life and crack growth. In most cases, these tools have been built or imported to support specific major test interpretation projects. Work has rarely been carried out to modify these tools for use in different applications, less so to fully verify and/or calibrate those tools for new applications.

Based on the availability, releasability, level of support and anticipated continued development, and soundness of the underlying models, a number of tools can be recommended for wider distribution within DSTO, or as worthy of further or more in-depth evaluation, or as a candidate for further development.

8.1.1 Fatigue Life Approaches and Tools

The stress-life approaches based on Miner's rule have been in use for many years at DSTO. These can still be undertaken using hand calculations or spreadsheets particularly in association with simplified spectra preparation methods. The stress-life method is also embedded in a number of aircraft fleet fatigue tracking programs such as PC-9, and is the approach used with the SAFE S-N method advocated by DEF STAN 00-970 and used within the F/A-18 test interpretation effort. A FORTRAN program developed under the P-3 SLAP project is currently available for use, but its material database needs to be expanded for other applications.

The strain-life tools available at DSTO, CI89 and FAMS, have been provided as a result of large collaborative test projects on the F/A-18 and P3, respectively. Transfer limitations apparently limit the use of CI89 to F/A-18 work only, a restriction that does not exist with FAMS. Both codes have been shown to produce compatible results in limited verification cases; however, there is currently an active program to improve the performance of FAMS within the P-3 SLAP area.

8.1.2 Crack Growth Approaches and Tools

Crack growth analysis at DSTO has overwhelmingly been based on linear elastic fracture mechanics, either explicitly in the direct use of models such as AFGRAW and FASTRAN, or implicitly in the EBA approach recently used for several F/A-18 analyses. Within the classical modelling approach, the tools available at DSTO such as CGAP/FASTRAN, METLIFE, AFGROW, CG90 and Broek's FractureResearch software could all be used for standard problems that do not involve severe notch plasticity. However, CG90 and Broek are not actively developed and supported.

For notch plasticity dominated problems or spectra with distinct retardation effects the state of the art is that current classical models do not produce reliable predictions, however the crack closure based models such as FASTRAN would seem to produce superior results.

METLIFE purportedly dealt with notch plasticity however verification work within the F-111 program showed up errors, and its proprietary software is not amenable to ongoing evaluation. However, some expertise in METLIFE would be worth retaining within DSTO as the crack growth codes in IMAT, CGRo (FZM-8964 2006) (used for JSF) appears to be at least partially based upon it. The in-house code, CGAP, combines the crack closure model and an advanced cyclic plasticity model to deal with crack growth in notch plasticity-affected zone. It also provides a module for probabilistic crack growth analysis based on Monte Carlo methods. Its graphical user interface, with full support of FASTRAN, greatly reduces the work load on input data preparation, simplifies case management, and maintains data consistency.

The effective block approach has been demonstrated to work well for selected cases in the F/A-18 program. The fundamental difficulty in the EBA is the non-transferability of the crack growth rate data from one spectrum to another. The current practice of using a third-party tool (e.g., AFGROW or CGAP/FASTRAN) to transfer the crack growth rate data is problematic: the log-log plots of the numerical results of da/dB versus K_{ref} for two different spectra may not always be linear or parallel to each other. Thus, in some case it may not be possible to uniquely transfer the crack growth rate data from one spectrum to another. One view of the current situation is that; since all models include empirical based adjustments to cope with difficulties such as retardation and as a result all need calibration to the particular problem at hand, it is best to choose the simplest model and adjust it until it 'works'. The other view is that the more 'advanced' models, even though they will still always need calibration, are more likely to correctly predict resulting crack growth behaviour over a wider range of associated spectra and configurations and are therefore likely to be more useful in the end. One error that does need to be watched, however, is the claim that one specific model is better than another based on the comparison of results from an uncalibrated model to one that has had significant effort applied to its calibration to a particular problem.

Classical models currently do not have the ability to predict crack growth in the 'short crack' regime, although success has been shown down to about 0.020" or 0.5 mm when improvements are made to SIF's. This would generally be more than sufficient for their use in determining damage tolerant based outputs such as inspection intervals or life to failure from rogue flaws. The only exceptions may be problems that use a_{NDI} of 0.010" or less such as in some F-111 applications.

The calculation of crack growth life or 'durability' from flaw sizes quoted as 'typical manufacturing flaws' in the airworthiness standards or guidance documents, i.e., 0.005" and less, cannot be expected to be modelled reliably such that predictions for different notch sizes, configurations (beta) and spectra cannot currently be made with confidence. In the same fashion, the EIFS values generated by 'back-projecting' from experimental data are entirely a function of the software tool, its material database, its retardation approach and the SIF solution used for the particular problem. EIFS values generated from one spectrum cannot be expected to correctly predict crack growth life for a second spectra using current classical tools, although applications involving repeated spectrum blocks and high stresses are more likely to be successful.

The alternative log-linear crack growth curve fitting approach has been shown to match experimental data down to very small sizes, but the restrictions on its claimed (and currently demonstrated) applicability are severe, i.e., no change in the geometry factor for SIF calculation, no load shedding, no plasticity, and limited spectra and stress variation. Within these limitations, however, the estimation of initial equivalent crack size and final crack size does allow the method to produce estimations of total life to failure.

8.1.3 Probabilistic Approaches

The discussion in Section 6 of probabilistic approaches to the prediction of fatigue and crack growth is not meant to be comprehensive, and reference is made to the publication from other DSTO groups working in this field. Probabilistic approaches fall into two categories: the first is to add a capability within the otherwise deterministic fatigue life and crack growth codes in order to analyse sensitivity of input data that are often stochastic in nature; and the second is to statistical analyse either test or real-world data to assess the scatter and then estimate risk. In the second category, one of the most limiting issues is the amount of data typically needed to enable an analysis to be made with the required confidence. Nevertheless, probabilistic approaches will have an essential place in the future development of fatigue life methods, for risk assessment of structural life management.

A summary of the attributes of the recommended software tools for crack initiation and growth analyses are given in Table 4 and Table 5.

8.2 Recommendations

The fatigue life and crack growth tools used by DSTO enable it to support its research into fatigue and its fatigue life test and analysis work for its ADF customers. The project based genesis of the various tools and their limited individual application within DSTO increases costs to each project, reduces corporate knowledge that would help widen the successful application of the best tools and reduces customer confidence in the ability of DSTO to produce work of a consistent standard. In light of the parallel activities to produce a knowledge information system that will tackle some of these problems, the following recommendations are made:

1. FASTRAN/CGAP and FAMS should be developed (in terms of structure, material database, verification and documentation) for submission to the planned DSTO web-based system of information on airworthiness standards and lifing tools such they become available as standard tools for future applications.
2. The CGAP/FASTRAN tool should be targeted as the platform for continued improvement of the classical crack growth modelling as identified in this report, including the issue of notch plasticity, short crack effect and spectrum effect.
3. The EBA, log-linear and similar crack growth fitting approaches should be considered for use with simple problems, problems where data are limited but where the classical approach has been unsuccessful. However, rigorous evaluation needs to be carried out to evaluate their applicability beyond their limited use under F/A-18, and identify their intrinsic advantages and limitations.

4. The compendium of benchmark problems assembled at the end of this report provide a stating point for further evaluation of existing tools as well as the validation and/or calibration of new tools or new versions of existing tools. The problems presented are not exclusive and should be built upon.
5. Probabilistic approaches to estimating fatigue lives and crack growth lives either as options to existing deterministic models, or as solutions to the interpretation of test data need to be part of DSTO's pursuit of improved fatigue analysis methodologies.

Table 4 Summary of tools for fatigue life analysis: input, output and capabilities

Tools		CI89 4.0	FAMS (including DSTO femsh 1.42)	S-N_fatigue_1-e.exe 1.3
Features				
Input	Material	$\varepsilon - N$ curve and other data	$\varepsilon - N$ curve and other data	$S - N$ curve and other data
	Geometry	K_t	Up to 10 K_n	Coupon-specific
	Load	Up to 100 stress levels	Spectrum	Spectrum
Output (Damage)	Line-by-Line	Yes	Yes	Yes
	Peak-Valley	Yes	Yes	Yes
	Truncation Levels	No	Yes	No
	Flight-by-Flight	No	Yes	No
Capabilities	Cycle Counting	Optional	Compulsory	Optional
	Pre-Strain Transition	Yes. A second $\varepsilon - N$ curve may be used	No	No
	Equivalent Strain Equations or Mean Stress Equation	F15, Morrow, Modified Goodman, Gerber, Soderberg, SWT, F-18, F18-Morrow	Morrow, Loopin, modified Loopin, Walker, SWT, F-18, LM-Aero Mod #1, and LM-Aero Mod #2	Modified Goodman, optional
	Residual Stress	Yes	Yes	No
	Notch Stress	Neuber's rule or Glinka's method	Neuber's Rule	N/A
	Multiple Pass Analysis	No	Yes	No
	Database	Tabulated material data	<ul style="list-style-type: none"> • Tabular material data • Parametric material data 	Tabular material data
	Source Availability	Yes	Yes	Yes

Table 5 Summary of tools for crack growth analysis: input, output and capabilities⁷

Tools Features		AFGROW 4.10.13.0	METLIFE 1.3	FASTRAN 3.8	CGAP 1.5	Log-Linear	EBA
Input	Primary Crack Growth Rate da / dN	CA $\frac{da}{dN} = C\Delta K^m$	CA $\frac{da}{dN} = C\Delta K^m$	CA $\frac{da}{dN} = C\Delta K_{eff}^m$	CA $\frac{da}{dN} = C\Delta K_{eff}^m$	$\frac{da}{dN} = \lambda a$	VA $\frac{da}{dN} = C_B K_{ref}^{m_B}$
	Crack Configuration	33 built-in User defined	More than 50	18 built-in User defined	21 built-in User defined	Coupon-specific	Coupon-specific
	Load	Tension Bending Bearing Combined	Tension Bending Bearing Combined	Tension Bending Combined	Tension Bending Combined	Test spectrum- specific	Test spectrum- specific
Output	Crack Growth Curve	Yes	Yes	Yes	Yes	Yes	Yes
	Beta Solution	Yes	Yes	No	Yes	No	No
Capabilities	Stress Ratio	Forman Walker Crack Closure	Forman Walker	Crack Closure	Crack Closure	All the effects are lumped in λ	All the effects are lumped in C_B and m_B
	Retardation	Wheeler Willenborg Crack Closure	Wheeler Willenborg	Crack Closure	Crack Closure		
	Short Crack Effect	Crack Closure	No	•Crack Closure •Fictitious Crack	•Crack Closure •Fictitious Crack		

⁷ ADAMSys, Broek and CG90 are not included due to their infrequent use and inactive support.

Tools Features		AFGROW 4.10.13.0	METLIFE 1.3	FASTRAN 3.8	CGAP 1.5	Log-Linear	EBA
	<i>Notch Plasticity</i>	No	Yes	No	Yes		
	<i>Initial Residual Stress</i>	Yes	Yes	No	Yes		
	<i>Residual Strength</i>	Yes	For multiple stress levels	•Elastic Fracture •Elastic-plastic Fracture	•Elastic Fracture •Elastic-plastic Fracture	No	No
	<i>Probabilistic Crack Growth</i>	No	No	No	Monte Carlo	No	No
	<i>Graphical User Interface</i>	Yes	No	No	Yes	No	No
	<i>Database Support</i>	Material Beta	Material Beta	No	Material Crack config Load Case	No	No
	<i>Source Availability</i>	No	No	Yes	Yes	Yes	Yes

Appendix A Various Implementations of the Stress-Life Method at DSTO

The most recent uses of the stress-life method for structural fatigue analysis in DSTO were in the PC-9 full scale fatigue tests (FSFT) and P3-C Service Life Assessment Program (SLAP). The PC-9 FSFT program was conducted by DSTO between 1993 and 2000 and the test interpretation effort used a stress-life approach along with fixed test scatter factors taken from the UK MoD DEF STAN 00-970 issue 1. A description of the fatigue life algorithm used can be found in (Kashyap and Anderson 1995), which includes a FORTRAN routine called 'minsum.for'.

The P3-C SLAP test interpretation process was initiated in about 2002 and intended to use a strain-life approach, consistent with the intent of the other members of the P-3 SLAP effort, including the USN. However, in order to assess the performance of the proposed USN sourced strain-life program FAMS, the DSTO P-3 SLAP team embarked on building a number of stress-life based computer programs in order to compare the results. In the end four algorithms were built into a single piece of software: S-N_Fatigue_1-3.exe documented in (Phillips 2004). The four algorithms were: the ESDU $S-N$ algorithm, the PC-9 sourced minsum algorithm, an algorithm sourced from the P3-C Service Life Monitoring Program (SLMP) software written by Aerostructures Australia and the modified Goodman algorithm that applied the Goodman adjustment for mean stress to the PC-9 algorithm.

A.1. ESDU S-N Algorithm

The ESDU $S-N$ algorithm consists of performing a straightforward log-linear interpolation to estimate the fatigue life N , at a given stress value between data points identified on the ESDU $S-N$ curve. The accuracy of the estimation depends on the quality of the data used. The data used in this case were the $S-N$ data given in the ESDU data sheet 89046.

This data sheet provides $S-N$ curve data on low-load transfer joints with different fasteners and materials. Depending on the circumstances different data can be used for the analysis. In this case the data used were based on a clearance fit Hi-lok fastener for the material 7010-T765 derived from constant amplitude loading and a mean stress of 56 MPa. This material was selected for two reasons: the material data are the closest representation to 7075-T651 which is the predominant material on the P3-C, and the Hi-lok fastener data represented the most conservative analysis results. Other data could, of course, be added to the program as required.

One of the limitations of the current data is the endurance range which covers all data between 3,000 and 20,000,000 cycles. If the stress level is such (lower than the stress corresponding 3,000 cycles or higher than the stress corresponding to 20,000,000 cycles) that the endurance limitations are exceeded at either extreme, the corresponding extreme value is taken as the fatigue life.

The second limitation of this algorithm is that it is limited to performing the life calculation at an R -ratio that is inherent in the $S-N$ data used. For variable amplitude spectra the

successive stress pairs may have different mean stresses so this limitation could be significant. One of the ways to circumvent this problem is to incorporate the Goodman/Gerber algorithm for mean stress adjustment into this algorithm.

A.2. PC-9 Minsum Algorithm

The PC9 algorithm utilises a cubic function to determine the corresponding life from a given stress amplitude. This analysis can be performed for R -ratios ranging from -0.5 to 0.2 incremented by 0.1 . One of the limitations of this approach is that the exact R -ratio will not necessarily be available and hence the data used will have to be the closest R -ratio to the actual value. This could result in either overly conservative or non-conservative results depending on the R -ratio approximation used, especially for certain locations on the P3-C where the R -ratio for the sequence is -1.0 .

The PC-9 *minsum* algorithm data also has the limitation of calculating the endurance value between 2,500 and 10,000,000 cycles. Similar to the ESDU algorithm, if the stress amplitude indicates that the endurance is outside the extremes of the data the maximum or minimum number of cycles is assumed.

A.3. P-3 SLMP Algorithm

The P-3 SLMP program was developed by Aerostructures Australia as a replacement to the Lockheed-Martin SLEP process that was derived in the 1980s based on the RAAF usage at that time. Analyses of later usage of RAAF aircraft showed that it was considerably different to the usage of the 1980s. In order to more accurately track the aircraft, an Australian developed program based on the actual usage of the aircraft was proposed. The algorithm extracted from the SLMP for this analysis was "algorithm 6" which is called the K_t damage algorithm, whilst the tabular $S - N$ data for a range of R -ratios was for 7075-T6, however its original source could not be verified.

The algorithm uses the mean stress, stress amplitude, and the K_t of the location to determine the damage. The first stage of the algorithm is to calculate the endurance which is done by fitting a quadratic surface over the three K_t values that are closest to the K_t of the location. The three K_t are picked from a pre-defined list of K_t values. Damage is then calculated for the three K_t values based on the number of occurrences and the endurance for each of these values. Finally the damage for the required K_t is calculated by interpolating the damage results from the other three K_t values.

As a result of the complexity of the analysis there are some limitations to the P-3 SLMP algorithm; however, these are primarily limited to the original specification of the algorithm in (Murtagh 2001). The P-3 SLMP algorithm was written according to this specification; however, small discrepancies were still identified. The first is that the interpolation formula was found to result in realistic endurance values for only a certain case. The interpolation did not work if the desired K_t value fell between the second and third fixed K_t values, as the calculated endurance was less than the calculated endurance for the third fixed K_t .

Following this discovery, the P-3 SLMP algorithm was altered to utilise three different interpolation methods. The first method is the original P-3 SLMP interpolation method. The second method utilises the same interpolation formula as that specified for the P-3 SLMP, but ensures that the specified K_t falls between the first and the second fixed K_t values. The third interpolation method is simply a logarithmic linear interpolation between the two bounding fixed K_t values. Generally the endurance values obtained for the modified SLMP algorithm are similar to those obtained for the log-linear interpolation, which are far better to those obtained for the original P-3 SLMP interpolation.

It should be noted that all compressive cycles have a damage value of zero in the SLMP algorithm. This was not always the case, as the SLMP algorithm would calculate a large endurance value for a compressive cycle. Although the damage for the compressive cycle was rather small, it was thought to be more complete if these compressive cycles were assumed to not contribute to the overall damage.

A.4. Modified Goodman Algorithm

This algorithm was written to address some of the limitations of the PC9 algorithm. The modified Goodman equation (45) converts the stress amplitude for a R -ratio that is not equal to minus one to an equivalent stress amplitude at an R -ratio of -1 . Therefore, the limitations of the usable R -ratios taken from the PC9 data are removed.

$$S_a = S_{a0} \left[1 - \left(\frac{S_{mean}}{S_{ult}} \right) \right] \quad (45)$$

The material information for an R -ratio of -1 was generated by curve-fitting data points obtained for 7075-T6 sheet having a K_t of 3.6 (Schwarmann 1988) with cubic polynomial. The comparison of the Schwarmann data and the curve fit are illustrated in Figure 41. This is currently the only material data available for this algorithm in the current version of the software but additional data could of course be added as required.

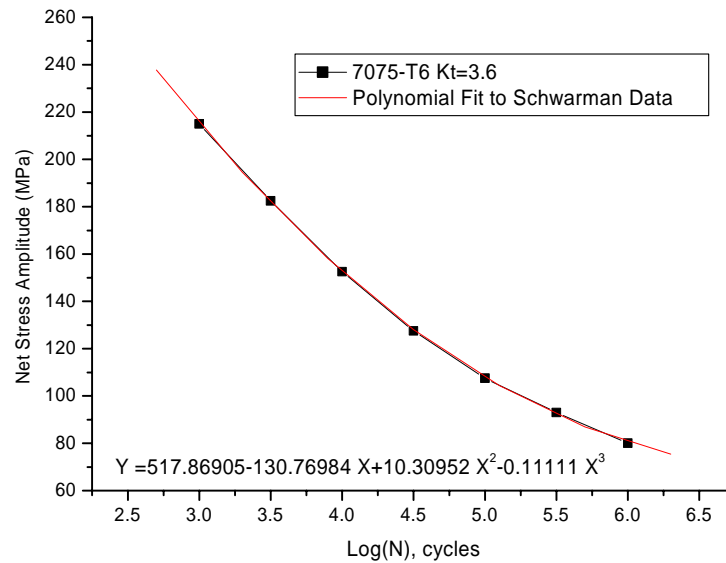


Figure 41 Stress-life data for 7075-T6 (Schwarman 1988), with cubic curve-fitting

The curve fit limitations for this cubic were extrapolated slightly to an endurance value that is between $10^{2.5}$ and 10^7 (These limits can be modified by altering the material data file). Similar to the previous algorithms if the endurance falls outside the limits of the data available, the endurance is approximated to the extreme value.

A.5. Case Study

As was the original purpose in the P-3 SLAP test interpretation, a comparison was made between the DSTO developed stress-life algorithms and the version of the strain-life program FAMS that was in use at the time. The experimental data used as the benchmark for comparison were a set of test results from K_t (net) = 4 coupons that were run using P-3C lower wing stress sequences representative of the usage from each of the P-3C SLAP participants (RAAF, the Netherlands and the Canadian Force (CF)) as well as the proposed FSFT sequence. The results from the various analytical methods were then compared to the total life results obtained for a coupon spectrum tested by the National Aerospace Laboratory (NLR) in the Netherlands. The four different spectra were run through the $S - N$ program, with each algorithm multiplied by a stress factor so that the time to failure for the FSFT spectrum was the same as that recorded in the coupon tests performed by NLR, see (Veul and Ubels 2003) for published results.

Reference (Technical Data Analysis Inc 2003) performed a correlation analysis of FAMS using the same spectra for FCA301 outlined in Reference (Veul and Ubels 2003). In this analysis the calculated life for all the spectra were normalised to the FSFT spectrum. If the predictions are exactly the same as the actual lives the points should all place along the 1-1 line. In order to see the relative effectiveness of the four algorithms, the calculated lives for the four algorithms were plotted against the test lives in a similar manner to that done in (Technical Data Analysis

Inc 2003). Again the calculated life for each spectrum was normalised by the calculated life of the FSFT spectrum on the y-axis, with the coupon test results normalised by the coupon test result for the FSFT on the x-axis. The resulting graph is presented as Figure 42.

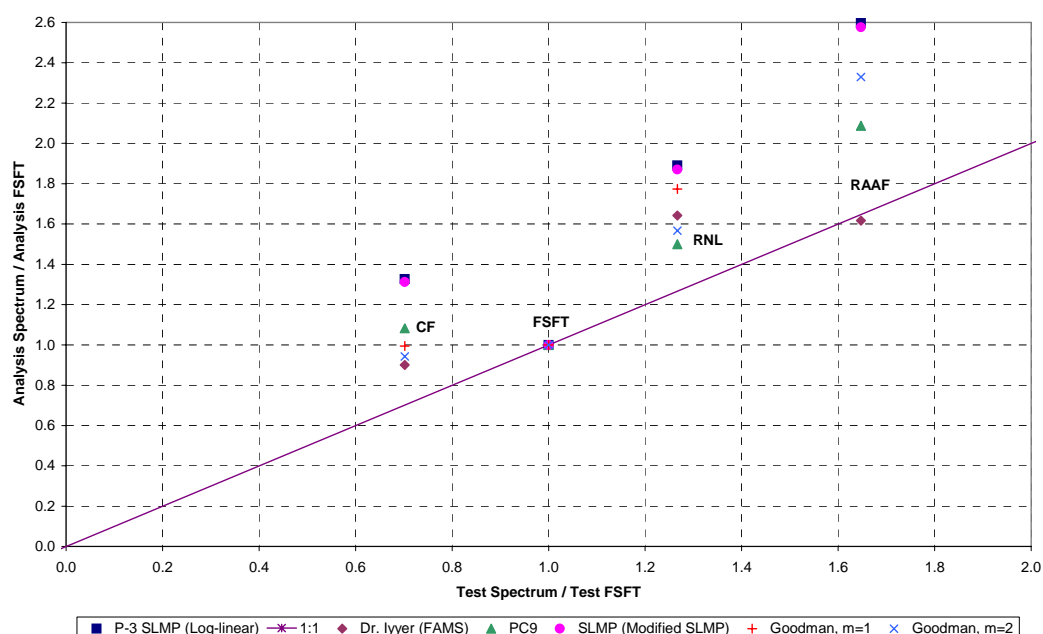


Figure 42 S-N algorithms & FAMS normalised fatigue lives for FCA301

A stress multiplication factor was applied to the S-N fatigue algorithms to ensure that the calculated life was the same as that determined for the coupon tests under the FSFT spectrum (i.e., 17,677 hours). The resulting ratios are presented according to the fatigue algorithm, along with the corresponding stress multiplication factor applied to the sequence.

Table 6 Analysis Results from Algorithm Comparison Case Study for FCA301

Analysis Method	Methodology / Algorithm	Spectrum				Stress Multiplier
		FSFT	CF	RAAF	RNLN	
Coupon Test	Coupon Test Results	1.0000	0.7019	1.6471	1.2668	N/A
FAMS	Technical Data Analysis	1.0000	0.9001	1.6167	1.6418	1.00
	DSTO Analysis	1.0000	0.8437	1.6496	1.4028	1.00
S-N Fatigue Program	PC9 (7075-T6 sheet, $K_t=3.6$)	1.0000	1.0826	2.0875	1.5004	1.3694
	P-3 SLMP (Log-linear)	1.0000	1.3266	2.5976	1.8901	0.8516
	SLMP (Modified SLMP)	1.0000	1.3124	2.5769	1.8706	0.83
	Goodman (m=1.0)	1.0000	0.9942	2.8041	1.7737	1.4454
	Goodman (m=2.0)	1.0000	0.9429	2.3295	1.5676	1.7208

It can be seen from Figure 42 and Table 6 that the Goodman $S - N$ analysis is the only stress-life algorithm that correctly predicts a shorter fatigue life for the Canadian Forces (CF) spectrum than that of the FSFT, as was demonstrated in the fatigue coupons. FAMS also predicted a shorter fatigue life for the CF spectra than that of the FSFT and shows generally a better prediction against experiment for all three of the fleet usage based sequences than did any of the stress-based algorithms. Whilst it was acknowledged at the time that improvements could have been made to the stress-based methods, for example using $S - N$ data for a K_t closer to that of the coupon, the conclusion was that the P-3 program would proceed with the FAMS software.

Appendix B Benchmark Problems for Fatigue Life Analysis

The objective of this section is to provide a list of problems for which there are experimental data available. Using these data it is then possible to generate predictions using crack initiation programs, the results of which can be compared to the experimental data to determine the accuracy of the software's predictive capability.

This section is split into two parts: constant amplitude loading and spectrum loading. The problems defined in this section are relatively straightforward and can be easily solved. Hence they are considered benchmark problems.

B.1. Benchmark Problems for Constant Amplitude Loading

This coupon test was conducted to generate sufficient constant amplitude load coupon data for aluminium 7075-T6 for varying R-ratios (Phillips, Hartley and Amaratunga 2005). The original test was performed for multiple coupons with varying stress concentration profiles; however this problem definition will focus on only 3 different stress concentrations.

B.1.1 Coupon Descriptions

The three different coupon geometries have theoretical stress concentration factors K_{tgross} of 1.00, 3.24, and 5.00. The coupons were sourced from either Lockheed Martin or DSTO. The coupons with $K_t = 1.0$ are dog-bone shaped while the other two sets of coupons were rectangular plates with a central hole and compound notches, as shown in Figure 43-Figure 45, respectively. More detailed information regarding the coupons may be found from (Phillips, Hartley and Amaratunga 2005).

Each coupon was tested to failure, and the time to crack initiation was determined using crack cameras. The crack initiation life was defined as the number of cycles at which a visible crack was observed from crack camera pictures. This particular method was used because it was the only one available at DSTO to determine the crack initiation when the experiment was conducted.

B.1.2 Coupon Data for K_t Equal to 3.24

Coupon Geometry

The coupon that has a gross stress concentration factor of 3.24 was manufactured from 0.125" 7075-T6 extrusion. These coupons have the geometry outlined in Figure 43. The stress concentration was derived from the hole in the middle of the coupon.

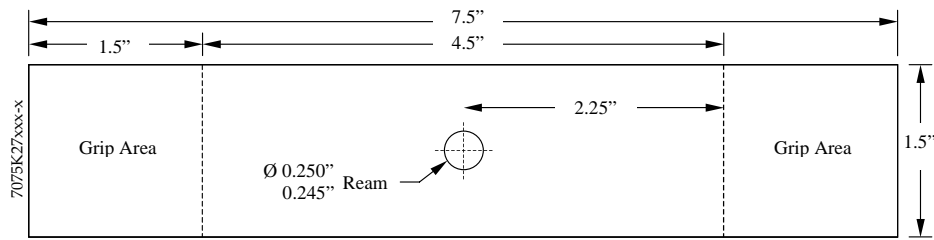


Figure 43 Geometry for coupons with $K_t = 3.24$

Test Results

The experimental results in terms of the total fatigue life obtained for these coupons are presented in Table 10, together with numerical results obtained from FAMS and CI89. It should be noted that all the numerical predictions are conservative.

B.1.3 Coupon Data for K_t Equal to 5.00

Coupon Geometry

The geometry for the gross stress concentration of 5.0 is shown in Figure 44. These coupons were manufactured from 0.125" 7075-T6 Alclad Sheet, and were sourced by DSTO. DSTO decided to use an Alclad sheet of 0.125" for the manufacture of these coupons instead of a 0.120" 7075-T651 extruded section. This was because the sheet was readily available at the time of manufacture. The coupon stress concentration is derived from the rabbit ear type notch in the centre of the coupon.

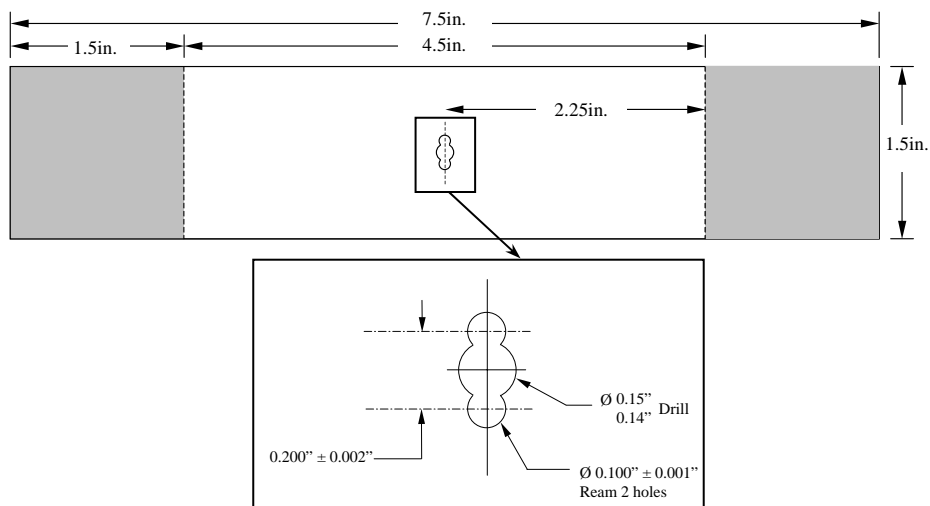


Figure 44 Geometry for coupons with $K_t = 5.00$

Test Results

The results obtained for these coupons are presented in Table 11 on p. 116.

B.1.4 Coupon Data for K_t Equal to 1.0

Coupon Geometry

The geometry of the coupons with $K_t = 1.00$ designed using ASTM standard E466-96 (ASTM 1996) is shown in Figure 45.

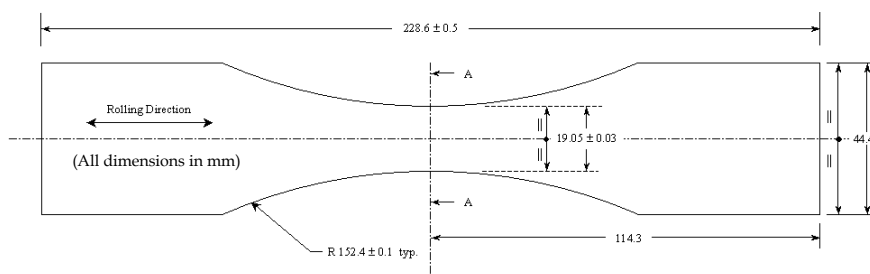


Figure 45 Geometry for coupons with $K_t = 1.00$.

Test Results

The results that were obtained for these coupons are presented in Table 12 on p. 117.

B.2. Benchmark Problems for Spectra Loading

B.2.1 Fighter Aircraft Spectrum Loading

Test Purpose

The purpose of this test program was to generate experimental data to validate CI89 and produce stress versus life curves for a practical range of stresses. A series of 7050-T7451 coupon tests were conducted to evaluate the fatigue lives of various F/A-18 spectra. Further details of these coupon tests and resulting analyses may be found in (Molent, Ogden and Pell 2000) and (Dickinson and Molent 2000). Only the results for one of F/A-18 spectrum are presented below.

Coupon Geometry

The coupons used for the test were of a “dog bone” configuration which was designed to represent the six inch radius of the F/A-18’s FS488 bulkhead lower lug flange fillet. The coupons were made from 7050-T7451, had a theoretical stress concentration factor of $K_t = 1.055$ and a test area of 177.8 mm². The coupons had an “as machined” surface finish with a roughness grade number of N5 or N6. Figure 46 shows the geometry of the coupons.

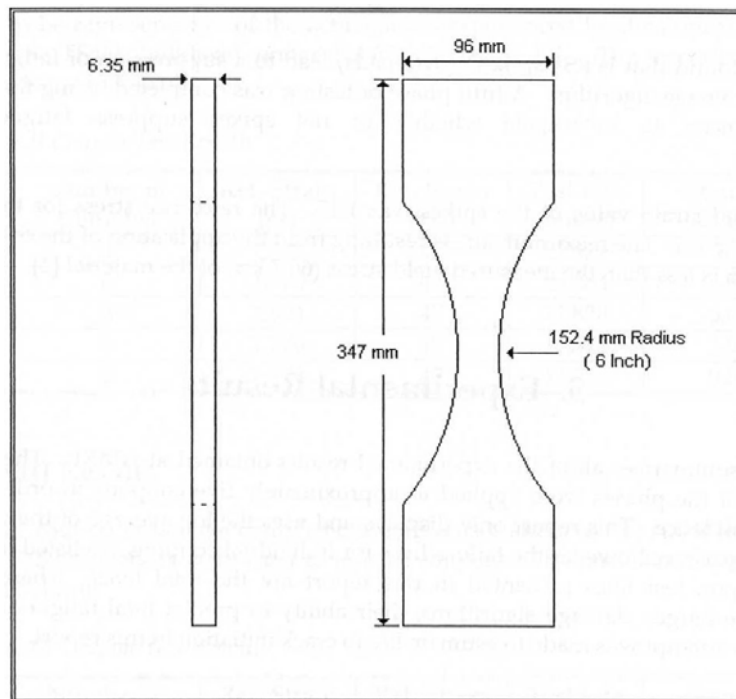


Figure 46 Geometry for FS488 Flange Fillet Coupons

Test Spectra

APOL (Australian Post-LEX (Leading Edge eXtension)) is an F/A-18 spectrum which represents RAAF usage after the addition of the LEX fence. The spectrum represents a wing root strain sequence for a fighter aircraft. The APOL coupon test sequence contains 22,062 points and represents 294.1 hours of usage.

Test Results

The results from the coupon tests under the APOL spectrum are presented in Table 13 on page 117 for a number of applied stresses. These results were taken from (Dickinson and Molent 2000). Approximately five coupons were tested at each stress level. Note that the coupon test lives provided are total lives.

B.2.2 Transport Aircraft Spectrum Loading

Test Purpose

The purpose of this test program was to obtain fatigue life data for 7075-T6 coupons under P-3C representative spectra loading. Tests were performed using the RAAF P-3C spectrum and the sequence applied to the USN P-3C wing-fuselage Full Scale Fatigue Test (FSFT) which is representative of 85th percentile USN usage.

Coupon Geometry

Notched coupons that had a gross stress concentration of $K_t = 5.00$ were used for this test program, as illustrated in Figure 44. These coupons were manufactured from 0.125" 7075-T6 Alclad sheet, and were sourced by DSTO-PSL.

Test Spectra

The coupons tests utilised spectra at fatigue critical area (FCA) 301 and FCA 361. Both FCAs are situated on the front lower spar beam of the outer wing with FCA301 at the wing root (BL 65) and FCA 361 at the inboard engine nacelle (WS 209). These two locations were selected because they provided examples of a tension-tension dominant spectrum (FCA 301) and tension-compression dominated spectrum (FCA 361). The RAAF P-3C spectrum for these locations was generated from the Database Interface / Spectra Sequencing Tool using Phase IIB loads (Matricciani and Jackson Unpublished) while the FSFT spectrum was obtained from Lockheed Martin. The test matrix for the spectrum analysis coupon is presented in Table 7. Due to the large number of cycles in each spectrum, it was decided that the spectrum would be applied at 20 Hz to reduce the amount of test machine running time.

Table 7 Test Matrix for the Spectrum Analysis Coupons

FCA Location	Spectrum	Clipping Level (ksi)	Spectrum Size (Cycles)	Max Test Load (N)	Min Test Load (N)	Freq. (Hz)	N° of Coupons
FCA301	FSFT	None	440,674	24,790	-5,475	20	3
	P-3C	None	1,048,807	23,088	-5,920	20	3
FCA361	FSFT	None	427,952	20,296	-12,717	20	3
	P-3C	-21.829	1,269,031	18,206	-18,206	20	3

The equivalent flight hours for a block of data differ for the FSFT and the RAAF P-3C DBI/SST spectra. A FSFT spectrum block corresponds to 14,994 equivalent flight hours, while the DBI/SST corresponds to 15,292 hours. The appropriate hours need to be used when converting the number of cycles to equivalent flight hours.

The applied loading for each coupon was calculated using the maximum stress, which was converted to a force using a gross area of 0.1875 in.² (1.5"×0.125").

Test Results

The results obtained for the FCA301 and FCA361 coupons are presented in Table 14 and Table 15, respectively. The crack initiation time values are only approximate, because they are limited to intervals when the crack camera photos are taken. Furthermore a crack was only identified once it was clearly visible on the surface of the coupon.

Appendix C Challenging Problems for Fatigue Life Analysis

The main objective of this section is to present coupon test data for problems which are considered more challenging for the existing numerical tools. The results from the crack initiation programs are presented, with the estimated lives orders of magnitude greater than the test results, as shown in Table 16 through Table 18. These problems highlight the deficiencies of the existing methods/tools.

C.1. Challenging Problems for Constant Amplitude Loading

C.1.1 Low Load Transfer Joint Coupon Tests

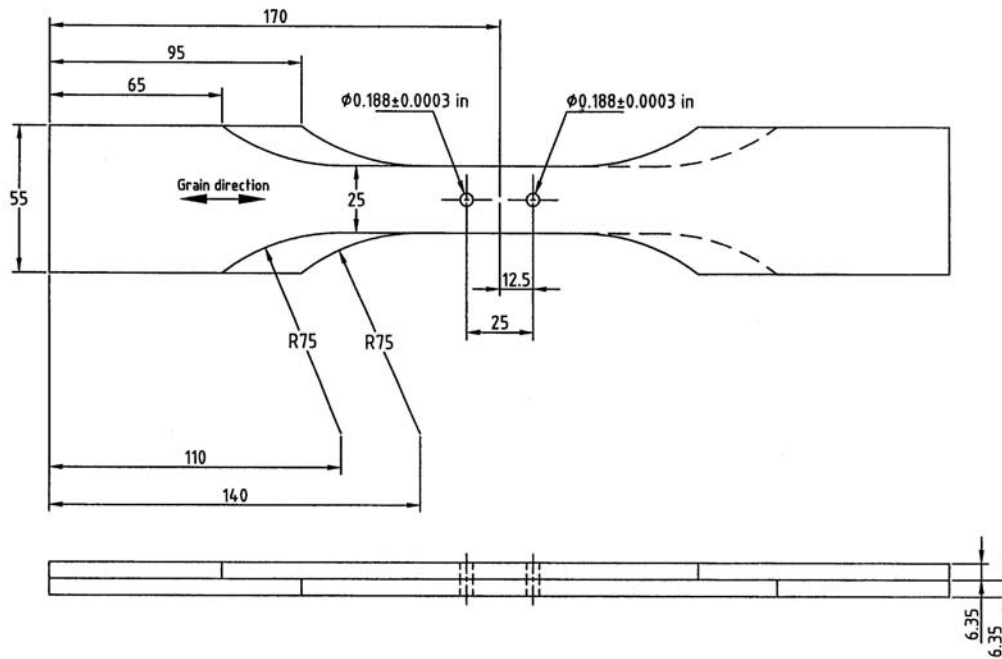
Test Purpose

The Australian P-3C empennage FSFT article completed 60,000 simulated flight hours of testing. Analysis of the structure has led to the generation of several FCAs, which have a structural configuration similar to that of a low load transfer joint.

In order to verify the predictive capabilities of the crack initiation software, a coupon test was conducted where the coupons simulated a low load transfer lap joint.

Coupon Geometry

The coupon specimens consisted of two 7075-T6 aluminium plates (340mm x 55mm x 6.35mm) that were joined face to face with two 3/16" diameter Huck Lockbolt fasteners (see Figure 47). The total coupon thickness was 0.5". It should be noted that the fasteners were installed with a slight clearance fit, which is the worst-case scenario for joint fatigue life.



Note: (dimensions in mm unless stated otherwise)

Figure 47 Geometry for Low Load Transfer Coupons

Test Spectrum

Whilst this problem definition calls for a constant amplitude sequence the example presented here is one with spectrum loading. However, the load sequence is fully reversed with an R ratio of -1. The sequence utilised in the coupon testing is represented by FCA811 which is located on the front spar at the root of the vertical tail. As the sequence is reasonably benign, initial testing was conducted with the basic FCA811 spectrum factored up by 1.8 times to gain some idea as to the duration each test will take prior to failure. This factored spectrum became known as Spectrum E.

It was found that the test took too much time and hence Spectrum E became the baseline sequence to which additional multiplication factors were applied to further speed up the test. Table 8 outlines the coupon test program that was developed, which includes the end loads for each test as well as the number of coupons to be run for each case. The revised test program basically consisted of scaled load spectra (factors of 0.9, 1.1 and 1.2) based upon FCA811 Spectrum E.

Table 8 Coupon Test Program

Spectrum Label	Multiplication Factor	End Load (Kn)	Number of Coupons	Test Frequency (Hz)
Spectrum E	0.9	38.38	4	10
	1.0	42.619	4	10
	1.1	46.88	4	10
	1.2	51.14	4	10

It should be noted that the spectrum multiplication factor of 1.2 is the highest stress level that can be tested using this coupon configuration and load spectrum before localised plastic yielding will occur at the highest point of stress concentration.

Test Results

A total of 18 coupon tests were run. Two tests were deemed invalid because the coupon test machine erroneously applied a large compressive load during testing and buckled the test specimen (see Coupon N° 14 and 15). Table 16 on p. 118 shows an overview of the results obtained. The total life value recorded is taken as the number of turning points applied to completely fail both halves of the test specimen.

C.2. Challenging Problems for Spectra Loading

C.2.1 Discrimination Level Coupon Tests

Test Purpose

Five coupons were tested using an F-111 service life spectrum to determine the impact discrimination has on the total life of the coupon. Many crack initiation programs have a minimum threshold below which the cycles are not counted towards calculating the damage of a sequence. As a result by discriminating sequences and running it through this prediction software there is no change in the damage. This test was conducted to check the impact of discriminating the sequence on the total life of the coupon.

Coupon Geometry

The test coupons were manufactured from 7075-T6 Alclad sheet (7.5" × 1.5" × 0.125"), with a net stress concentration factor $K_t = 5.00$. The test specimen contains three holes, which are required to generate the stress concentration, as illustrated in Figure 44.

Test Spectrum

The test spectrum used for this analysis was the F-111 wing spectra DADTA2b from location FAS226. The sequence details are shown in Table 9.

Table 9 F-111 Sequences used for Coupon Test

Sequence	N° of Coupons	Turning Points	Sequence Description
DADTA2b (Disc 1% max peak)	3	1,789,548	RAAF F-111 wing service spectrum at FASS 226 discriminated at 1% of the maximum peak load.
DADTA2b (Disc 12% max peak)	2	65,904	RAAF F-111 wing service spectrum at FASS 226 discriminated at 12% of the maximum peak load.

The DADTA2b sequence was subject to some discrimination as it was a very long sequence and the estimated test time without discrimination was deemed unreasonable. The discrimination level (rise-fall) was set at 1% of the maximum peak stress in the sequence. Two coupons were also subsequently run using a DADTA2b sequence discriminated to 12% of the maximum peak to significantly reduce the number of turning points.

Test Results

Table 17 on p. 118 shows the total life results for the coupon tests.

With the DADTA2b sequence, coupons 27 and 28 had problems during the test. During the testing of coupon 27, the machine stopped at an error detection routine. Once the problem had been rectified the machine started at the beginning of the block rather than continuing on from where it had stopped. This resulted in only half of one block being completed before the sequence restarted.

The test values for coupon 28 are not available as after the completion of four blocks a fault in the test machine caused the machine to shut down. Once the problem was rectified the first load the machine applied was an overload that snapped the coupon.

The results show a significant change in the life between the two sequences. However it must be noted that there is a significant difference between the numbers of turning points between the two.

C.2.2 Overload Coupon Tests

Test Purpose

The predictability of crack initiation software can be greatly affected by the presence of spikes in a sequence. The inclusion of a tensile overload can increase the predicted fatigue life significantly. Consequently, a series of coupon tests were performed to evaluate the effects of overloads. Further details of these coupon tests and resulting analysis may be found in references (Molent, Ogden and Pell 2000) and (Dickinson and Molent 2000). Only the results for one of F/A-18 spectrum are presented below.

Coupon Geometry

The coupons used for testing were of a “dog bone” configuration which was designed to duplicate the six-inch radius of the F/A-18’s FS488 bulkhead lower lug flange fillet. The coupons were made from 7050-T7451, had a theoretical stress concentration factor K_t of 1.055

and a test area of 177.8 mm². The coupons had an “as machined” surface finish with a roughness grade number of N5 or N6. Figure 46 provides an illustration of the coupon.

Test Spectrum

FT55 is an F/A-18 spectrum which was applied to the IFOSTP centre fuselage full-scale fatigue test and is representative of Canadian Forces usage. The spectrum provided represents a wing root strain sequence which was recorded from the FT55 full-scale fatigue test. The basic FT55 coupon test sequence contains 12,172 turning points and represents 323.4 hours of usage. An overload, with a normalised strain value of 1.15 was used to represent an overload in the FT55 sequence.

Test Results

The results from the coupon tests under the FT55 spectrum are presented in Table 1 on p. 119 for a spectrum with and without an overload. These results were taken from reference (Dickinson and Molent 2000). Note that the coupon test lives provided are total lives.

Table 10 Experimental and numerical total fatigue lives for the coupon with a gross stress concentration factor of $K_t = 3.24$ subjected to constant amplitude loading

Test Condition and Results				FAMS Output				CI89 Output					
Stress Ratio	$S_{n,max}$ [psi]	$S_{n,min}$ [psi]	Average Fatigue Life	Morrow	Error %	F18	Error %	Morrow	Error %	F18	Error %	Mod F18	Error %
0.3	35417	10625	25613	5339	-79	11354	-56	8000	-69	7000	-73	16000	-38
0.2	28125	5625	42126	19461	-54	19624	-53	22000	-48	11000	-74	27000	-36
-0.2	26042	-5208	28239	8946	-68	7074	-75	4000	-86	4000	-86	4000	-86
-0.6	31250	-18750	9526	1243	-87	1109	-88	3000	-69	3000	-69	3000	-69
-1	16000	-16000	88145	41503	-53	41499	-53	49000	-44	49000	-44	49000	-44
-1	20833	-20833	28224	7755	-73	7754	-73	11000	-61	11000	-61	11000	-61
-1	26000	-26000	12214	1978	-84	1978	-84	4000	-67	4000	-67	4000	-67

Table 11 Experimental and numerical total fatigue lives for the coupon with a gross stress concentration factor of $K_t = 5.00$ subjected to constant amplitude loading

Test Condition and Results				FAMS Output				CI89 Output					
Stress Ratio	$S_{n,max}$ [psi]	$S_{n,min}$ [psi]	Average Fatigue Life	Morrow	Error %	F18	Error %	Morrow	Error %	F18	Error %	Mod F18	Error %
-2.5	6400	-16000	232089	193029	-17	84985	-63	570000	146	10000000 000	4308592	1000000000 0	4308592
-0.2	20000	-4000	15894	10576	-33	7875	-50	12000	-24	10000	-37	11000	-31
-1.0	15000	-15000	20120	13359	-34	13358	-34	16000	-20	16000	-20	16000	-20
-1.0	20000	-20000	7841.667	2202	-72	2202	-72	4000	-49	4000	-49	4000	-49

Table 12 Experimental and numerical total fatigue lives for the coupon with a gross stress concentration factor of $K_t = 1.00$ subjected to constant amplitude loading

Stress Ratio	$S_{n,max}$ [psi]	$S_{n,min}$ [psi]	Average Fatigue Life	FAMS Output				CI89 Output					
				Morrow	Error %	F18	Error %	Morrow	Error %	F18	Error %	Mod F18	Error %
-1.0	50400	-50400	38402	8622	-78	8622	-78	11000	-71	11000	-71	11000	-71
0.3	42860	12858	38362	2747	-93	2746	-93	5000	-87	5000	-87	5000	-87
-1.0	60480	-60480	45850	2747	-94	2746	-94	5003	-89	5003	-89	5003	-89

Table 13 Coupon Test Results for F/A-18 APOL Spectrum

Stress Level			FAMS Output				CI89 Output					
$S_{g,max}$ [psi]	$S_{n,max}$ [psi]	Average Fatigue Life	Morrow	Error %	F18	Error %	Morrow	Error %	F18	Error %	Mod F18	Error %
47000	49585	25284	2198975	8597	368432	1357	154048	509	34669	37	24374	-4
52000	54860	14767	1189923	7958	260891	1667	91201	518	22917	55	17401	18
57500	60663	9761	728570	7364	201221	1961	54736	461	15870	63	12550	29
62200	65621	7898					36494	362	11939	51	9624	22

Table 14 Spectrum Analysis results for FCA301

Test Condition and Results			FAMS Output				CI89 Output					
Spectrum	$S_{n,max}$ [psi]	Average Fatigue Life	Morrow	Error %	F18	Error %	Morrow	Error %	F18	Error %	Mod F18	Error %
FSFT	149	40430	24233	-40	12130	-70	32751	-19	28258	-30	18603	-54
RAAF	138	27825	40565	46	15393	-45	47371	70	30969	11	27602	-1

Table 15 Spectrum Analysis results for FCA361

Test Condition and Results			FAMS Output				CI89 Output					
Spectrum	$S_{n,max}$ [psi]	Average Fatigue Life	Morrow	Error %	F18	Error %	Morrow	Error %	F18	Error %	Mod F18	Error %
FSFT	122	10046	6038	-40	3665	-64	3096	-69	1812	-82	2494	-75
RAAF	109	12007	11834	-1	5346	-55	8797	-27	2499	-79	6800	-43

Table 16 Low Load Transfer Coupon Test results

Test Condition and Results			FAMS Output				CI89 Output					
Spectrum	$S_{n,max}$ [psi]	Average Fatigue Life	Morrow	Error %	F18	Error %	Morrow	Error %	F18	Error %	Mod F18	Error %
Spectrum E	65613	372311	748079	101	742598	99	788943	112	795396	114	724589	95
Spectrum E x 1.1	72175	166496	383352	130	381230	129	390969	135	387165	133	235442	41
Spectrum E x 1.2	78737	87046	216122	148	169041	94	219449	152	216268	148	132524	52
Spectrum E x 0.9	59052	361672	1550640	329	1536885	325	1641235	354	1641237	354	1645718	355

Note: Spectrum E contains 438,976 turning points, which corresponds to 15,000 test hours.

Table 17 Total Life recorded for the FASS 226 Fatigue Life Coupons

Test Condition and Results			FAMS Output				CI89 Output					
Disc Levels	$S_{n,max}$ [psi]	Average Fatigue Life	Morrow	Error %	F18	Error %	Morrow	Error %	F18	Error %	Mod F18	Error %
1% of Max	88100	3775.16	13146	248	3843	2	18456	389	8915	136	9859	161
12% of Max	88100	8833.07	13146	49	3843	-56	18456	109	11284	28	9859	12

Table 18 Coupon Test Results for F/A-18 FT55 Spectrum. Stress Level: 57.5 ksi

Test Condition and Results			FAMS Output				CI89 Output					
	$S_{n,max}$ [psi]	Average Fatigue Life	Morrow	Error %	F18	Error %	Morrow	Error %	F18	Error %	Mod F18	Error %
Loading No Overload	57500	9121	21783	139	6056	-34	28795	216	8097	-11	6483	-29
With Overload	57500	13679	29870	118	7808	-43	33636	146	12595	-8	8148	-40

Appendix D Benchmark Problems for Fatigue Crack Growth Analysis

D.1. Mirage Spectrum Loading Example

D.1.1 Background

This example consists of a series of tests on simple centre crack tension (CCT) specimens manufactured from 7075-T651 aluminium alloy plate material (Walker 1987; Walker 1997). The specimens were pre-cracked and then subjected to a simplified semi-blocked fighter aircraft (Mirage) load sequence. The load sequence was subtly modified to simulate the imposition of a placard flight restriction. A placard type flight restriction is sometimes proposed as a means of reducing fatigue damage and therefore increasing life. The effect in this case was however dramatic and opposite, i.e., the spectrum with the simulated “placard” produced more rapid crack growth and reduced lives. The crack growth behaviour in this case can be successfully modelled (Walker 1997), provided that the load sequence (retardation/acceleration) effect is accurately accounted for. Previous analysis experience (Walker 1997) has shown that the analytical crack closure modelling method as per FASTRAN can model the behaviour very well. Conventional retardation models such as Wheeler and Willenborg do not work as well.

Specimen geometry

The geometry of the specimens is shown in Figure 48.

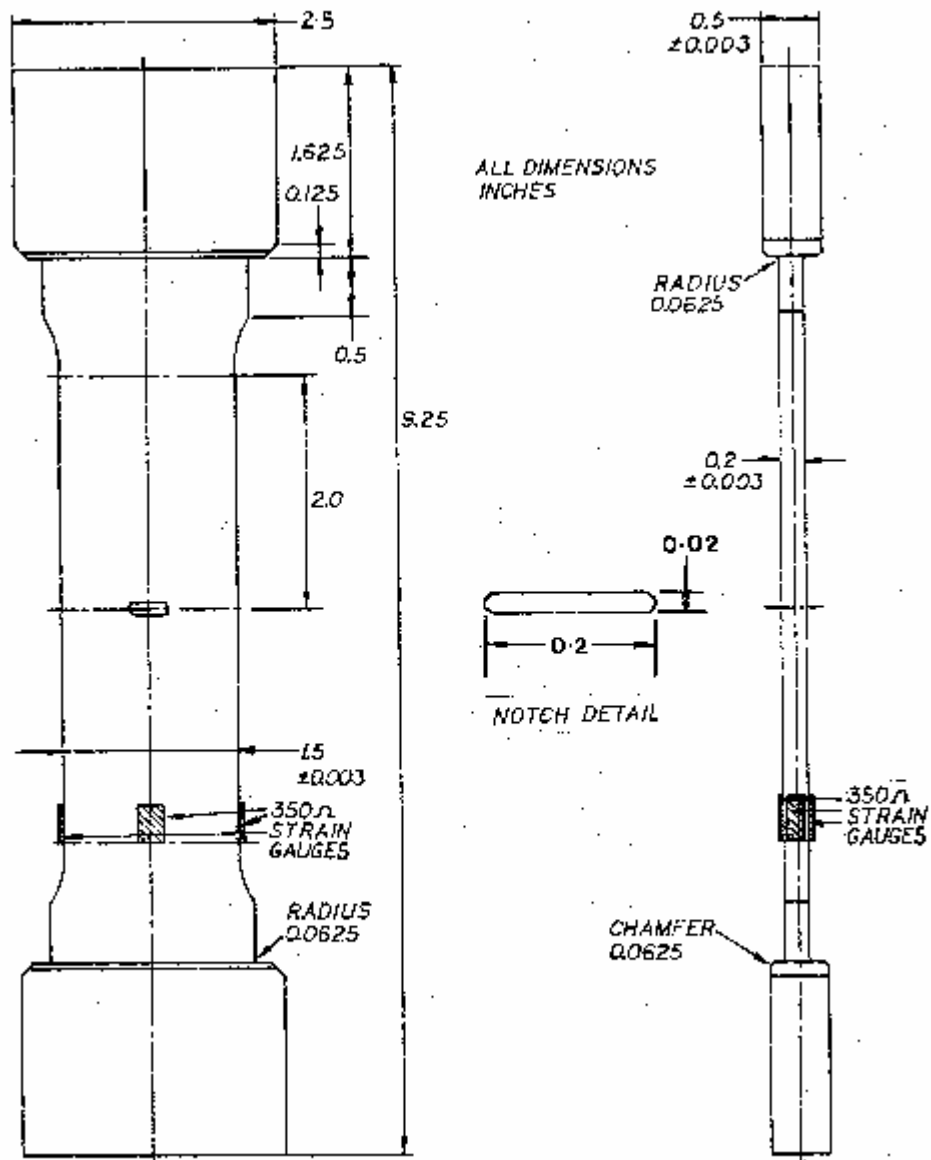


Figure 48 Fixed End Centre Crack 7075-T651 Specimen

Load spectra

The specimens were subjected to four variations of a simplified Mirage fighter aircraft spectrum as follows:

1. The unmodified spectrum;
2. Clipped at 6.5 g;
3. Clipped at 5 g; and
4. With the 7.5 g peak (which occurs once in a 100 flight, 66.6 hour block) increased to 8.5 g.

The spectra are detailed in Figure 49 and Figure 50 and Table 19 and Table 20.

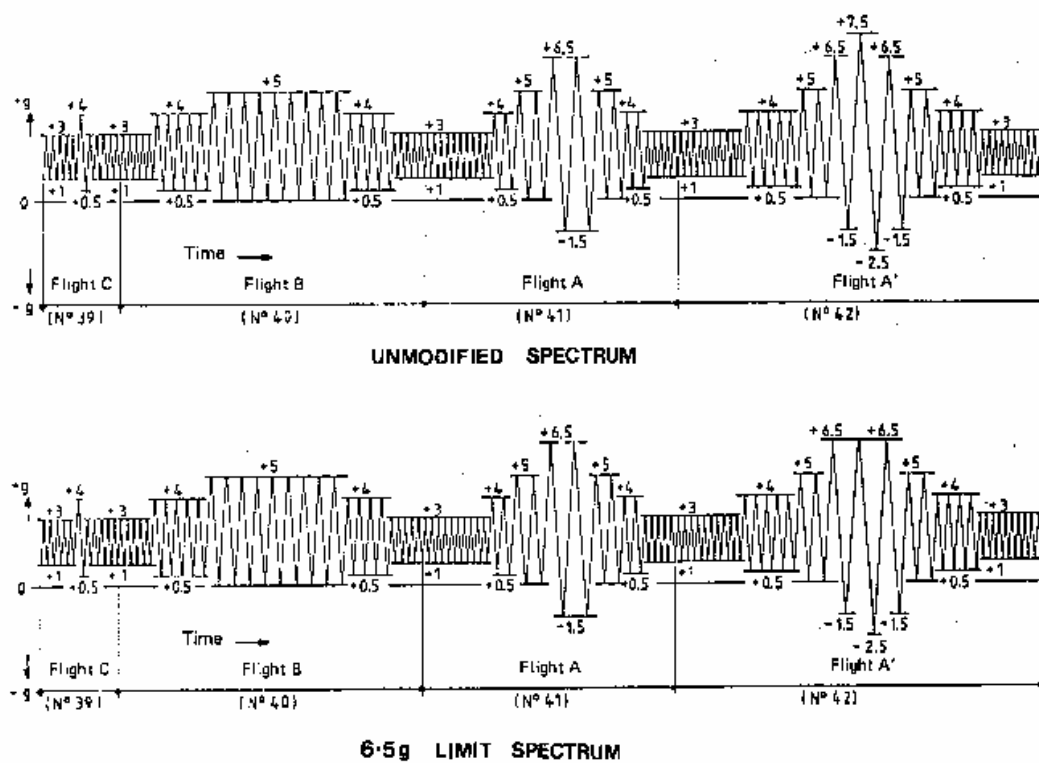


Figure 49 Representative segments from the Unmodified and 6.5 g limit spectra

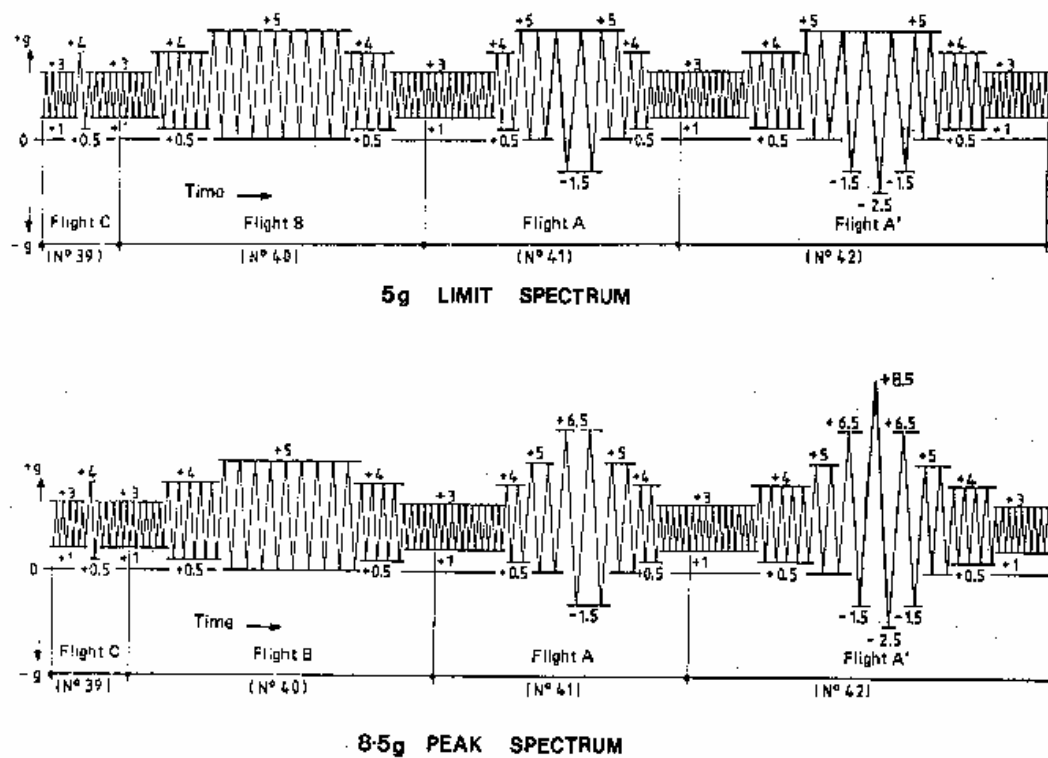


Figure 50 Representative segments from the 5 g limit and 8.5 g peak spectra

Table 19 Flight segment spectra

Flight	Spectra	STEP								
		1	2	3	4	5	6	7	8	9
A'	Unmodified	10 cycles +3/+1	5 cycles +4/+0.5	2 cycles +5/0	1 cycle +6.5/-1.5	1 cycle +7.5/-2.5	1 cycle +6.5/-1.5	2 cycles +5/0	4 cycles +4/+0.5	10 cycles +3/+1
A'	6.5 g Limit	10 cycles +3/+1	5 cycles +4/+0.5	2 cycles +5/0	1 cycle +6.5/-1.5	1 cycle +6.5/-2.5	1 cycle +6.5/-1.5	2 cycles +5/0	4 cycles +4/+0.5	10 cycles +3/+1
A'	5 g Limit	10 cycles +3/+1	5 cycles +4/+0.5	2 cycles +5/0	1 cycle +5/-1.5	1 cycle +5/-2.5	1 cycle +5/-1.5	2 cycles +5/0	4 cycles +4/+0.5	10 cycles +3/+1
A'	8.5 g Peak	10 cycles +3/+1	5 cycles +4/+0.5	2 cycles +5/0	1 cycle +6.5/-1.5	1 cycle +8.5/-2.5	1 cycle +6.5/-1.5	2 cycles +5/0	4 cycles +4/+0.5	10 cycles +3/+1
A	Unmodified 6.5 g Limit 8.5 g Peak	10 cycles +3/+1	5 cycles +4/+0.5	2 cycles +5/0	2 cycles +6.5/-1.5	2 cycles +5/0	2 cycles +4/0.5	5 cycles +3/+1	-	-
A	5 g Limit	10 cycles +3/+1	5 cycles +4/+0.5	2 cycles +5/0	2 cycles +5/-1.5	2 cycles +5/0	2 cycles +4/0.5	5 cycles +3/+1	-	-
B	ALL	5 cycles +3/+1	5 cycles +4/+0.5	9 cycles +5/0	4 cycles +4/+0.5	5 cycles +3/+1	-	-	-	-
C	ALL	5 cycles +3/+1	1 cycle +4/+0.5	5 cycles +3/+1	-	-	-	-	-	-

Table 20 Sequence of flight segments in a block representing 100 flights, 66.6 hours (1989 cycles)

1	2	3	4	5	6	7	8	9	10	11	12	13	14	15
B	C	C	B	C	C	C	A	C	C	B	B	A	C	C
16	17	18	19	20	21	22	23	24	25	26	27	28	29	30
C	B	A	C	B	B	B	A	C	C	C	A	A	C	C
31	32	33	34	35	36	37	38	39	40	41	42	43	44	45
B	B	B	C	B	A	B	C	C	B	A	A'	B	C	C
46	47	48	49	50	51	52	53	54	55	56	57	58	59	60
A	A	B	B	C	C	B	C	C	B	C	B	B	C	C
61	62	63	64	65	66	67	68	69	70	71	72	73	74	75
C	A	B	A	C	C	C	B	A	B	B	B	C	B	C
76	77	78	79	80	81	82	83	84	85	86	87	88	89	90
C	A	B	C	B	A	B	C	C	B	A	A	B	C	C
91	92	93	94	95	96	97	98	99	100	-	-	-	-	-
B	C	C	B	B	C	B	C	A	C	-	-	-	-	-

Test procedure and results

A central slot was machined into the specimens using electrical discharge machining (EDM) and the specimens were then subjected to constant amplitude pre-cracking until a crack length of 0.15 inch ($a=0.15$ inch, $2a=0.30$ inch) was reached. The final maximum load during pre-cracking was 3,000 pounds. The spectrum loading applied later was such that this load level was exceeded in the first 10 cycles. Residual effects from pre-cracking were therefore not anticipated. The ends of the specimens were clamped, and the tests conducted using a computer-controlled electro-hydraulic testing machine. Three specimens were subjected to the unmodified spectrum, two specimens to the 6.5 g limit spectrum, three specimens to the 5 g limit spectrum and one specimen to the 8.5 g limit spectrum. All specimens were tested to failure which occurred at a half crack length a of between 0.5 and 0.6 inch. The crack growth curves are plotted below. There is very little scatter in the results where several tests were

performed under the same spectrum. It is therefore considered reasonable to conclude that the differences in crack growth rate can be attributed solely to the differences in the load spectra.

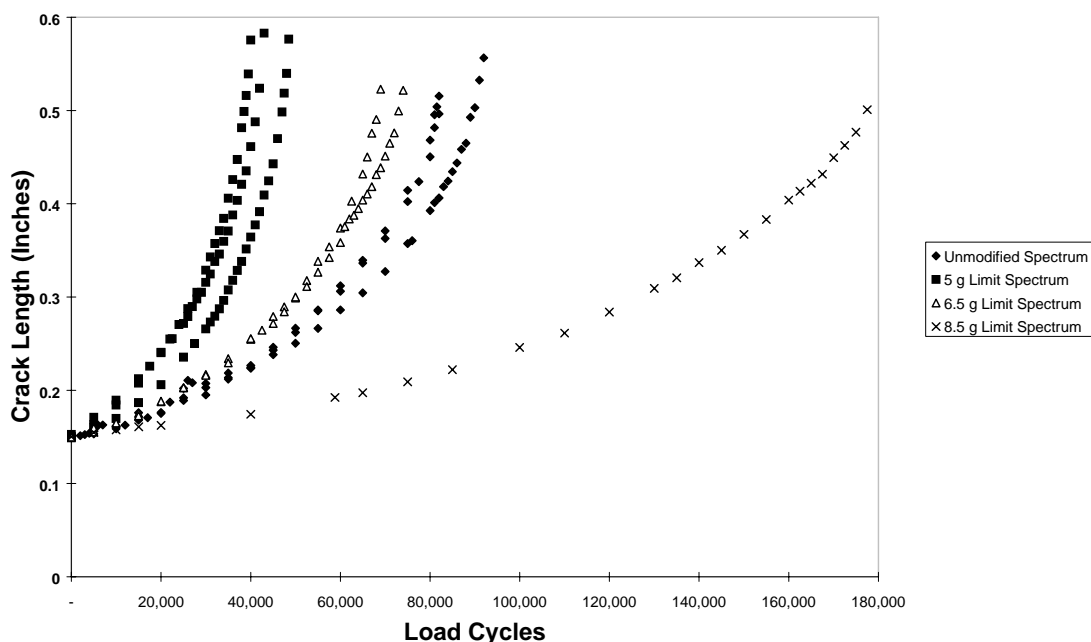


Figure 51 Experimental crack growth results for four Mirage spectra variations.

Computer files

The relevant computer files for this example are as follows⁸:

File name	Details
kev7_5g.dat	Fastran input file which includes the unmodified 7.5 g peak spectrum
kev5g.dat	Fastran input file which includes the 5 g peak spectrum
Kev6_5g.dat	Fastran input file which includes the 6.5 g peak spectrum
Kev8_5g.dat	Fastran input file which includes the 8.5 g peak spectrum
Thesis Check 1.dax	AFGROW problem definition file
miraun.spc	AFGROW spectrum file unmodified 7.5 g spectrum
miraun01.sub	AFGROW spectrum file unmodified 7.5 g spectrum
mira5.spc	AFGROW spectrum file 5 g spectrum
mira501.sub	AFGROW spectrum file 5 g spectrum
mira65.spc	AFGROW spectrum file 6.5 g spectrum
mira6501.sub	AFGROW spectrum file 6.5 g spectrum
mira85.spc	AFGROW spectrum file 8.5 g spectrum
mira8501.sub	AFGROW spectrum file 8.5 g spectrum
Figure4.xls	Experimental results

⁸ The computer files referred to in this section and the next one are available on the accompanying CD.

D.2. F-111 Wing Pivot Fitting Lower Plate Cracking Example

Background

Structural integrity for the F-111 aircraft is generally assured under a durability and damage tolerance analysis (DADTA) and safety by inspection (SBI) basis. The approach is underpinned by analysis and testing. Many of the locations considered for the DADTA are located in the high strength D6ac steel used in the critical structural areas of the F-111. One of these is known as DADTA Item (DI) 86 in the lower plate of the WPF at fuel flow vent hole (FFVH) number 58. Cracks occurred at this location during the A4 right hand wing fatigue test conducted by the manufacturer⁹ in the late 1960s (General Dynamics 1970; General Dynamics 1973). The fracture surface from the crack was subjected to fractographic analysis and a crack growth curve obtained. The manufacturer claimed at the time to have obtained a good correlation between analysis and test (General Dynamics 1970; General Dynamics 1973); however attempts at DSTO to reproduce that result (Murtagh 1997) were only partially successful. This is considered to be a good example for this report because:

1. The geometry is reasonably simple and well defined;
2. The material has been well characterised;
3. There is a crack growth curve from a full scale wing fatigue test under a known spectrum available for comparison;
4. The loading does not exceed the material yield stress. The peak spectrum stress (local) is 169 ksi compared with a material monotonic yield of 190 ksi. However, this does exceed the cyclic proportional limit for the material of 133 ksi.

Geometry

The DI 86 location is detailed in Figure 52 (reproduced from General Dynamics 1987).

⁹ At the time the manufacturer was known as General Dynamics. The Company is now part of the Lockheed Martin Corporation.

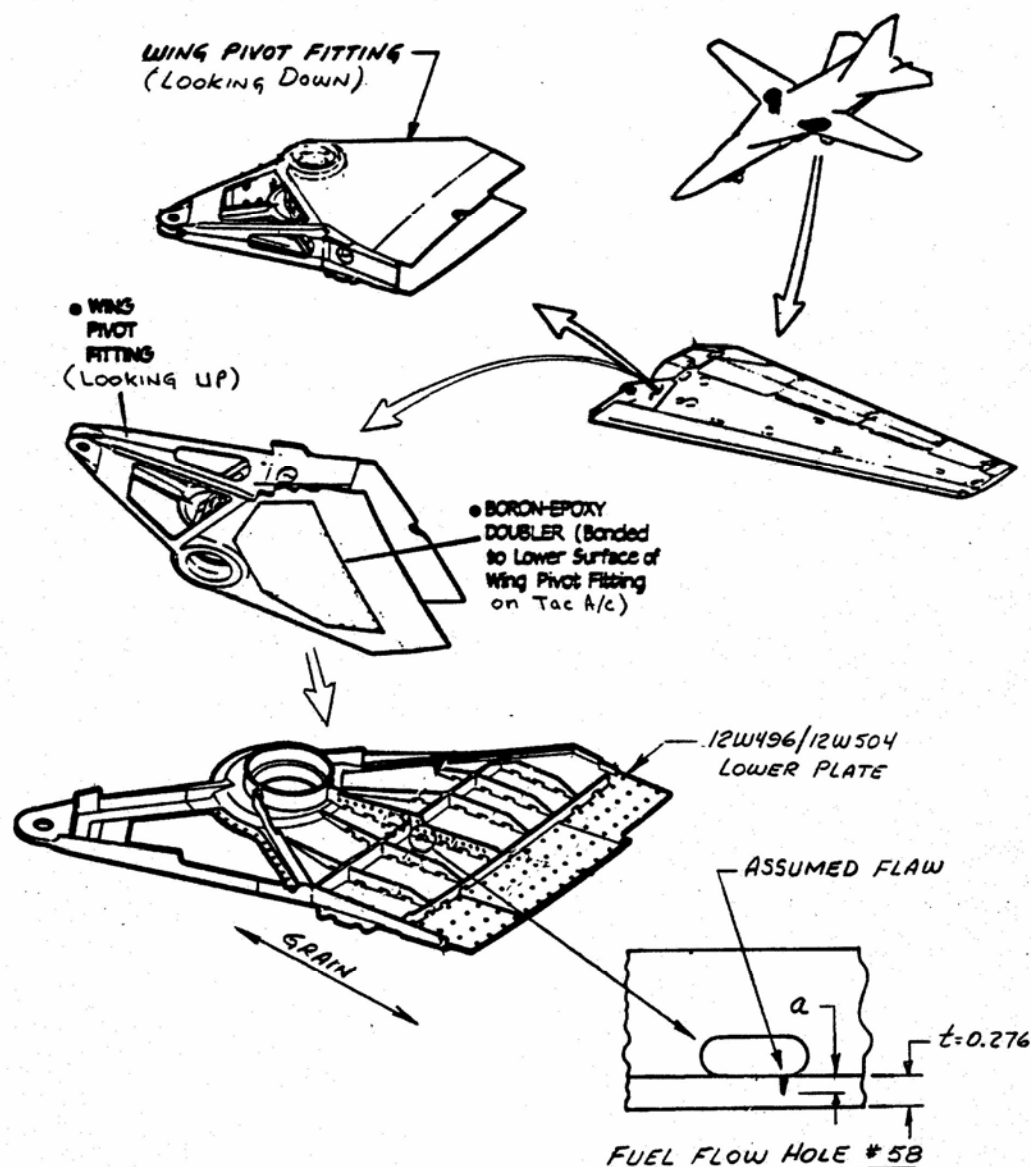


Figure 52 DADTA Item 86

Load Spectrum

The load spectrum applied to the A-4 right hand wing is shown in Table 21, from (General Dynamics 1973). The spectrum is expressed in terms of applied load; Wing pivot bending moment (WPBM). From (General Dynamics 1973), a stress equation was known to convert from local load (WPBM) to applied stress (σ). The stress equation is as follows

$$\sigma(\text{ksi}) = (11.31 - 15.42 \times X) \times \text{WPBM} \quad (46)$$

Where:

X = depth, in inches, below the inner surface

WPBM = wing pivot bending moment in millions of inch pounds (MIPS)

The thickness of the plate is 0.276 inches. The stress profile described can be considered as a situation of combined tension and out of plane bending, or a linear stress profile through the thickness.

Table 21 A-4 Right Hand Wing Fatigue Test Blocked Spectrum

Maximum WPBM (MIPS)	Minimum WPBM (MIPS)	Cycles per 400 Hr. Block
6.84	0.99	255
8.54	0.99	196
10.19	2.88	29
12.22	2.88	5
14.96	2.88	1
6.84	0.99	1
2.88	-2.4	4
2.88	-3.59	1
2.88	-2.4	1
6.9	0.58	1044
8.49	0.58	321
10.08	2.79	267
11.21	2.79	46
12.99	2.79	1
6.9	0.58	1
2.79	-1.5	5
2.79	3.07	1
2.79	-1.5	1
5.49	0.65	142
7.97	1.58	34
9.87	1.58	15
11.82	1.58	5
14.9	1.58	2
5.49	0.65	1

Test Procedure and Results

The wing was subjected to representative flight loading in block form such that the load at the WPF was as described. Each block represented 400 flying hours. The resultant crack growth curve and the original OEM analysis are shown in Figure 53 (from (General Dynamics 1973))

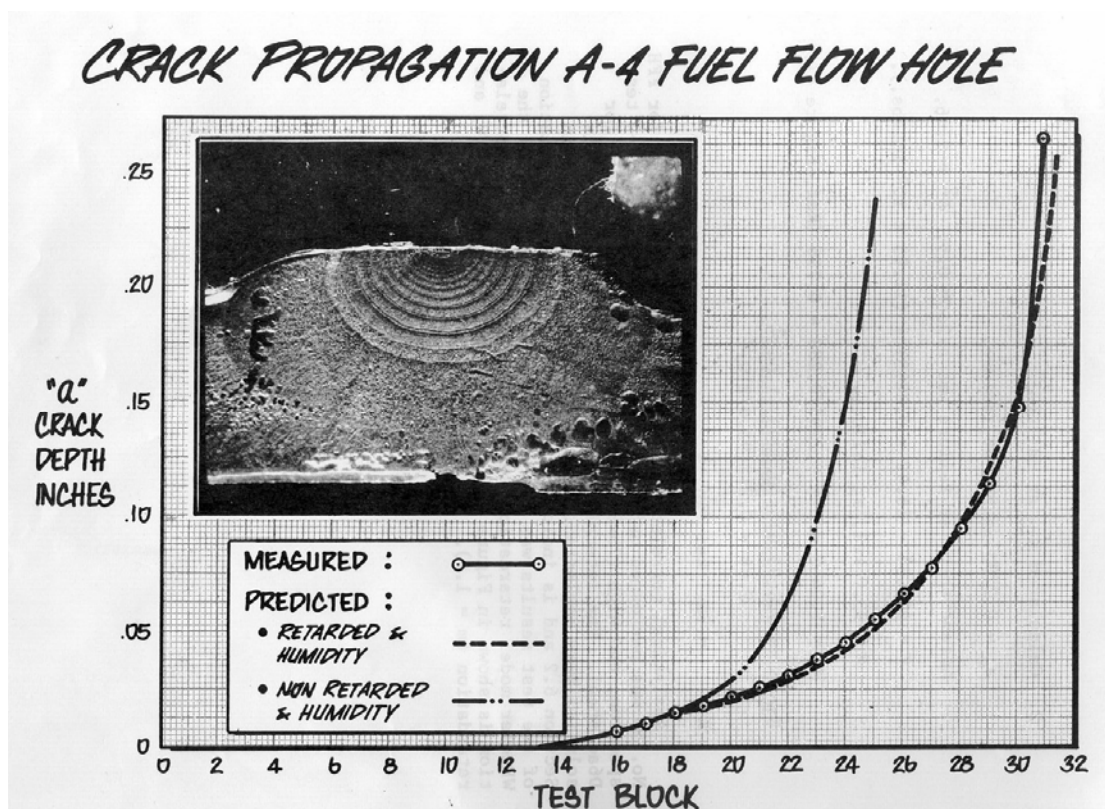


Figure 53 Comparison of Observed Crack Growth with Analysis

Details of more recent DSTO efforts to re-create the analysis are detailed in (Murtagh 1997). At that time, three analysis codes were used as follows:

- a. FractuREsearch,
- b. AFGROW, and
- c. FASTRAN II.

The results of the DSTO analyses compared with the data in Figure 53 are shown in Figure 54.

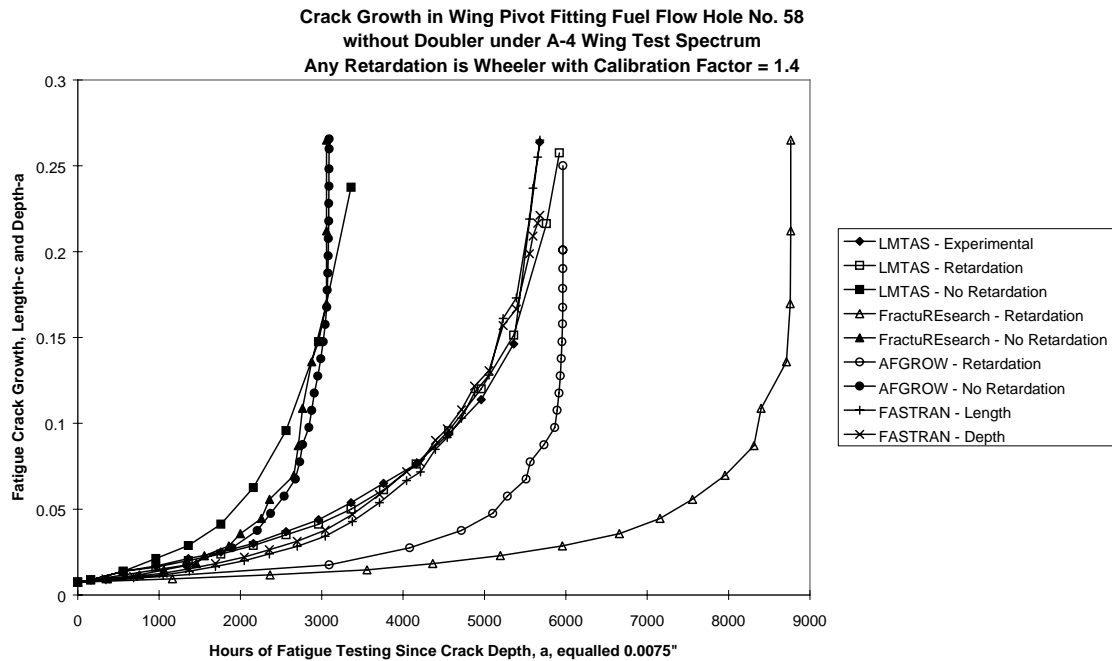


Figure 54 A-4 Right Hand Wing Fatigue Test Observed Crack Growth Compared with Analyses

In summary, the DSTO work concluded that FASTRAN II provided the best modelling result with a match in terms of both the final crack size/time and the shape of the curve itself¹⁰.

In theory at least, this example should be a very simple, straightforward example for crack growth analysis. However, it is clear from (Murtagh 1997) that this is not necessarily the case.

Computer Files

The relevant computer files for this example are as follows (see footnote 8 on p. 96 for the location of these files)

File name	Details
d6a4di86.dax	AFGROW problem definition file
d6a4.sp3	AFGROW A4 Spectrum file
d6a401.sub	AFGROW A4 Spectrum file
exdelkha.dat	Experimental (raw) crack growth rate data file for DKEFFNEW/FASTRAN
mndelkha.dat	Mean crack growth rate data file for DKEFFNEW/FASTRAN
Mnd6a4ha.dat	FASTRAN II input file, uses mean curve data

¹⁰ In other words, the analysis matched the crack size and time throughout the analysis, not just the final crack size and time. This is an important consideration when determining inspection intervals which relies on knowing the time corresponding to both the detectable and critical crack sizes.

D.3. F-111 Horizontal Tail Pivot Shaft Example

Background

This example is based on an F-111 location known as DI 36, which concerns potential cracking from an open hole below the horizontal tail pivot shaft (see Figure 55).

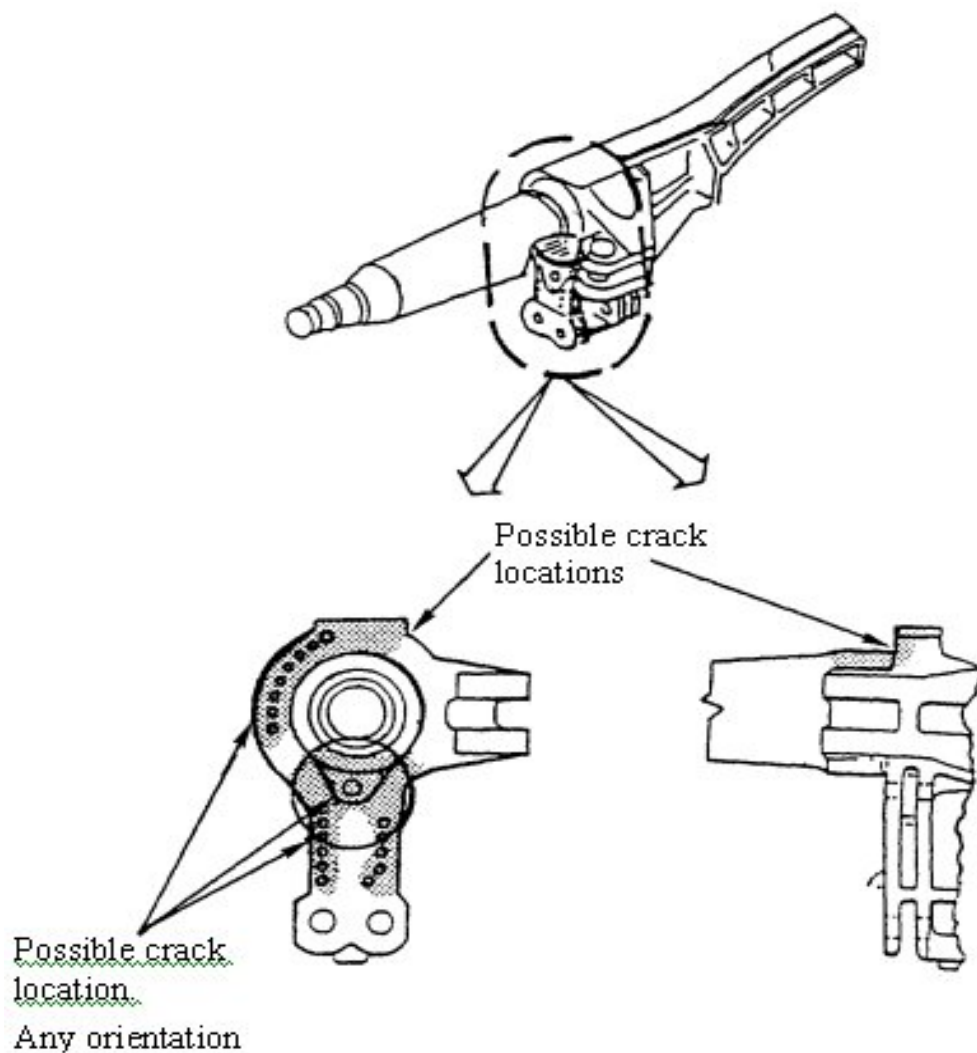


Figure 55 DADTA Item 36

Geometry

A series of coupon tests were conducted on D6ac steel coupons representing the DI36 location (Ignjatovic 2002). This location was of interest because the stresses are such that local plastic deformation (notch plasticity) was expected at the edge of the hole. The typical geometry of the coupons is shown in Figure 56, but the diameter of the hole varies.

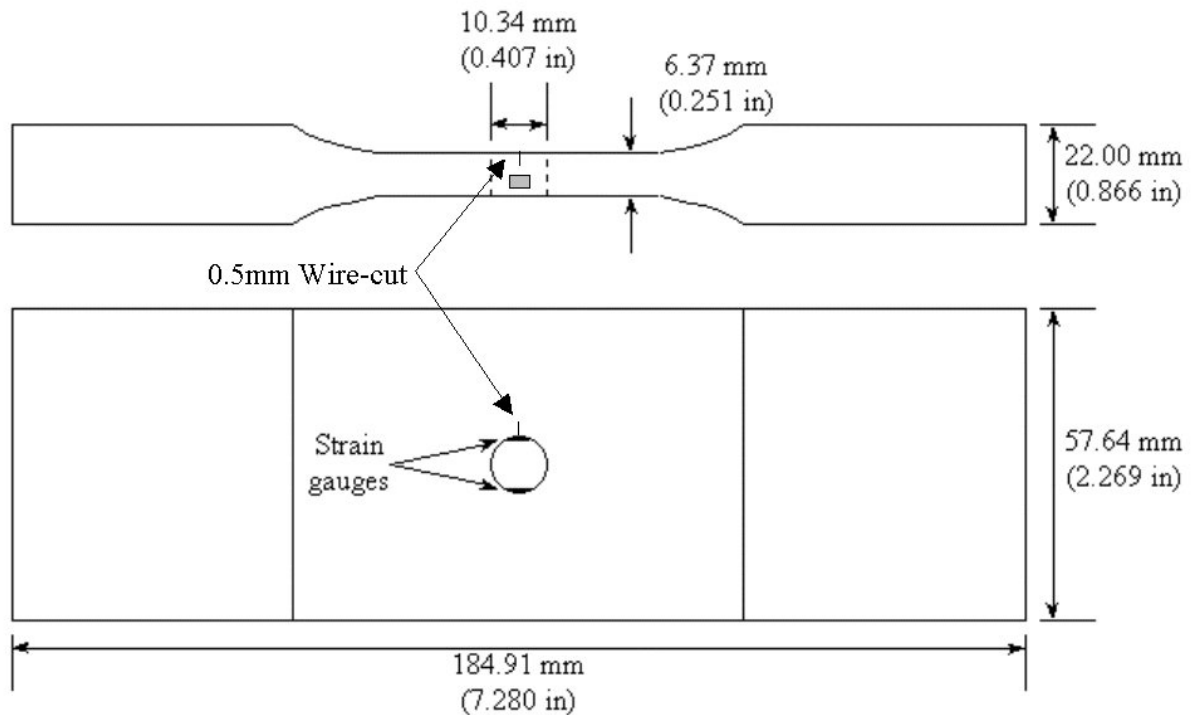


Figure 56 Typical Coupon Dimensions

Load Spectrum

The load spectrum applied to the coupons consisted of a sequence of loads known as the CPLT followed by a representative service sequence. The overall sequence represents 2000 hours of RAAF F-111 usage. In terms of remote applied load, the maximum and minimum of the service usage were 42.81 and -26.29 ksi respectively. The CPLT sequence consists of a sequence of six stress points, with remote stress values of 0, 79, -79, 24.66, -45.85 and 0 ksi.

Test Procedure and Results

The test procedure and results are detailed in (Ignjatovic 2002). One particular case is chosen here, known as Test ID 4. Two specimens were tested, with serial numbers EL7AA1 and EL3AL1. These particular specimens were pre-cracked following the introduction of a through thickness EDM slot. The hole was then reamed out to a diameter of 16.27 mm for EL7AA1 and 16.38 mm for EL3AL1. Following the testing, fractographic analysis was conducted and an analysis performed using METLIFE (Stoessiger 2002a; Stoessiger 2002b). The METLIFE analysis was conservative, and an improved result was obtained using CGAP in 2005 (Walker, Hu, Walker and Ignjatovic 2005). The test data and the METLIFE/CGAP analysis results are shown in Figure 57.

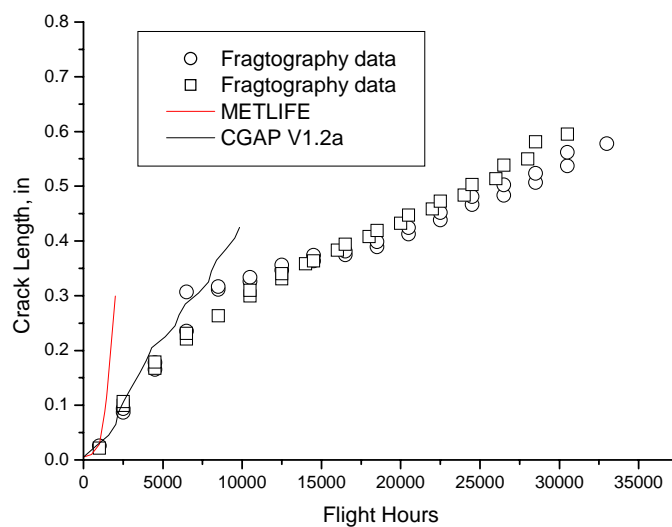


Figure 57 DI 36 coupon crack growth test and analysis results

Computer Files

The relevant computer files for this example are as follows (see footnote 8 on p. 96 for the location of these files):

File name	Details
cgap.exe	Version 1.5
di36BH.ntc	Notch definition file
di36-d2b_cplt.fsp	Spectrum file with CPLT load sequence
test ID4 (TC Variable).xls	Experimental and METLIFE data

D.4. F-111 Wing Pivot Fitting Upper Plate Fuel Flow Vent Hole Example

Background

This example is also based on the F-111, and also involves D6ac steel. The location is known as DI 92b, at the lower inboard corner of FFVH 13 in the WPF upper plate (see Figure 58).

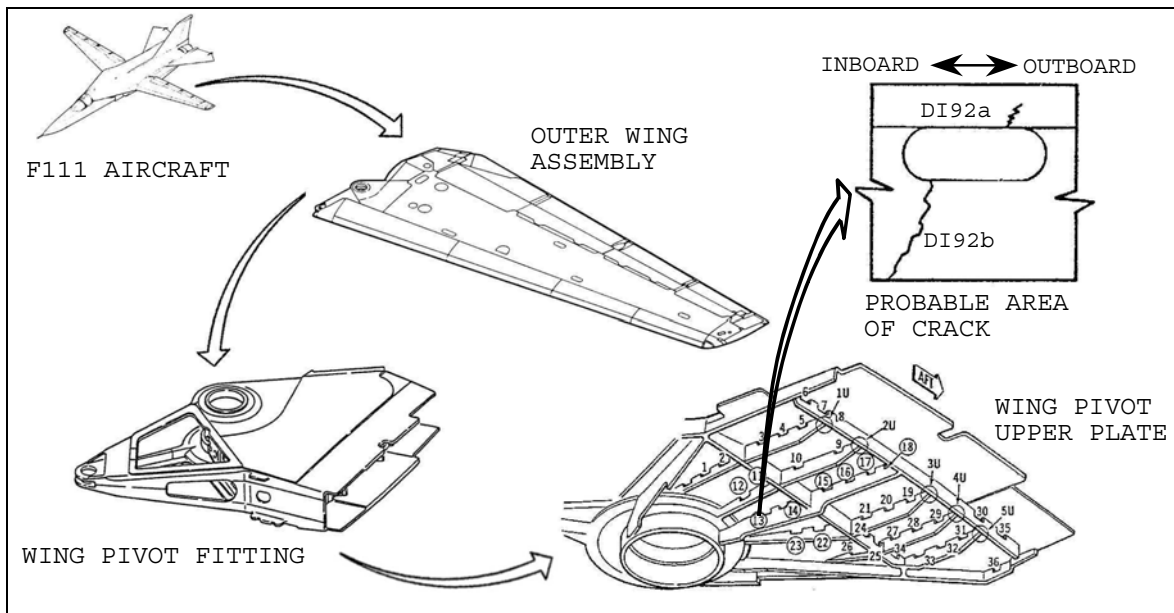


Figure 58 DI 92b

Geometry

Coupons representing the DI 92b location were designed and tested. The coupon geometry is shown in Figure 59, with an approximate stress concentration factor of $K_t = 3.78$.

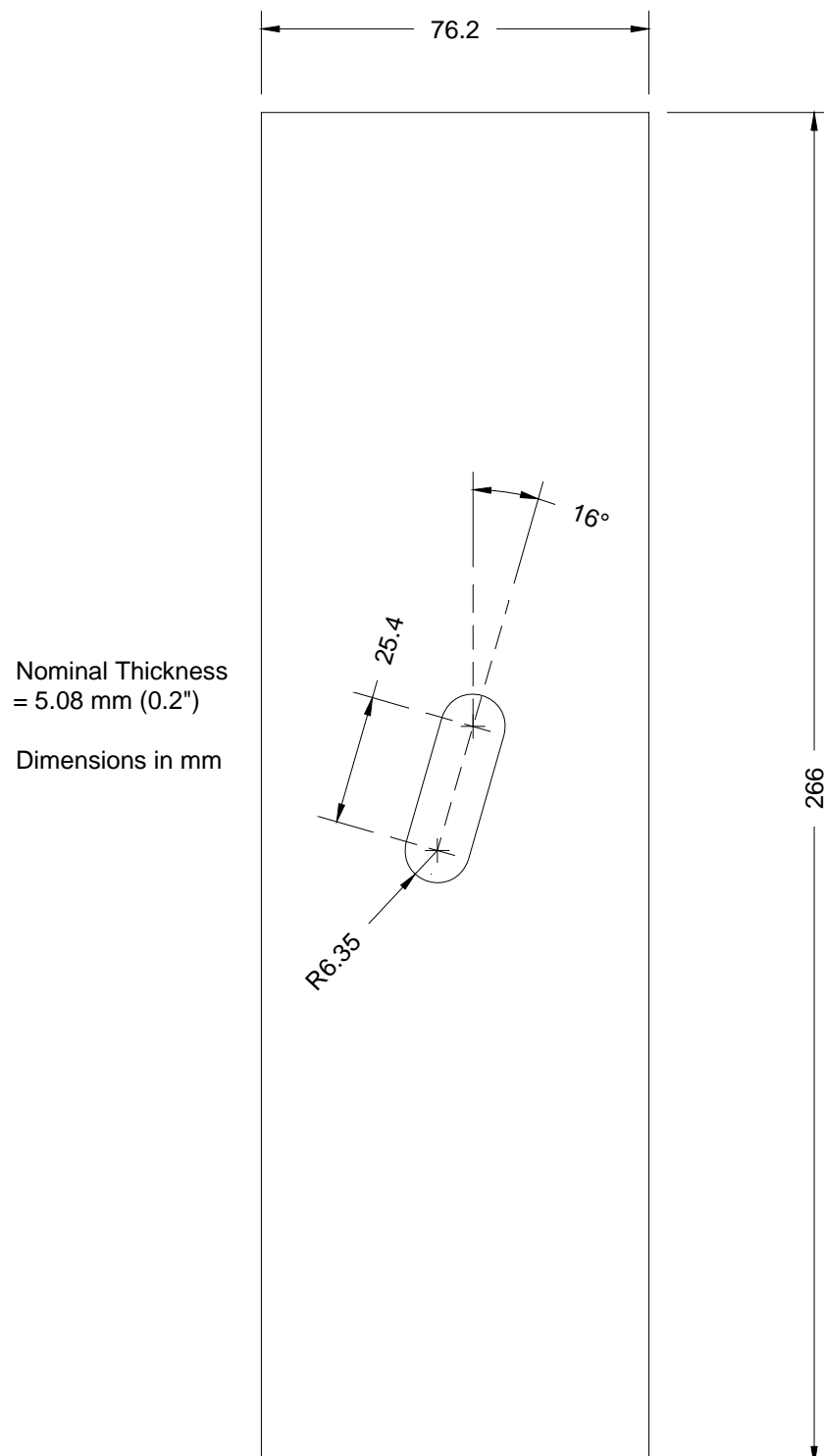


Figure 59 DI 92b coupon

Load Spectrum

The load spectrum applied to the coupons consisted of a sequence of loads known as the CPLT followed by a representative service sequence. The overall sequence represents 2000 hours of RAAF F-111 usage. In terms of remote applied load, the maximum and minimum of the service usage were 40.3 and -99.8 ksi respectively. The CPLT sequence consists of a sequence of six stress points, with remote stress values of 0, 51.2, -110.9, 62.6, -110.9 and 0 ksi.

Test Procedure and Results

The test procedure and results are detailed in (Weller 2002). A METLIFE analysis was performed (Walker 2001). The test data and the METLIFE analysis results are shown in Figure 60.

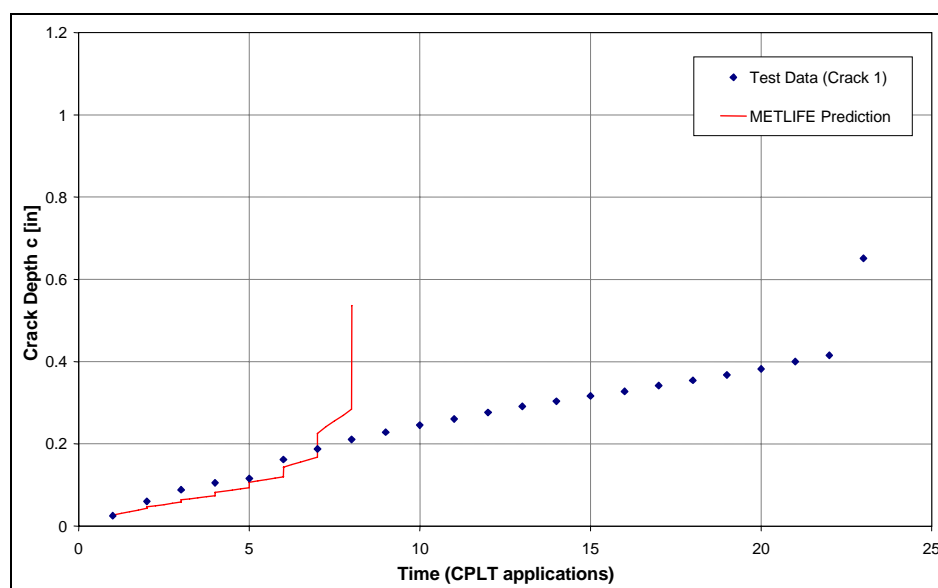


Figure 60 DI92b coupon crack growth and analysis data

Computer Files

The relevant computer files for this example are as follows:

File name	Details
SpectrumKSI.txt	Load spectrum applied to coupons in units of ksi

References

- Anderson, T. L. (1995). *Fracture Mechanics: Fundamentals and Applications*, CRC Press.
- ASTM (1996) *Standard Practice for Conducting Force Controlled Constant Amplitude Axial Fatigue Tests for Metallic Materials*. ASTM Standard E466-96. E466-96.
- ASTM (2000). *Annual Book of ASTM Standards, Metals Test Methods and Analytical Procedures*, West Conshohocken, PA.
- Athiniotis, N., S. Barter and G. Clark (1999) *Summary of fatigue cracking in RAAF Macchi MB326H wing spar*. DSTO. ARL-MAT-TR-0747.
- Ayling, J. and L. Molent (1998) *An Investigation into the Program FAMS (Fatigue Analysis of Metallic Structures)*. DSTO. DSTO-TR-0681.
- Ball, D. L. (1990). Proposed integration of notch-strain and fatigue crack-growth analysis. *Journal of Aircraft* **27**(4): 358-367.
- Ball, D. L. (1997a) *AFGROW evaluation*. Lockheed Martin Tactical Aircraft Systems VPDI-WBS-32CO-003.
- Ball, D. L. (1997b) *SPCGEN v1.3 technical approach, revision B, volume 2*. Lockheed Martin Tactical Aircraft Systems. MR(FF)-1037.
- Ball, D. L. (2005a) *METLIFE v1.3 technical approach, revision C, volume 2*. Lockheed Martin Tactical Aircraft Systems. MR(FF)-1022.
- Ball, D. L. (2005b) *METLIFE v1.3 user's guide, revision C, volume 1*. Lockheed Martin Tactical Aircraft Systems
- Barter, S. (1998) *Fractographic Inspection of the Cracking in FT488/2 Removed at Program 79*. DSTO. DSTO-TN-0170.
- Barter, S., N. Athiniotis and L. Lambianidis (1990) *Examination of the microstructure of several samples of 7050 aluminium alloy. Aircraft material memorandum*. DSTO. ARL-MAT-TM-403.
- Barter, S., L. Molent, N. Goldsmith and R. Jones (2005). An experimental evaluation of fatigue crack growth. *Journal of Engineering Failure Analysis* **12**(1): 99-128.
- Barter, S. A. (2003) *Fatigue Crack Growth in 7050T7451 Aluminium Alloy Thick Section Plate with Surface Condition Simulating Some Regions of the F/A-18 Structure*. DSTO-TR-1458. Air Vehicles Division, Platform Sciences Laboratory, DSTO.
- Barter, S. A., B. Bishop and G. Clark (1991) *Defect Assessment on F/A-18 488 Bulkhead Tested at ARL. Aircraft Material Report 125*. Aeronautical Research Laboratory, DSTO.
- Basquin, O. H. (1910). The exponential law of endurance tests, ASTM, West Conshohocken, PA.
- Blom, A. F. (1988). Fatigue crack growth under variable amplitude loading. *The third international spring meeting of the French Metallurgical society*.
- Blom, A. F. and D. K. Holm (1985). An experimental and numerical study of crack closure. *Engineering Fracture Mechanics* **22**(6): 997-1011.
- Breitung, K. (1984). Asymptotic Approximation for Multi-normal Integrals. *Journal of Engineering Mechanics, ASCE* **110** (3): 357-366.
- Broek, D. (1986). *Elementary engineering fracture mechanics*, Martinus Nijhoff Publishers.
- Broek, D. (1988). *The practical use of fracture mechanics*, Kluwer Academic Publishers.
- Broek, D. (1998) *Software for practical fracture mechanics and damage tolerance Version 98*.
- Bueckner, H. F. (1970). A novel principle for the computation of stress intensity factors. *Z. Angew. Math. Mech.* **50**(9): 529-546.

- Chaboche, J. L. (1986). Time independent constitutive theories for cyclic plasticity. *International Journal of Plasticity* **2**: 149-188.
- Clayton, J. Q. (1989). Modelling delay and thickness effects in fatigue. *Engineering Fracture Mechanics* **32**(2): 289-308.
- Dickinson, T. and L. Molent (2000) *Validation of fatigue damage models used for F/A-18 life assessment using fatigue coupon test results*. Defence Science and Technology Organisation. DSTO-TR-0940.
- Dugdale, D. S. (1960). Yielding of Steel Sheets Containing Slits. *Journal of Mechanics and Physics of Solids* **8**: 100-4.
- El Haddad, M. H., K. N. Smith and T. H. Topper (1979). Fatigue crack propagation of short cracks. *Journal of Engineering Materials and Technology, Trans. ASME* **101**: 42-46.
- Elber, W. (1971). The damage tolerance in aircraft structures. *ASTM STP 486*: 230-242.
- Finney, J. M. (1994). Fatigue crack growth in metallic military aircraft structures. *Handbook of fatigue crack propagation in metallic structures*. A. Carpinteri, Elsevier Science B.V. **2**: 1539-1565.
- Finney, J. M., and Denton, A.D. (1986). Cycle counting and reconstruction with application to the aircraft fatigue data analysis system. *International Conference on Fatigue of Engineering Materials and Structure*, University of Sheffield.
- Fleck, N. A. and J. C. J. Newman (1988). Analysis of crack closure under plane strain conditions. *Mechanics of Fatigue Crack Closure, STP 982*. J. C. Newman, Jr. and W. Elber, ASTM.
- Forman, R. G., V. E. Kearney and R. M. Engle (1967). Numerical analysis of crack propagation in cyclic-loaded structures. *Trans. ASME, Journal of Basic Engineering* **89, Series D**: 459-464.
- Frost, N. E. and D. S. Dugdale (1958). The propagation of fatigue cracks in sheet specimens. *Journal of the Mechanics and Physics of Solids* **6**: 92-110.
- Frost, N. E., K. J. Marsh and L. P. Pook (1974). *Metal Fatigue*, Clarendon Press, Oxford.
- Fühling, H. and T. Seeger (1979a). Dugdale crack closure analysis of fatigue cracks under constant amplitude loading. *Fracture Mechanics, ASTM STP 677*. C. W. Smith, American Society for Testing and Materials: 144-167.
- Fühling, H. and T. Seeger (1979b). Dugdale crack closure analysis of fatigue cracks under constant amplitude loading. *Engineering Fracture Mechanics* **11**: 99-172.
- General Dynamics (1970) *F-111 A-4 Right Hand Wing Fatigue Test 30.5 Blocks Report*. General Dynamics. FZS-12-325 Volume I of III.
- General Dynamics (1973) *Fracture Mechanics Volume II - Analysis for operational aircraft usage*. General Dynamics. FZM-12-13647.
- General Dynamics (1987) *DADTA : F-111 A/E/D/F and FB-111A Final Analysis Details*. General Dynamics. FZS-12-495, Revision A.
- Glinka, G. (1985). Energy density approach to calculation of inelastic strain-stress near notches and cracks. *Engineering Fracture Mechanics* **22**(3): 485-508.
- Glinka, G. (1985a). Calculation of inelastic notch tip strain-stress histories under cyclic loading. *Engineering Fracture Mechanics* **22**(5): 839-854.
- Goldsmith, N. T. and G. Clark (1990). Analysis and interpretation of aircraft component defects using quantitative fractography. *Quantitative methods in fractography*. S. M. Bernard and P. K. Susil, ASTM International.
- Graham, D. A. and G. D. Mallinson (1984) *NERF-A Computer Program for the Numerical Evaluation of Reliability Functions User Manual*. DSTO. 131.

- Grandt, A. F. (2004). Fundamentals of structural integrity, damage tolerant design and nondestructive evaluation, John Wiley and Sons USA.
- Grooteman, F. (1999). Advanced Stochastic Method for Probabilistic Analysis. *Euromech 405*, Valenciennes, France.
- Harter, J. A. (2004) *AFGROW user's guide and technical manual*. AFRL-VA-WP-TR-2004.
- Head, A. K. (1953). The growth of fatigue cracks. *Phil. Mag.* **44**(7): 925-938.
- Hovey, P. W., A. P. Berens and J. S. Loomis (1998) *Update of the Probability of Fracture (PROF) Computer Program for Aging Aircraft Risk Analysis*. Air Vehicles Directorate, Air Force Research Laboratory, Air Force Materiel Command, Wright-Patterson Air Force Base, OH 45433-7542. AFRL-VA-WP-TR-1999-3030. 96.
- Hovey, P. W., A. P. Berens and D. A. Skinn (1991) *Risk Analysis for Aging Aircraft-Volume 1-Analysis*. Flight Dynamics Directorate, Wright Laboratory, Wright-Patterson AFB, OH 45433-6553.
- Hu, W. and K. F. Walker (2004). An analysis of fatigue crack growth of a notched aircraft component under compression-dominated spectrum loading. *SIF2004 Structural Integrity and Fracture*, Brisbane, Australia, Australian Fracture Group Inc.
- Hu, W. and K. F. Walker (2006a) *Crack Growth in Notch Plasticity: The Methodology and Implementation of CGAP*. Defence Science and Technology Organisation. DSTO-RR-xxxx (to be published).
- Hu, W. and K. F. Walker (2006b). Fatigue Crack Growth from a Notch under Severe Overload and Underload. *The International Conference on Structural Integrity and Failure*, Sydney, Australia.
- Hu, W. and C. H. Wang (2000). Modelling of the Cyclic Ratchetting and Mean Stress Relaxation Behaviour of Materials Exhibiting Transient Cyclic Softening. *Structural Failure and Plasticity (IMPLAST 2000)*, Melbourne.
- Hu, W., C. H. Wang and S. Barter (1999) *Analysis of cyclic mean stress relaxation and strain ratchetting behaviour of aluminium 7050*. Aeronautical and Maritime Research Laboratory. DSTO-RR-0153.
- Ignjatovic, M. (2002) *Fatigue testing of D6ac steel coupons in support of F-111 DADTA capability - Test IDs 4, 5 and 6*. AMRL Structures Laboratory Report No 9/01.
- Irwin, G. R. (1957). Analysis of stresses and strains near the end of a crack traversing a plate. *Journal of Applied Mechanics* **24**: 361.
- Jones, R., L. Molent and S. Pitt (2006). Crack growth of physically small cracks. *Proceedings of International Conference on Fatigue Damage of Structural Materials VI*, Hyannis, USA.
- Kashyap, R. and I. Anderson (1995) *PC9/A Fatigue Test - Description of Computer Programs Used to Process Flight Data, test Loads and to Assess Fatigue Life*. Defence Science and Technology Organisation. DSTO-DDP-0289.
- Kitagawa, H. and S. Takahashi (1976). Applicability of fracture mechanics to very small cracks or the cracks in the early stage. *2nd international conferences on mechanical behaviour of materials*, Boston, MA.
- Latzko, D. G. H., C. E. Turner, J. D. Landes, D. E. McCabe and T. K. Hellen (1979). Post-yield fracture mechanics, Elsevier Applied Science Publishers.
- Leis, B. N., A. T. Hopper, J. Ahmad, D. Broek and M. F. Kanninen (1986). Critical review of the fatigue growth of short cracks. *Engineering Fracture Mechanics* **23**(5): 883-898.
- Leist, R. T. and C. R. Saff (1981) *CNTKSPC user's manual - contact stress model fatigue crack growth computer program*. McDonnell Douglas MDC IR0245.

- Lincoln, J. W. (1985). Risk Assessment of an Aging Military Aircraft. *Journal of Aircraft* **22**(8): 687-691.
- Liu, H. W. (1963). Fatigue crack propagation and applied stress range. *J. Basic Eng., ASME Trans.* **85D**(1): 116-122.
- Liu, H. W. (1991). A review of fatigue crack growth analyses. *Theoretical and Applied Fracture Mechanics* **16**(2): 91-108.
- Liu, Q., P. Hamel, W. Hu, A. Lahousse, P. K. Sharp and G. Clark (2005) *Experiments and modelling of stable tearing on aircraft structure*. DSTO. DSTO-TR-1657.
- Lockheed Martin (2001). Increased scope of Lockheed Martin Aeronautics Company RAAF F-111 study.
- Lockheed Martin (not-dated) *ADAMSys users guide for F-111 program*.
- Lockheed Martin Aeronautics Company (2001) *Increased scope of Lockheed Martin Aeronautics Company RAAF F-111 DADTA study for Royal Australian Air Force*. FZS-12-38002.
- Matriccioni, E. and P. Jackson (Unpublished) *Development of RAAF P-3C Fatigue Sequence for P-3 SLAP Test Interpretation*. DSTO. DSTO-TR-XXXX.
- McClung, R. C. and J. H. Feiger (not dated) *Small crack effect assessment, model implementation and evaluation for F-16 durability analysis*. Southwest Research Institute. MR(FF)-1207 Attachment B. B1-B23.
- McDonald, M., L. Molent and A. J. Green (2006) *Assessment of Fatigue Crack Growth Prediction Models for F/A-18 Representative Spectra and Material*. Defence Science and Technology Organisation. DSTO-RR-0312.
- McDonnell Douglas (1991a) *CG90 User's Manual for the Predication of Crack Growth*.
- McDonnell Douglas (1991b) *Computer program documentation for C_CI89*.
- Meeker, W. Q. and L. A. Escobar (1998). *Statistical Methods for Reliability data*, Wiley series in probability and statistics.
- Melchers, R. E. (1999). *Structural reliability analysis and prediction*. John Wiley & Sons Ltd, John Wiley & Sons Ltd.
- Miner, M. A. (1945). Cumulative damage in fatigue. *Journal of applied mechanics* **12**: A159-A164.
- Moews, J. (2003) *Certification basis description for the F-/A-18 aft fuselage/empennage*. Aerostructures. ER-F18-51-ASM343.
- Molent, L. (2005) *The History of structural fatigue testing at Fishermans Bend Australia*. Defence Science and Technology Organisation. DSTO-TR-1773
- Molent, L., R. Jones, S. Barter and S. Pitt (2006). Recent developments in fatigue crack growth assessment. *International Journal of Fatigue* **38**(12): 1759-1768.
- Molent, L., R. Ogden and R. Pell (2000) *F/A-18 FS488 bulkhead fatigue coupon tests*. Defence Science and Technology Organisation. DSTO-TR-0941.
- Murtagh, B. (2001) *Functional specifications for the P-3 structural life monitoring program*. Aerostructures. ES-P3-51-ASM021.
- Murtagh, B. a. W., K. (1997) *Comparison of analytical crack growth modelling and the A-4 wing test experimental results for a fatigue crack in an F-111 wing pivot fitting fuel flow hole number 58*. DSTO. DSTO-TN-0108.
- Naval Air Warfare Center (1995). *Fatigue Analysis of Metallic Structures (FAMS) - A Computer Program to Calculate Fatigue Damage by Local Stress/Strain Approach*.
- Navarro, A. and E. R. de los Rios (1988). Short and long fatigue crack growth: a unified model. *Philosophical Magazine A* **57**(1): 15-36.

- Neuber, H. (1961). Theory of stress concentration for shear-strained prismatical bodies with arbitrary non-linear stress-strain law. *Transactions of the ASME, Journal of Applied Mechanics*: 544-550.
- Newman, J. C. (1984). A crack opening stress equation for fatigue crack growth. *International Journal of Fracture* **24**: R131-R135.
- Newman, J. C., Jr. (1981a). A crack-closure model for predicting fatigue crack growth under aircraft spectrum loading. *Methods and Models for Predicting Fatigue Crack Growth under Random Loading*, ASTM STP 748. J. B. Chang and C. M. Hudson, ASTM: 53-84.
- Newman, J. C., Jr. (1992a) *FASTRAN II - A fatigue crack growth structural analysis program*. NASA. NASA TM-104159.
- Newman, J. C. and E. P. Phillips (1999) *Fatigue analyses under constant- and variable-amplitude loading using small-crack theory*. NASA. TM-1999-209329, ARL-TR-2001.
- Newman, J. C. J. (1981b). A crack closure model for predicting fatigue crack growth under aircraft spectrum loading. *ASTP STP 748*: 53-84.
- Newman, J. C. J. (1992b) *FASTRAN-II: A Fatigue Crack Growth Structural Analysis Program*. NASA, NASA TM 104159. NASA TM 104159.
- Newman, J. C. J. and H. J. Armen (1975). *AIAA Journal* **13**(8): 1017-1023.
- Newman, J. C. J. and I. S. Raju (1983). Stress-intensity factor equations for cracks in three-dimensional finite bodies. *Fracture Mechanics: Fourteenth Symposium - Volume I: Theory and Analysis*, ASTM STP 791. J. C. Lewis and G. Sines, ASTM. **I**: I-238-I-265.
- Orisamolu, I. R. (2001). Performance and Damage Prognostics for United Technologies Products. *LANL Damage Prognostics Workshop*, Tempe, Arizona.
- Palmgren, A. (1923). The endurance of ball bearings. *Z Ver Deut Ing* **68 No 14**: 339-41.
- Paris, P. C. (1964). Fatigue - an interdisciplinary approach. *Proceedings of the Tenth Sagamore Conference*, Syracuse New York USA, Syracuse University Press.
- Paris, P. C. and F. Erdogan (1963). A critical analysis of crack propagation laws. *Journal of Basic Engineering. Transactions of ASME* **85**: 528-534.
- Phillips, M. (2004) *P-3C SLAP Stress-Life Fatigue Analysis Program Documentation*. Defence Science and Technology Organisation.
- Phillips, M., D. Hartley and R. Amaratunga (2005) *DSTO Coupon Testing Documentation in Support of the P-3 Service Life Assessment Program*. DSTO. DSTO-TR-1764.
- Ritchie, R. O. (1979). Near-threshold fatigue-crack propagation in steels. *International Metallurgical Review* **20**: 205-230.
- Ritchie, R. O. and J. Lankford (1986). Small fatigue cracks: A statement of the problem and potential solutions. *Materials Science and Engineering* **84**: 11-16.
- Rose, L. R. F. and P. F. Preston (1999) *A strategic plan for fracture research*. Defence Science and Technology Organisation. DSTO-GD-0226.
- Rose, L. R. F. and C. H. Wang (2001). Self-similar analysis of plasticity-induced closure of small fatigue cracks. *Journal of the Mechanics and Physics of Solids* **49**: 401-429.
- Sadananda, K. and A. K. Vasudevan (1995). Analysis of fatigue crack closure and thresholds. *Fracture Mechanics: 25th Volume*. F. Erdogan. Philadelphia, ASTM. **STP 1220**: 484-501.
- Schijve, J. (2003). Fatigue of structures and materials in the 20th century and the state of the art. *International journal of fatigue* **25**: 679-702.
- Schwarman, L. (1988). Material data of high-strength aluminium alloys for durability evaluation of structures – fatigue strength, crack propagation, fracture toughness, Dusseldorf, West Germany : Aluminium-Verlag.

- Scott, C. F., J. C. Newman, Jr. and R. G. Forman (2002). Evaluation of fatigue crack thresholds using various experimental methods. *Fatigue and Fracture Mechanics*, ASTM STP 1417. W. G. Reuter and R. S. Piascik. West Conshohocken, American Society for Testing and Materials. 33.
- Shah, B. (2004). P-3C SLAP Program Phase II/III (Slides). Reno, Nevada, Lockheed Martin Aeronautics Co.
- Sharp, P. K., R. Byrnes and G. Clark (1998) *Examination of 7050 Fatigue Crack Growth Data and its Effect on Life Prediction*. Aeronautical and Maritime Research Laboratory DSTO. DSTO-TR-0729. 48.
- Sharpe, W. N. J. and K. C. Wang (1991). Evaluation of a modified monotonic Neuber relation. *Journal of Engineering Materials and Technology* **113**: 1-8.
- Sharpe, W. N. J., C. H. Yang and R. L. Tregoning (1992). An evaluation of the Neuber and Glinka relations for monotonic loading. *Transactions of the ASME* **39**: S50-S59.
- Silva, F. S. (2004). Crack closure inadequacy at negative stress ratios. *International journal of fatigue* **26**: 241-252.
- Southwest Research Institute (1991) *Probabilistic Structural Analysis Methods (PSAM) for Select Space Propulsion System Components-II (6th Annual Report)*. NASA. NASA-CR-187200. 343.
- Stephens, R. I., A. Fatemi, R. R. Stephens and H. O. Fuchs (2001). *Metal Fatigue in Engineering*, John Wiley & Sons, Inc.
- Stoessiger, M. (2002a) *Fracture and camera image analysis of D6ac steel coupons in support of F-111 DADTA*. Aerostructures. ER-F111-51-APM145.
- Stoessiger, M. a. I., M. (2002b) *Crack growth analysis of pseudo DI 36 coupons using METLIFE*. Aerostructures. ER-F111-51-APM164.
- Suresh, S. and R. O. Ritchie (1984). Propagation of short fatigue cracks. *International Metals Reviews* **29**(6): 445-476.
- Swanton, G. (2005) *A critical review of the METLIFE software in support of the RAAF F-111 durability and damage tolerance analysis (DADTA) program*. DSTO. DSTO-TR-1713.
- Technical Data Analysis Inc (2003) *Coupon Test - FAMS analysis correlations*. TDA. TDA-TR-01-010102x.
- Teunisse, B., M. Phillips, P. Jackson, E. Matricciani, Weiping Hu, R. Amaratunga, D. Hartley and D. Mongru (2006) *Computer Programs and Methodology used for DSTO P-3C SLAP Test Interpretation*. Defence Science and Technology Organisation. DSTO-TR-1834.
- Tong, Y. C. (2006). Probabilistic fatigue life analysis methods for aerospace vehicles. *School of Aerospace, Mechanical and Mechatronic Engineering*, The University of Sydney.
- Tong, Y. C. and R. A. Antoniou (2005) *Risk Analysis of TF30 2nd and 3rd LPT*. DSTO. DSTO-CR-2005-0256.
- Tong, Y. C., J. Hou and R. A. Antoniou (2005) *Probabilistic Damage Tolerance Assessment: The Relative Merits of DARWIN, NERF AND PROF*. DSTO. DSTO-TR-1789.
- Tong, Y. C., P. White, K. C. Watters and R. A. Antoniou (2006) *Reliability analysis of F-111C wing life*. Air Vehicles Division, DSTO. DSTO-CR-2006-0433.
- UK DEFSTAN, -. (1987). General Specifications for Aircraft Gas Turbine Engines,. *UK Defence Standard*.
- UK Ministry of Defence (1999), Defence Standard 00-970, Design and Airworthiness Requirements for Service Aircraft, Issue 2.

- Veul, R. P. G. and L. C. Ubels (2003) *Results of the FMS spectra loading coupon tests performed within the framework of the P-3C Service Life Assessment Program*. Royal Netherlands Navy (RNLN). NLR-CR-2003-DRAFT.
- Walker, K. (1970). The effect of stress ratio during crack propagation and fatigue for 2024-T3 and 7075-T6 aluminium. *Effects of Environment and Complex Load History of Fatigue Life*, ASTM STP 462: 1-14.
- Walker, K. (1987). The effect on fatigue crack growth under spectrum loading of an imposed placard "G" limit, Purdue University.
- Walker, K. (1997). An evaluation of empirical and analytical models for predicting fatigue crack propagation load interaction effects. *United States Air Force Aircraft Structural Integrity Program (ASIP)*, San Antonio Texas USA.
- Walker, K. (1998) *Review of DADTA Item 86 analysis*.
- Walker, K., W. Hu, J. Walker and M. Ignjatovic (2005). Fatigue crack growth in high strength metallic F-111 aircraft structures involving significant cyclic notch plasticity. *The Eleventh Australian International Aerospace Congress*, Melbourne, Australia.
- Walker, K., Marsden, P., and Weller, S. (2001). Elastic plastic analysis of fatigue cracking in the F-111 wing pivot fitting upper plate fuel vent hole number 13. *9th Australian International Aerospace Congress AIAC 2001*, Canberra, ACT, Australia.
- Walker, K., Walker, J., and Swanton, G. (2004) *Structural integrity assurance for the F-111 outer lower wing skin through a condition assessment program*.
- Wang, C. H., W. Hu and J. P. G. Sawyer (2000). Explicit numerical integration algorithm for a class of non-linear kinematic hardening model. *International Journal of Computational Mechanics* **26**: 140-147.
- Wang, G. S. (2000). Probabilistic Fatigue Crack Growth Analyses for Critical Structural Details. *AIAA Journal* **Vol. 38**(No. 5): 882-892.
- Weller, S. (2002) *Fatigue testing of open elongated hole specimens for METLIFE validation*. DSTO. AVD Structures Laboratory Report No 8/01.
- Wheeler, O. E. (1970) *Crack growth under spectrum loading*. General Dynamics/Fort Worth Division. FZM-5602.
- Wheeler, O. E. (1972). Spectrum loading and crack growth. *J. Basic Engineering, Transactions, ASME* **94**: 181-186.
- White, P., L. Molent and S. Barter (2005). Interpreting fatigue test results using a probabilistic fracture approach. *International Journal of Fatigue* **27**(7): 752-767.
- Willenborg, J. D., R. M. Engle and H. A. Wood (1971) *A crack growth retardation model using an effective stress concept*. Air Force Flight Dynamics Laboratory. TM-FBR-71-1.
- Wood, C. and R. A. Antoniou (2005) *Reliability Assessment of RAAF F404-400 No. 4 Bearings*. DSTO-CR-2005-0250, Platform Sciences Laboratory, Defence Science and Technology Organisation.
- Wu, Y. T. (1985). Demonstration of a new, fast probability integration method for reliability analysis. *Advances in aerospace structural analysis: Proceedings of the Winter Annual Meeting*, Miami Beach, FL, American Society of Mechanical Engineers.
- Wu, Y. T., M. P. Enright and H. R. Millwater (2002). Probabilistic methods for design assessment of reliability with inspection. *AIAA Journal* **40**(5): 937-946.
- Zion, L. (1996) *A Risk-Based Methodology for Rotorcraft Component Retirement Time Substantiation*. Georgia Tech Research Institute, GTRI Project A-5144, Technical report, Final report-Rev-1.

Zuidema, J., F. Veer and C. Van Kranenburg (2005). Shear lips on fatigue fracture surfaces of aluminium alloys. *Fatigue & Fracture of Engineering Materials & Structures* **28**(1): 159-167.

DISTRIBUTION LIST

"As per the Research Library's *Policy on electronic distribution of official series reports* (<http://web-vic.dsto.defence.gov.au/workareas/library/aboutrl/roles&policies/mission.htm>) Unclassified (both Public Release and Limited), xxx-in-confidence and Restricted reports and their document data sheets will be sent by email through DRN to all recipients with Australian defence email accounts who are on the distribution list apart from the author(s) and the task sponsor(s). Other addressees and Libraries and Archives will also receive hardcopies."

A Review and Assessment of Current Airframe Lifting Methodologies and Tools in Air Vehicles Division

W. Hu, Y.C. Tong, K.F. Walker, D. Mongru, R. Amaratunga, P. Jackson

AUSTRALIA

DEFENCE ORGANISATION

	No. of copies
Task Sponsor	
DGTA (OIC ASI Section) S&T Program	2 Printed
Chief Defence Scientist	1
Deputy Chief Defence Scientist Policy	1
AS Science Corporate Management	1
Director General Science Policy Development	1
Counsellor Defence Science, London	Doc Data Sheet
Counsellor Defence Science, Washington	Doc Data Sheet
Scientific Adviser to MRDC, Thailand	Doc Data Sheet
Scientific Adviser Joint	1
Navy Scientific Adviser	Doc Data Sht & Dist List
Scientific Adviser – Army	Doc Data Sht & Dist List
Air Force Scientific Adviser	1
Scientific Adviser to the DMO	Doc Data Sht & Dist List
Deputy Chief Defence Scientist Platform and Human Systems	Doc Data Sht & Exec Summary
Chief of Air Vehicles Division	Doc Data Sht & Dist List
Research Leader: D. Graham	1 Printed
Task Manager: Phil Jackson (AVD)	1 Printed

Author(s):	
W. Hu	1 Printed
Y.C. Tong	1 Printed
K.F. Walker	1 Printed
D. Mongru	1 Printed
R. Amaratunga	1 Printed
Others:	1 Printed
R. Boykett	1 Printed
L. Molent	1 Printed
C.H. Wang	1 Printed
M. Heller	1 Printed
K. Watters	1 Printed
G. Chen	1
M. McDonald	1
L. Meadows	1
D. Lombardo	1
S. Pitt	1
W. Zhuang	1
B. Wicks	1
DSTO Library and Archives	
Library Fishermans Bend	1 Printed
Library Edinburgh	1 Printed
Defence Archives	1 Printed
Capability Development Executive	
Director General Maritime Development	Doc Data Sheet
Director General Capability and Plans	Doc Data Sheet
Assistant Secretary Investment Analysis	Doc Data Sheet
Director Capability Plans and Programming	Doc Data Sheet
Chief Information Officer Group	
Head Information Capability Management Division	Doc Data Sheet
Director General Australian Defence Simulation Office	Doc Data Sheet
AS Information Strategy and Futures	Doc Data Sheet
Director General Information Services	Doc Data Sheet
Strategy Executive	
Assistant Secretary Strategic Planning	Doc Data Sheet
Assistant Secretary International and Domestic Security Policy	Doc Data Sheet
Navy	
Maritime Operational Analysis Centre, Building 89/90 Garden Island Sydney NSW	Doc Data Sht & Dist List
Deputy Director (Operations)	
Deputy Director (Analysis)	

Director General Navy Capability, Performance and Plans, Navy Headquarters	Doc Data Sheet
--	----------------

Director General Navy Strategic Policy and Futures, Navy Headquarters	Doc Data Sheet
---	----------------

Air Force

SO (Science) - Headquarters Air Combat Group, RAAF Base, Williamtown NSW 2314	Doc Data Sht & Exec Summary
---	-----------------------------

Staff Officer Science Surveillance and Response Group	Doc Data Sht & Exec Summary
---	-----------------------------

OIC ASI - DGTA	1
----------------	---

Army

Australian National Coordination Officer ABCA (AS NCO ABCA), Land Warfare Development Centre, Puckapunyal	Doc Data Sheet
---	----------------

J86 (TCS GROUP), DJFHQ	Doc Data Sheet
------------------------	----------------

SO (Science) - Land Headquarters (LHQ), Victoria Barracks NSW	Doc Data Sht & Exec Summary
---	-----------------------------

SO (Science) - Special Operations Command (SOCOMD), R5-SB-15, Russell Offices Canberra	Doc Data Sht & Exec Summary & Dist List
--	---

SO (Science), Deployable Joint Force Headquarters (DJFHQ) (L), Enoggera QLD	Doc Data Sheet
---	----------------

Joint Operations Command

Director General Military Strategic Commitments	Doc Data Sheet
---	----------------

Chief of Staff Headquarters Joint Operations Command	Doc Data Sheet
--	----------------

Commandant ADF Warfare Centre	Doc Data Sheet
-------------------------------	----------------

Director General Strategic Logistics	Doc Data Sheet
--------------------------------------	----------------

Intelligence and Security Group

AS Concepts, Capability and Resources	1
---------------------------------------	---

DGSTA , Defence Intelligence Organisation	1
---	---

Manager, Information Centre, Defence Intelligence Organisation	1
--	---

Director Advanced Capabilities	Doc Data Sheet
--------------------------------	----------------

Defence Materiel Organisation

Deputy CEO	Doc Data Sheet
------------	----------------

Head Aerospace Systems Division	Doc Data Sheet
---------------------------------	----------------

Head Maritime Systems Division	Doc Data Sheet
--------------------------------	----------------

Program Manager Air Warfare Destroyer	Doc Data Sheet
---------------------------------------	----------------

Guided Weapon & Explosive Ordnance Branch (GWEO)	Doc Data Sheet
--	----------------

CDR Joint Logistics Command	Doc Data Sheet
-----------------------------	----------------

OTHER ORGANISATIONS

National Library of Australia	1
-------------------------------	---

NASA (Canberra)	1
-----------------	---

Library of New South Wales	1
----------------------------	---

UNIVERSITIES AND COLLEGES

Australian Defence Force Academy	
Library	1
Head of Aerospace and Mechanical Engineering	1
Hargrave Library, Monash University	Doc Data Sheet

OUTSIDE AUSTRALIA

INTERNATIONAL DEFENCE INFORMATION CENTRES

US Defense Technical Information Center	1
UK Dstl Knowledge Services	1
Canada Defence Research Directorate R&D Knowledge & Information Management (DRDKIM)	1
NZ Defence Information Centre	1

ABSTRACTING AND INFORMATION ORGANISATIONS

Library, Chemical Abstracts Reference Service	1
Engineering Societies Library, US	1
Materials Information, Cambridge Scientific Abstracts, US	1
Documents Librarian, The Center for Research Libraries, US	1

INFORMATION EXCHANGE AGREEMENT PARTNERS

National Aerospace Laboratory, Japan	1
National Aerospace Laboratory, Netherlands	1

SPARES	5 Printed
--------	-----------

Total number of copies: 55 Printed: 23 PDF: 32

DEFENCE SCIENCE AND TECHNOLOGY ORGANISATION DOCUMENT CONTROL DATA					
				1. PRIVACY MARKING/CAVEAT (OF DOCUMENT)	
2. TITLE A Review and Assessment of Current Airframe Lifting Methodologies and Tools in Air Vehicles Division			3. SECURITY CLASSIFICATION (FOR UNCLASSIFIED REPORTS THAT ARE LIMITED RELEASE USE (L) NEXT TO DOCUMENT CLASSIFICATION) Document (U) Title (U) Abstract (U)		
4. AUTHOR(S) W. Hu, Y.C. Tong, K.F. Walker, D. Mongru, R. Amaratunga and P. Jackson			5. CORPORATE AUTHOR DSTO Defence Science and Technology Organisation 506 Lorimer St Fishermans Bend, Victoria, 3207 Australia		
6a. DSTO NUMBER DSTO-RR-0321		6b. AR NUMBER AR 013-826		7. DOCUMENT DATE December 2006	
8. FILE NUMBER 2006/1080235/1		9. TASK NUMBER AIR 04/153		10. TASK SPONSOR DGTA (OIC ASI Section)	
				11. NO. OF PAGES 144	
				12. NO. OF REFERENCES 146	
13. URL on the World Wide Web http://www.dsto.defence.gov.au/corporate/reports/DSTO-RR-0321.pdf				14. RELEASE AUTHORITY Chief, Air Vehicles Division	
15. SECONDARY RELEASE STATEMENT OF THIS DOCUMENT <p style="text-align: center;"><i>Approved for public release</i></p>					
OVERSEAS ENQUIRIES OUTSIDE STATED LIMITATIONS SHOULD BE REFERRED THROUGH DOCUMENT EXCHANGE, PO BOX 1500, EDINBURGH, SA 5111					
16. DELIBERATE ANNOUNCEMENT No Limitations					
17. CITATION IN OTHER DOCUMENTS Yes					
18. DSTO Research Library Thesaurus Empirical methods, modelling methods, techniques, numerical modelling, probabilistic modelling, numerical simulation, plastic theory, science and technology advice					
19. ABSTRACT The Air Vehicles Division of Defence Science and Technology Organisation (DSTO) owns and/or uses a large number of software tools for crack-initiation and crack-growth analyses of aircraft structures. These tools represent a substantial body of knowledge of fatigue and fracture of engineering materials and structures that has been created and accumulated over the years. This report presents a review and assessment of the methods underpinning the more commonly-used software tools and approaches in Air Vehicles Division. The key points of the principle of each method are discussed, and different implementation considerations are highlighted, to demonstrate the similarity and difference between the models. A start is made on the compilation of a compendium of benchmark problems and challenging problems in order to assist the evaluation and consistent validation of existing and newly-developed tools. The objectives of the review are to help to increase the responsiveness and robustness of the advice DSTO provides to its clients by identifying the strengths and limitations of the commonly-used methods and tools; identifying and recommending software platforms for future improvement, and horizon-scanning the field of fatigue and fracture for new and emerging methodologies for aircraft structural life prediction. It is expected that the recommendations presented in this review will be addressed in follow-on work.					